DEVELOPMENT OF DIFFUSION BONDED MATERIALS FOR ELECTRONICS COOLING APPLICATIONS

A THESIS SUBMITTED TO
THE GRADUATE SCHOOL OF NATURAL AND APPLIED SCIENCES
OF
MIDDLE EAST TECHNICAL UNIVERSITY

BY

SILA ECE ATABAY

IN PARTIAL FULFILLMENT OF THE REQUIREMENTS
FOR
THE DEGREE OF MASTER OF SCIENCE
IN
METALLURGICAL AND MATERIALS ENGINEERING

SEPTEMBER 2017

Approval of the thesis:

DEVELOPMENT OF DIFFUSION BONDED MATERIALS FOR ELECTRONICS COOLING APPLICATIONS

submitted by **SILA ECE ATABAY** in partial fulfillment of the requirements for the degree of **Master of Science in Metallurgical and Materials Engineering Department, Middle East Technical University** by,

Prof. Dr. Gülbin Dural Ünver _____
Dean, Graduate School of **Natural and Applied Science**

Prof. Dr. C. Hakan Gür _____
Head of Department, **Metallurgical and Materials Engineering**

Prof. Dr. Arcan F. Dericioğlu _____
Supervisor, **Metallurgical and Materials Eng. Dept., METU**

Examining Committee Members:

Prof. Dr. Kadri Aydınol _____
Metallurgical and Materials Engineering Dept., METU

Prof. Dr. Arcan F. Dericioğlu _____
Metallurgical and Materials Engineering Dept., METU

Prof. Dr. Caner Durucan _____
Metallurgical and Materials Engineering Dept., METU

Assoc. Prof. Dr. Benat Koçkar _____
Mechanical Eng. Dept., Hacettepe University

Assist. Prof. Dr. Mert Efe _____
Metallurgical and Materials Engineering Dept., METU

Date: 07.09.2017

I hereby declare that all information in this document has been obtained and presented in accordance with academic rules and ethical conduct. I also declare that, as required by these rules and conduct, I have fully cited and referenced all material and results that are not original to this work.

Name, Last name: Sıla Ece Atabay

Signature :

ABSTRACT

DEVELOPMENT OF DIFFUSION BONDED MATERIALS FOR ELECTRONICS COOLING APPLICATIONS

Atabay, Sıla Ece

M.S., Department of Metallurgical and Materials Engineering

Supervisor: Prof. Dr. Arcan F. Dericioğlu

September 2017, 124 pages

Failure of most of the electronic systems are originating from deterioration of the components due to excessive heat flux generation. The unstoppable demand for more complex and miniaturized electronic systems makes the development of more suitable and feasible production methods for their cooling systems and components compulsory. In the scope of this study diffusion bonding behavior of the aluminum (Al) 6063 alloy was investigated to make this bonding method and alloy system available for the electronic cooling systems. In diffusion bonding every parameter has an important effect on the properties of the resulting joints. These effects were investigated in this study to determine the optimum bonding parameters in terms of the resulting mechanical properties of the joints. Consequently, maximum bond shear strength was achieved under 13 MPa pressure at 520°C for three hours when the bonded samples were cooled in air. Preserving the physical and chemical properties of the base metal is essential along with obtaining high bond strengths for the formation of a solid joint. To minimize the degradation in the properties of the alloy without altering the composition, silver, nickel and gold interlayers were applied to the bond interface. However, interlayer addition was proven to be unsuccessful in terms of bond

formation. Rather than using an interlayer, addition of copper (Cu) and tin (Sn) as alloying elements to the Al 6063 was also studied to examine their effect on the properties of both the base metal and diffusion bonded joints. Cu alloying was found to be preventing the loss in the mechanical properties of the base metal without causing any increase in the bond strength. On the other hand, enhancement of joint formation was observed in the Sn containing alloys along with a slight decrease in the strength of the base metal.

Keywords: Solid State Joining, Diffusion Bonding, Al-Mg-Si Alloys, Interlayer Addition, Alloy Production, Mechanical Testing.

ÖZ

ELEKTRONİK SOĞUTMA SİSTEMLERİ İÇİN DİFÜZYONLA BAĞLAMA YÖNTEMİYLE MALZEME ÜRETİMİ VE KARAKTERİZASYONU

Atabay, Sıla Ece

Yüksel Lisans, Metalurji ve Malzeme Mühendisliği Bölümü

Tez Yöneticisi: Prof. Dr. Arcan F. Dericioğlu

Eylül 2017, 124 sayfa

Elektronik sistemlerdeki bozulmaların pek çoğu sistem parçalarının aşırı ısı akışı nedeniyle çalışmayı durdurmasından kaynaklanmaktadır. Üretilen sistemlerin karmşıklığının artması konusundaki önlenemeyen talep, daha kompleks soğutma sistemlerinin ve sistem parçaları için üretim metodlarının geliştirilmesi gereğini doğurmuştur. Bu çalışma kapsamında elektronik soğutma sistemlerinde kullanılmak üzere alüminyum 6063 alaşımının difüzyonla bağlanması incelenmiştir. Difüzyonla bağlama sırasında kullanılan her değişkenin birleşim noktasının özellikleri üzerinde önemli bir etkisi olduğu bilinmektedir. İdeal değişkenleri belirlemek adına her birinin etkisi incelenmiş ve numuneler 13 MPa basınç altında 520^{o}C sıcaklıkta 3 saat süreyle tutulup daha sonra havada soğutulduğunda en yüksek bağ kuvvetinin elde edildiği gözlenmiştir. Başarılı bir bağlanmadan söz edebilmek için, ana maddenin fiziksel ve kimyasal özelliklerinin korunması da en az yüksek bağ kuvvetleri elde etmek kadar önem arzetmektedir. Difüzyonla bağlanma sırasında oluşan bozunmaları başlangıç malzemesinin kompozisyonunu değiştirmeden en aza indirgemek adına arayüzeye gümüş, nikel veya altın katmanlar eklenmiştir. Arakatman uygulanarak hazırlanan

numuneler bağ oluşumu açısından başarılı olmamıştır. Alaşım elementlerinin ana malzeme ve bağ kuvvetine etkisini incelemek amacıyla başlangıç alaşımına değişen miktarlarda bakır ve kalay eklenmiş ve etkileri gözlemlenmiştir. Bakır ile alaşımlanan nemunelerin bağ kuvvetinde herhangi bir artış olmamasına rağmen bağlanma sırasında yaşanan mekanik zayıflamanın engellendiği gözlemlenmiştir. Kalay eklenen numunelerde ise ana malzemede mekanik olarak hafif bir bozunma ile birlikte bağ kuvvetinde önemli artışlar olduğu görülmüştür.

Anahtar Kelimeler: Katı Halde Birleştirme, Difüzyonla Bağlama, Al-Mg-Si Alaşımları, Arakatman Eklemesi, Alaşım Üretimi, Mekanik Test.

To My Beloved Family

ACKNOWLEDGEMENTS

I would like to thank my supervisor Prof. Dr. Arcan F. Dericioğlu for his continuous support and encouragement throughout my graduate study. I am grateful to him for widening my academic vision and background with his experience. He consistently allowed this thesis to be my own work, but steered me in the right direction whenever he thought I needed it.

I am very grateful to Assoc. Prof. Dr. Ziya Esen for his helpful comments, remarks and support throughout this thesis study. I also need to thank my substitute supervisor Prof. Dr. Caner Durucan for his support and guidance. I would like to acknowledge Assoc. Prof. Dr. Yunus Eren Kalay for his favour.

I am thankful to all the staff of the Department of Metallurgical and Materials Engineering and Ergül Makina for their suggestions and help during this study.

I would like to express my gratitude to my lab mates and friends Güney Mert Bilgin, Simge Tülbez, Ezgi Bütev and Tuğçe Altuntop for their huge support, help and insightful comments and suggestions.

I owe my heartfelt thanks to my friends and colleagues Doğancan Sarı, Bengisu Yaşar, Özgün Köse, Ayşe Merve Genç Ünalan and Gökhan Polat for their constant support in daily struggles and being there whenever I need.

Above all, I would like to express my deepest gratitude to Fatih Sıkan, this thesis could not be accomplished without his unfailing support, continuous encouragement and patience. He was always there to lighten up my mood and stood by me through the good times and bad.

Finally, I want to thank my family Semine, Fikret and Doğa Atabay for their heartwarming support, encouragement and appreciation throughout my entire life.

TABLE OF CONTENTS

LIST OF TABLES

TABLES

LIST OF FIGURES

FIGURES

CHAPTER 1

INTRODUCTION

Wide variety of electronic components are being used in daily life from home appliances to personal computers. In addition, they also have a key importance in the military and aerospace applications such as unmanned aerial vehicles, radars and surveillance. Failure of these systems especially in military and aerospace applications can lead to catastrophic accidents resulting in loss of both life and financial resources. Most of the failures is caused by the degradation or malfunction of the electronic system due to excessive heat flux generation at any level. The increasing demand towards the miniaturization of electronic systems has resulted in a dramatic rise in the amount of heat generated per unit volume, which is comparable in magnitude to those encountered in nuclear reactors or at the surface of the sun. Therefore, development of cooling systems for the electronic components is essential in order to minimize the temperature rise of the components and to improve the reliability and service life.

Cooling systems can be integrated to the electronic components at the chip, board or system level depending on the amount of heat that need to be dissipated. Every level in the hierarchy of thermal management includes different solutions such as use of thermal pastes at the chip level, cold plates at the board level and liquid coolant systems at the package level. However, heat sinks are being used to carry away the heat from the system at each level making the design of the heat sinks significant on the development of thermal management techniques for electronic systems.

Most of the heat sinks used in the engineering products are produced from aluminum alloys due to their good combination of mechanical and physical properties including high specific strength, high wear, corrosion and creep resistance, relatively high

thermal conductivity along with light weight and easy processing. Depending on the required amount of heat dissipation and thermal resistance of the device various production techniques are used to produce aluminum heat sinks. Commercially used heat sinks are generally produced via extrusion, die casting, forging, folding or skiving.

Increase in the generated heat flux due to continuous increase in the complexity of the electronic systems makes the improvement in the efficiency of the heat sinks necessary. In order to meet this requirement more complex shaped heat sinks must be produced for increased area of the heat dissipation. Since it is impossible to produce this complex shapes as monolithic parts using commercial fabrication techniques, bonding of the components is required. Thermal pastes, brazing and welding are generally used as bonding methods for the bonded heat sink production. Although bonded heat sinks offer 200-300% increased efficiency, all of the mentioned bonding techniques have their disadvantages. Pastes generally act as a thermal barrier and decrease the thermal conductivity of the heat sink. Both welding and brazing involve solidification of a liquid phase that may cause defects like porosity, segregation etc. during assembly. Pressure applied during brazing causes the liquid metal to fill the cavities and results in a decrease in the effective cooling area. Therefore, further increase in the efficiency of heat dissipation requires development of a bonding method that can be conducted at low temperatures without the presence of any liquid metal. Solid state diffusion bonding is a promising method for this purpose.

Compared to conventionally used joining techniques diffusion bonding has many advantages. It can be applied on both similar and dissimilar materials without causing any macroscopic deformation. Microstructural defects due to solidification or uncontrolled phase transformations are not associated with the diffusion bonded joints unlike brazing and welding. Furthermore, thermal resistance accompanied by the use of pastes is eliminated, since the properties of the diffusion bonded joints are similar to those of the parent or base materials.

Properties of the diffusion bonded joints are controlled mainly by 3 important process parameters; time, temperature and pressure. Bonding should be carried out at a

temperature range between 0.5-0.8 of the melting point of the processed material. Applied pressure should be kept below the yield strength of the material at the process temperature to prevent plastic deformation during bonding. Holding time should be high enough to form a solid joint. All of the mentioned parameters should be adjusted precisely to obtain a solid bond with high bond strength, without causing any degradation in the microstructural, physical and chemical properties of the base material.

In this method bonding is achieved via atomic diffusion through the initial contact established at the surface asperities of the base materials. In the case of the aluminum and its alloys, the stable native oxide film forms on the surface and inhibits the initial contact making diffusion bonding of aluminum alloys further challenging. Careful surface preparation and use of a protective atmosphere during bonding along with introduction of interlayers or alloying elements were reported in several studies. However, there are no commercially applied processes reported to date for the diffusion bonding of the aluminum alloys.

This master thesis contains five chapters to give information about diffusion bonding behavior of the aluminum 6063 alloy. In Chapter 2, a literature review consisting of several parts has been presented to give a theoretical background about the topics covered in this study. Firstly, necessity of the cooling of the electronics was explained along with the important parts of the cooling systems emphasizing the heat sinks. Then, detailed information about the aluminum (Al) 6063 alloy was given, which is a commonly used alloy in the production of heat exchangers. In the last part of this chapter, an elaborative explanation on diffusion bonding was given focusing on the previous studies on diffusion bonding of the aluminum alloys. Chapter 3 presents the experimental setup and materials used in this study. Experimental parameters and characterization studies including SEM, XRD, DSC analyses as well as mechanical testing has been introduced in this chapter. Results and discussion given in Chapter 4 were again divided into sub-categories for the ease of tracking. In the first part of this chapter, determination of the optimum process parameters for the diffusion bonding

of the Al 6063 alloy was covered. In the next part, effect of variety of interlayer materials applied to the bond interface was presented. In the last part effect of the alloying element addition to this alloys system has been discussed using the data obtained from the diffusion bonding of the cast alloys. Finally, conclusion with the future remarks are presented in Chapter 5.

CHAPTER 2

LITERATURE REVIEW

2.1. Cooling in Electronics Applications

Electronic devices are needed in every part of modern life from toys and home appliances to high performance computers. To increase the service life and reliability of a system its essential to increase the reliability of its electronic components. Failure of most of the electronic components is due to the excessive heat generation during the service, since current flow through the resistors is accompanied by heat generation [1]. As the trend towards highly integrated electronics and simultaneous miniaturization escalates, heat flux generated by the electronic components has increased to the levels comparable to the heat flux generated by a nuclear blast, where the former one occurs at relatively lower temperatures (Figure 2.1).

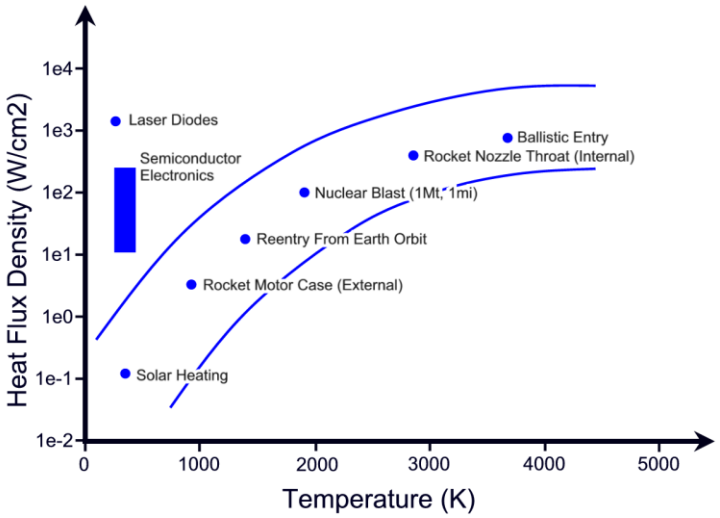

Figure 2. 1. Heat fluxes for various events as a function of temperature [2]**.**

Increase in the heat flux causes an increase in the temperature of the system which results in the loss of the efficiency of the system due to activation of failure mechanisms and degradation of the materials [3]. Furthermore, thermal stresses generated lead to the failure of the solder joints of the components mounted on the circuit board. Therefore, cooling of electronic equipment is crucial to increase the performance and operation life [4].

2.2. Heat Transfer

Cooling of an electronic system requires the operation of several heat transfer mechanisms to transfer the heat from one medium to another. There must be a temperature difference between these media for the heat transfer to occur [5]. Heat always flows from the higher to lower temperature medium following the path that has the lowest thermal resistance for the heat flow. Heat transfer occurs basically in three different mechanisms which are conduction, convection and radiation [1].

Conduction is the transfer of heat energy via molecules, atoms, ions etc. from high temperature medium to low temperature medium. Thermal conductivity of the material, temperature gradient between the two medium and the size and shape of the heat transfer path will determine the rate of heat conduction [6].

When heat is carried away with the aid of a fluid it is called convection. There are two types of convectional heat flow depending on the force that causes the heat transfer. Heat transfer due to the density and temperature gradient between the media is called natural convection, while heat transfer due to an external force is called forced convection [7].

Radiation is the transfer of heat from one body to another via electromagnetic radiation waves [6].

2.3. Thermal Management Techniques

Thermal design and management in electronic devices has a hierarchical order, where all parts of the system should be considered individually. Thermal characterization should begin at the chip level, then thermal management of the board, on which all of these parts are mounted, should be conducted. Final stage of the thermal management is at the system level where all of the circuit boards are brought together inside an enclosed chamber [8].

Thermal management at the chip level includes conduction of heat from the chip to the package surface followed by convection of this heat from the outer surface via heat sinks (Figure 2.2) [2]. For effective cooling materials with low thermal resistance such as adhesives loaded with diamond, silver or particles of other highly conductive materials as well as thermal greases, thermal epoxies and phase changing materials are used to attach the die to the heat spreader, which is also a material with high thermal conductivity, to spread the heat at the outer surface [9]. Heat sinks are attached to the spreader to increase the surface area for heat dissipation. Heat removal through heat sinks occurs via natural or forced convection depending on the heat flux generated by the system. Determination of the coolant fluid in the case of liquid cooling is also dependent on the heat flux that must be removed from the system [10].

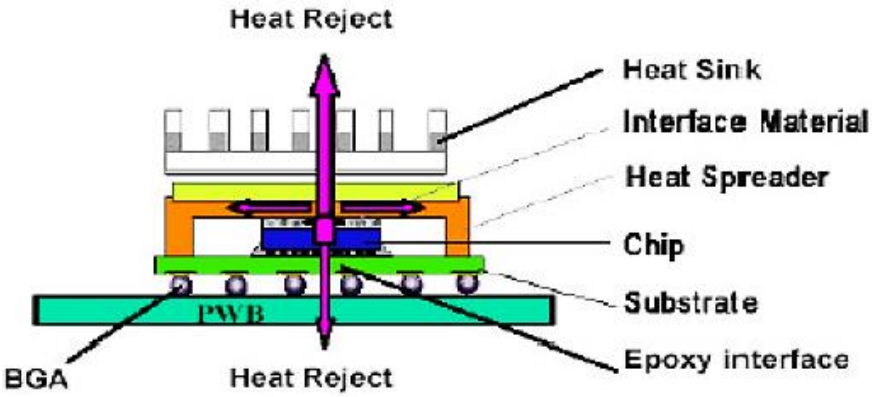

Figure 2. 2. Schematic of thermal packaging [2].

Cooling at the circuit board level is maintained via conduction through printed circuit boards (PCBs) or via natural air convection. For higher heat fluxes heat sinks or cold plates are attached to the back of the PCBs. Cold plates are generally preferred for harsh environments where use of air cooling is limited due to low gravity and air density at high altitudes of operation [2].

System level includes stacking of PCBs inside a rack, chassis or cabinet. At this level cooling can be maintained via natural air convection as shown in Figure 2.3 or via circulation of a fluid through the walls the housing structure. If the system is cooled with the aid of a liquid coolant thermal packaging requires integration of refrigeration systems, heat pipes, heat exchangers and pumps [11].

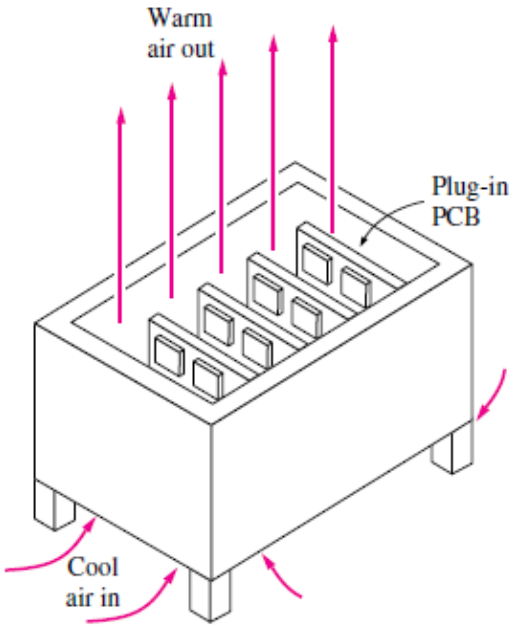

Figure 2. 3. Schematic of an air cooled chassis system [1].

Although there are different solutions at every level in the hierarchy of the thermal management, heat sinks are used to carry away the heat from the system at each level. Thus, design, production and joining of the heat sinks play an important role on the development of thermal management techniques for electronic systems [12].

2.4. Heat Sink Design

Heat sinks are designed depending on several factors including the amount of heat that must be dissipated from the system, maximum allowable junction temperature and thermal resistance of the device. Efficiency of the heat sink depends on the areas of heat dissipation and amount of fluid flow through it [13]. Most commonly used ones are air cooled heat sinks with natural or forced convection [14]. However, with increasing miniaturization and complexity of the systems the heat flux that must be removed increases, where liquid cooled heat sinks are used for such systems [15].

2.4.1. Heat Sink Materials

The most important material property to consider in heat sink material selection is the thermal conductivity of the material. Table 2.1. shows thermal properties of various metallic alloys commonly used in heat sink production [14]. Although there are materials which have higher thermal conductivity values such as silver, diamond and gold, they are not preferred as heat sink materials due to cost concerns [16].

Table 2. 1. Thermal properties of various metallic alloys available for heat sinks[17].

Material type	Thermal expansion coefficient [ppm]	Thermal conductivity [W/mK]	Heat flow kg/m3]
Aluminium	23	204	2710
Copper	17	390	8960
Copper-Molybdenum	7.2	195	-
Copper-Graphite	2	350	-
AlSiC	6.5-8.0	180-210	3000

Aluminum (Al) and its alloys are the most commonly used materials for the production for heat sinks due to their relatively high thermal conductivity, light weight, easy processibility and relatively low cost. Another metallic material that is often used in

heat sinks is copper. Thermal conductivity of copper is two times higher than that of aluminum; however, it is three times heavier than aluminum and processing of copper can be problematic [16].

Radiation characteristics of the heat sink material is another issue to consider during material selection. It is better for heat sink materials to emit infrared radiation. At this point, another advantage of Al alloys as heat sink material is that surfaces of these alloys can be subjected to oxidizing, blacking or anodizing to increase their infrared radiation emission capacity [17].

2.4.2. Heat Sink Production

Various production techniques are used to produce heat sinks from aluminum and its alloys. Commercially heat sinks are produced by extrusion, die casting, forging, folding, skiving or bonding (Figure 2.4).

Extrusion is used to produce profiles for heat sinks. Typically billets of material are placed in an enclosure and extruded through a die to the desired dimension [17]. Generally, an additional machining process is required to attach other components to the extruded part. Thickness of the extruded fins usually changes between 0.6 and 2 mm. Heat sinks produced by this method are used for dissipating heat via natural convection or forced convection of air [18].

Die casting is an another popular technique for the production of heat sinks. Geometrical complexity of the parts are not as limiting as in extrusion, and also by this method dimensional accuracy of the produced parts are higher [19]. Therefore, more efficient heat removal can be obtained due to lower fin thickness and higher heat dissipation area by die casting; however, thermal conductivity of the cast alloys is lower compared to those of the extruded alloys. Solidification defects like porosity and inclusions are the most important drawback of the casting, because they cause scattering and decrease the thermal conductivity. Another issue with die casting is its high initial cost required [17].

Although, forging is not as common as extrusion and die casting, it has several advantages such as superior surface finish, high strength, structural rigidity, close tolerance capabilities, continuity of shape and high uniformity of material [18].

In skiving fins are machined using a special tool. Skiving is applied to produce extremely fine and curved finned heat sinks. It is only preferred when cost is not a limiting factor [14].

Some heat sinks are produced by folding the sheet metal into serpentine fin array. These folded arrays are then bonded to the base of the heat sink [18].

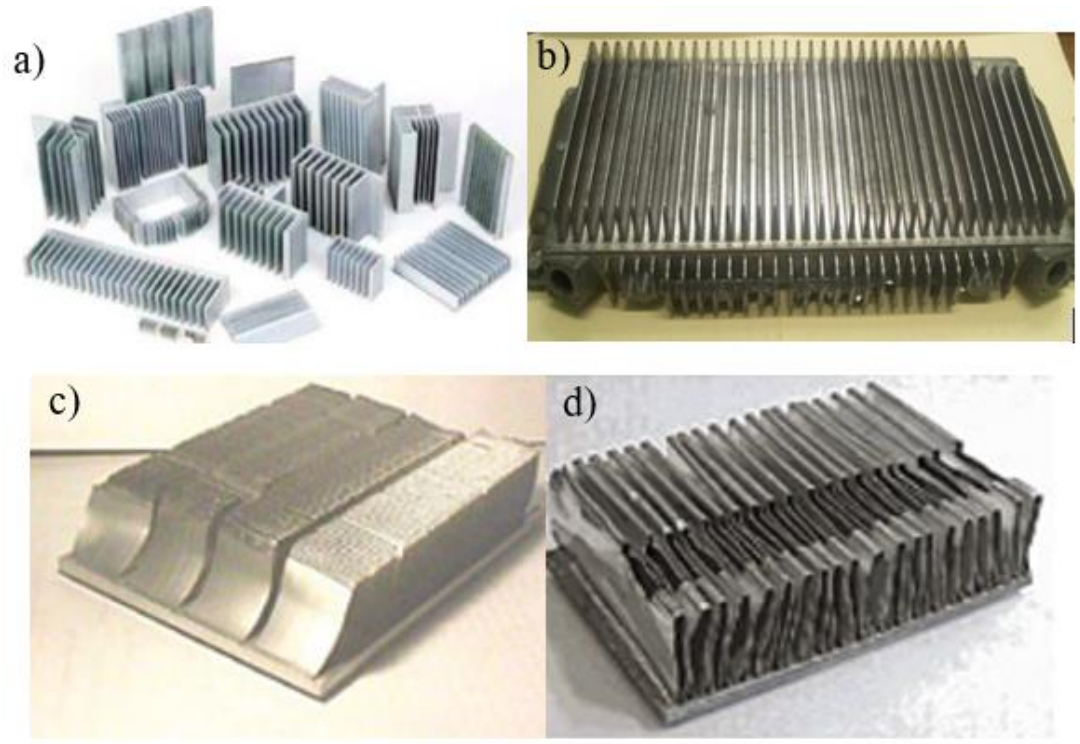

Figure 2. 4. Examples of heat sinks produced by a) extrusion b) die casting c) skiving d) folding [17]–[19].

To improve the efficiency of the heat dissipation the area of the cooling surface should be increased by using structures with relatively complex shapes. To produce such complex shapes assembly of the individual parts are required [14], [20]. Bonding is used to assemble extruded or folded heat sinks on to a base [19].

2.4.3. Bonded Heat Sinks

Bonded heat sinks offer 200-300% increased cooling surface area compared to conventional bulk heat sinks [14]. Epoxy based adhesives, brazing and welding are generally used bonding methods for the heatsink production [17].

Using a bonding agent like epoxy generally acts as a thermal barrier and decreases the thermal conductivity of the heatsink [19]. Brazing has the advantage of low joining temperature which prevents distortion during the bonding. However, both welding and brazing involve solidification of the filler and/or the base material that may cause formation of defects like porosity, segregation etc. during assembly [21]. Presence of pressure during brazing causes the liquid metal to fill the cavities and results in a decrease in the effective cooling area [17].

For increased efficiency a joining method that can be conducted at lower temperatures without the presence of any liquid metal is required. Solid state diffusion bonding is a promising method for the production of heatsinks with high integrity preserving the ‘internally bound’ flow channels running throughout the core of the block. Although, there are some examples of diffusion bonded compact heat exchangers, this method requires further studying to optimize for the production of high efficiency heatsinks [22], [23].

2.5. Diffusion Bonding

2.5.1. Introduction and Its Applications

Diffusion bonding (DB) is a widely used industrial joining technique in which a monolithic joint formation is achieved through solid state diffusion [24]. Diffusion bonded engineering components are in use in variety of fields such as electronics/sensor industry, nuclear industry, aerospace and automotive industry as well as transportation [21].

Properties and microstructures of the joints obtained via diffusion bonding are similar to those of parent materials (Figure 2.5). Therefore, there are no limitations in service conditions of the diffusion bonded joints where no filler materials and their solidification are required as in the case of brazing and welding, which are associated with typical microstructural defects [25].

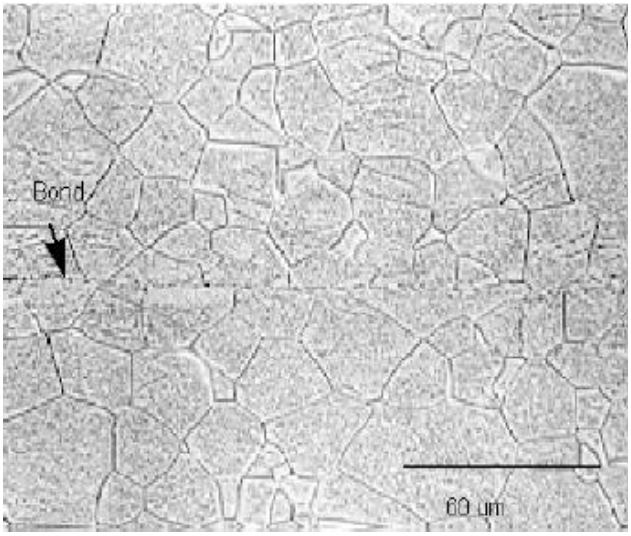

Figure 2. 5. Microstructure of a diffusion bonded joint [26].

Along with metals and ceramics, diffusion bonding is also a viable joining method for heat-sensitive materials, for materials with a tenacious oxide layer and for composites which are difficult to be joined by other processes [27]. Both similar and dissimilar

materials can be joined using DB with or without the use of an interlayer in between. Quality of the bond is determined depending on the chemical composition, microstructure and mechanical properties of the interface [28].

Unlike other joining methods no macroscopic deformations or uncontrolled phase transformations occur during diffusion bonding [29]. DB is a near net shaping process, that is to say no additional machining or forming operation is required for the bonded components [30]. Structural inhomogeneity associated with the temperature gradient is also minimized for diffusion bonded joints. Therefore, diffusion bonding is a cost effective method for the production of parts with minimum dimensional tolerances [30].

2.5.2. The Mechanism of Bond Formation Solid State Diffusion Bonding

In diffusion bonding joint formation is achieved by bringing two prepared surfaces together under pressure at elevated temperatures [31]. There are several hypotheses to explain the joint formation mechanism in DB. First one is the 'Film Hypothesis,' and it suggests that the difference in joinability of different materials is explained by the difference in their surface film characteristics. All metals can form a solid bond if stable surface oxide films can be ruptured and contact between two pristine surfaces can be established. On the other hand, according to the 'Recrystallization Hypothesis' when materials are subjected to high temperatures, deformation and strain hardening of the faying surfaces cause atoms to move between the two parent materials and bond formation is established. There is an energy threshold of the atoms for adhesion according to 'Energy Theory,' where heat and deformation increases the energy of the atom rendering the interface between the two pieces disappear. In the 'Dislocation Hypothesis' plastic deformation imposed during joining causes dislocations to move to the free surface rupturing the oxide film and producing steps on atomic scale which enhance the joint formation. 'Electron Hypothesis' claims that a stable electron configuration is formed at the interface as a result of metallic bond formation. The final and most widely accepted one is the 'Diffusion Hypothesis'. According to this

hypothesis due to the difference between the energy levels of the surface and bulk atoms interatomic diffusion of atoms into the bulk is responsible for the bond formation [32].

The mechanism of bond formation during solid state diffusion bonding can be summarized in three stages as illustrated in Figure 2.6. Asperities are formed at the surfaces to be joined during preparation prior to bonding. During the first stage of DB initial contact between these asperities is established and this contact area grows by yielding of the asperities and by creep deformation. Local disruption of the surface film enables metal to metal contact. At the end of this stage, a large volume of voids remains between localized bonded regions [33].

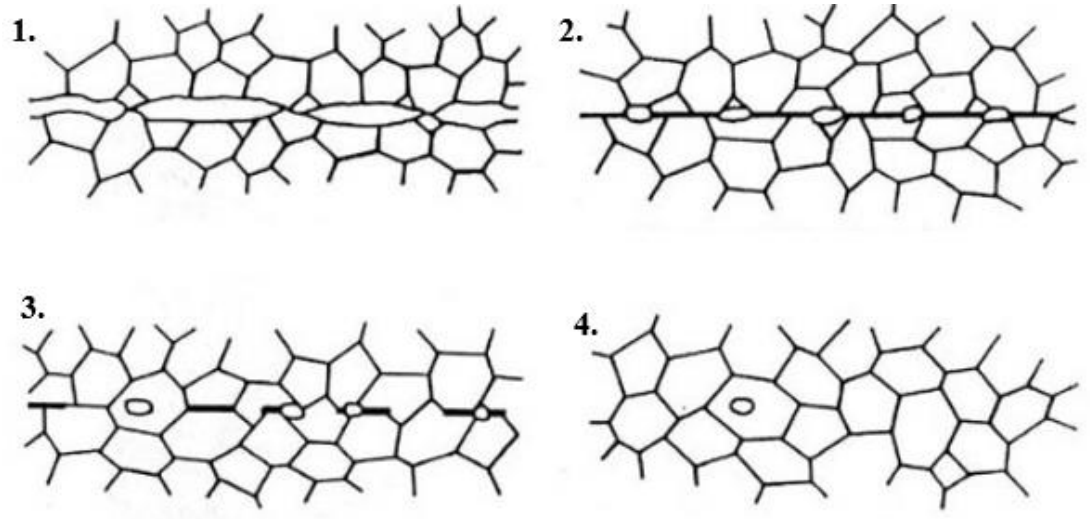

Figure 2. 6. Schematic illustration of stages of diffusion bonding [34].

In the second stage, void shrinkage occurs through grain boundary diffusion and metallic bond formation. During the last stage, remaining voids are eliminated via volume diffusion of atoms followed by recrystallization and grain growth [26].

2.5.3. Bonding Parameters

Quality of the diffusion bonded joints mainly depends on the parameters such as pressure, temperature, holding time and surface condition applied during the bonding process. These properties should be adjusted precisely to control the microstructure to obtain the desired properties [35]. Bonding temperature should be ~0.5-0.8 of the melting point (T_m) of the processed materials, and applied pressure should be below the yield strength of the material at the process temperature to prevent macroscopic deformation during the bonding process [36]. Holding time should be long enough to form a solid joint without causing any degradation in physical and chemical properties of the base material [32], [37].

2.5.3.1. Surface Preparation

Morphology and physical state of the surfaces play an important role on the joint quality, since bond formation directly depends on the contact between the mating surfaces [21]. Surface morphology is dependent on the production method (machining, milling, grinding etc.) and the surface finish applied. Macroscopic asperities on the surface is referred as waviness while microscopic ones are referred as roughness [32]. To ensure initial contact waviness of the surface should be minimum which can be achieved by improving the surface finish of the materials (Figure 2.7)

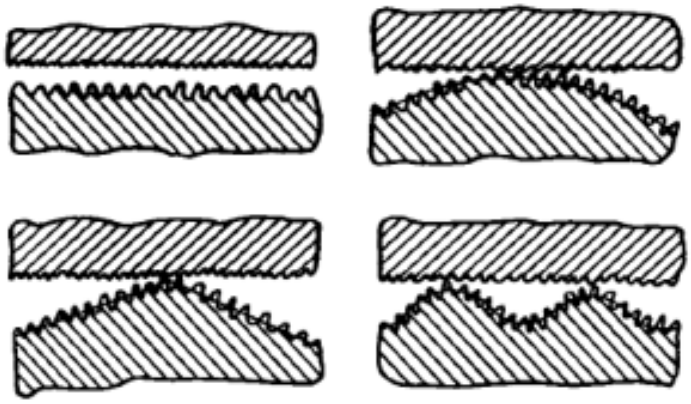

Figure 2. 7. Contact between wavy surfaces after machining [32].

Several studies have been conducted to understand the effect of surface geometry on the bond strength where it has been concluded that for effective diffusion bonding different surface geometries are required for materials with or without surface oxide films [38]. Higher bond strengths are obtained when smoother surfaces are brought together for oxide free materials due to an increase in the contact area [32]. In the case of materials with stable surface oxide films, increase in the roughness of the mating surfaces leads to an increase in the bond strength due to an increase in the local disruption in the oxide film [31].

Tensi et. al. studied the diffusion bonding of Al 7475 sheets with different surface finishes [39]. Figure 2.8 shows that coating the initial surface with copper yields an insufficient bond strength. Bond strengths are higher for the surfaces prepared by grinding and brushing due to disruption of the surface oxide film and establishment of metal to metal contact. Obtained bond strengths are higher for brushed surfaces compared to ground surfaces, since brushing results in a higher roughness values leading to an increase in local deformations. The highest peel strength is obtained for the specimens prepared under argon atmosphere, as fracture of oxide film under a protective atmosphere promotes the diffusion bond formation.

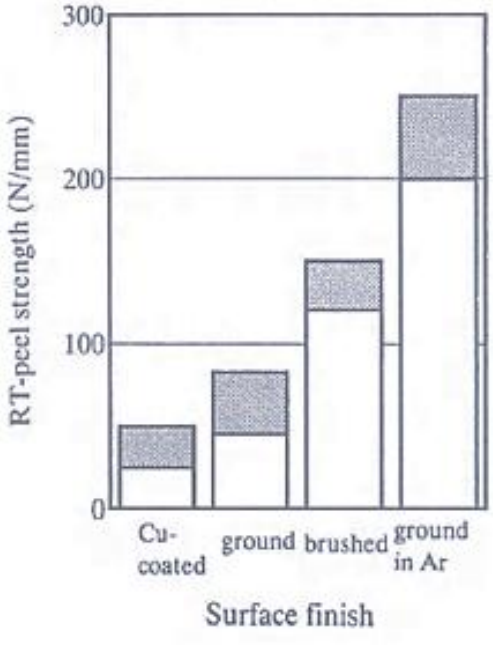

Figure 2. 8. Effect of surface finish on the peel strength of diffusion bonded Al 7475 sheets at room temperature [39].

These results are also in agreement with the study conducted by Zuruzi et. al., in which tensile properties of diffusion bonded Al 6061 alloy joints prepared using coarse and fine grinding papers were investigated [40]. The results revealed that the specimens ground with 180 grit SiC paper yielded bonds with higher integrity compared to the specimens ground with 1000 grit SiC paper (Figure 2.9).

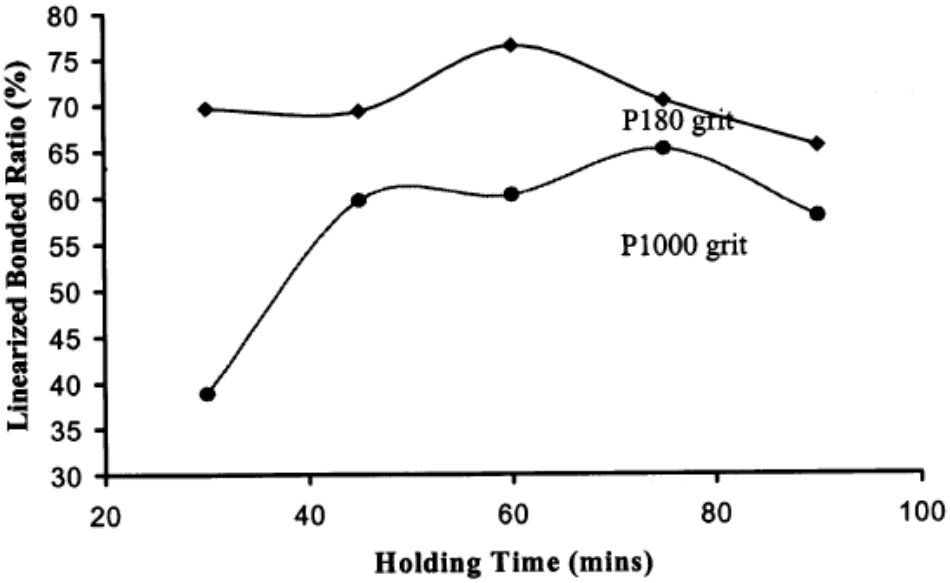

Figure 2. 9. Change in linearized bonded ratio, which is proportional to the bond strength, as a function of holding time for two different grinding conditions [40].

Cleaning of the surfaces also plays an important role on the property of the diffusion bonded joints. All surfaces are covered with layers of oxide films strongly bonded to surface as well as adsorbed layers of water and gases or layers of grease or oil. Rubbing the surfaces with alcohol or acetone or pickling with acids or alkalis are commonly used methods to remove these adsorbed layers. Although all of the above-mentioned methods were proven to be successful for the removal of the adsorbed surface layers, hence, the formation of effective joints to a certain extent, usage of chemical treatments involving acids and alkalis was shown to result in joints with the highest integrity [21], [30], [32].

2.5.3.2. Bonding Pressure

Pressure is required to deform the surface asperities at the first stage of the bonding process. Increase in the bonding pressure would lead to an increase in the deformation of these asperities leading to an increase in the contact area. Hence, integrity of the

bonds is expected to increase with increasing bonding pressure. However, applicable pressure is limited to the yield strength of the parent material at bonding temperature.

Bond strengths for several materials as a function of bonding pressure are shown in Figure 2.10 [32]. It is seen that increase in the pressure up to a certain value leads to an increase in the bond strength up to a threshold for all of the tested materials, where further increase in that value has almost no effect on the bond strength of the joints.

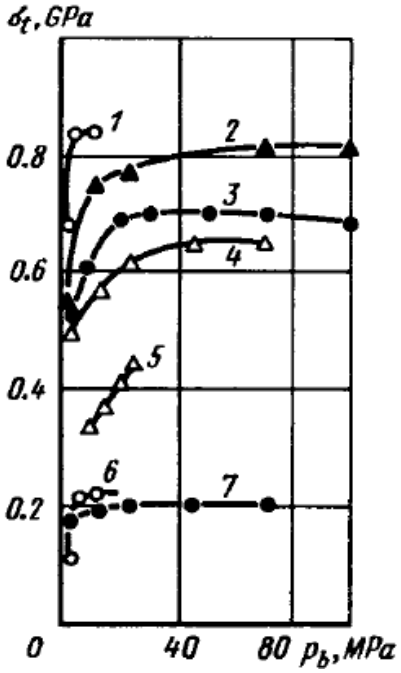

Figure 2. 10. Joint strength as a function of bonding pressure for 1) BT5-1 titanium alloy, 2) 45X14H14B2M alloy, 3) AISI 1050 steel (T = 1273 K), 4) AISI 1050 steel (T = 1173 K), 5) Kovar, 6) MB copper and 7) CM 18-36 cast iron [32].

Figure 2.11 shows the change in the bond strength for an Al 7075 alloy with the applied bonding pressure. These findings are also in agreement with the previous ones. At 500^{o}C bond formation starts under 2.5 MPa of pressure, and 20% increase in the specific bond strength is observed when pressure is increased to 4 MPa. Increasing pressure further does not have a significant effect on the bond formation and becomes less effective at higher temperatures. Therefore, it can be concluded that there is an

upper and a lower limit for the bonding pressure, and these limits are highly dependent on bonding temperature. Yield strength of the materials diminishes as the temperature increases along with both upper and lower limits of the bonding pressure [41].

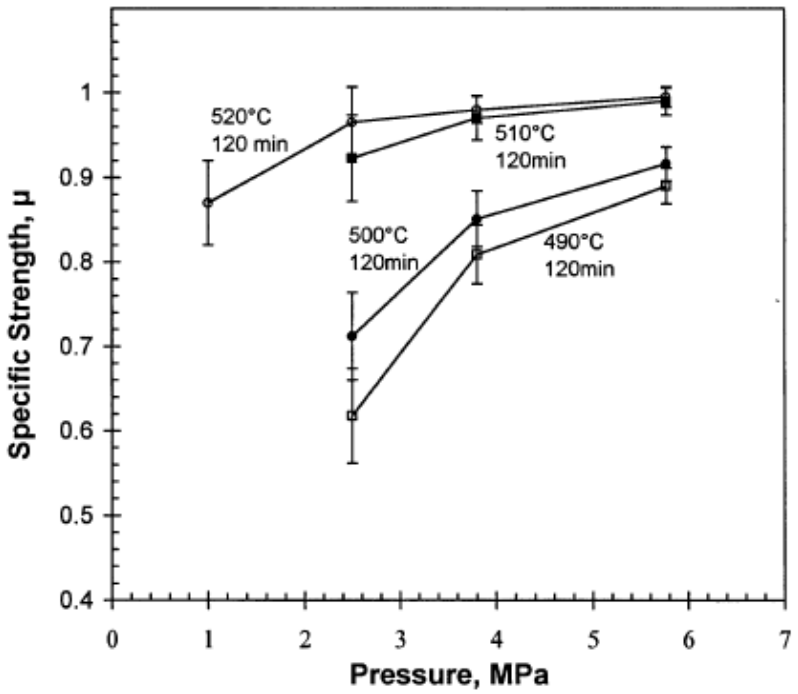

Figure 2. 11. The effect of bonding pressure on the specific bond strength of Al 7075 alloy [41].

2.5.3.3. Bonding Temperature

Proper selection of the bonding temperature is one of the most important issues in controlling the properties of the base metals and diffusion bonded joints. Bond formation occurs via grain boundary diffusion and self-diffusion after initial contact between two surfaces has been established [42]. Elevating temperature increases the diffusion rate due to an increase in the atomic mobility. In other words, increasing bonding temperature should enhance the bond formation. However, there is a limiting temperature for DB to preserve the mechanical properties of the base metal. Excessive

increase in the temperature is accompanied by rapid grain growth leading to loss in the strength of the base materials. Another reason why bonding temperature should be kept as low as possible is the decrease in the yield strength at elevated temperatures. Applied bonding pressures may cause gross plastic deformations at higher temperatures [32].

The study on diffusion bonding behavior of Al 7075 alloy conducted by Huang et.al. also proves that integrity of the bond increases with bonding temperature up to a limiting value. Further increase in temperature does not contribute to the improvement of the bond strength, on the contrary, it causes degradation of the material properties due to grain growth (Figure 2.12) [41].

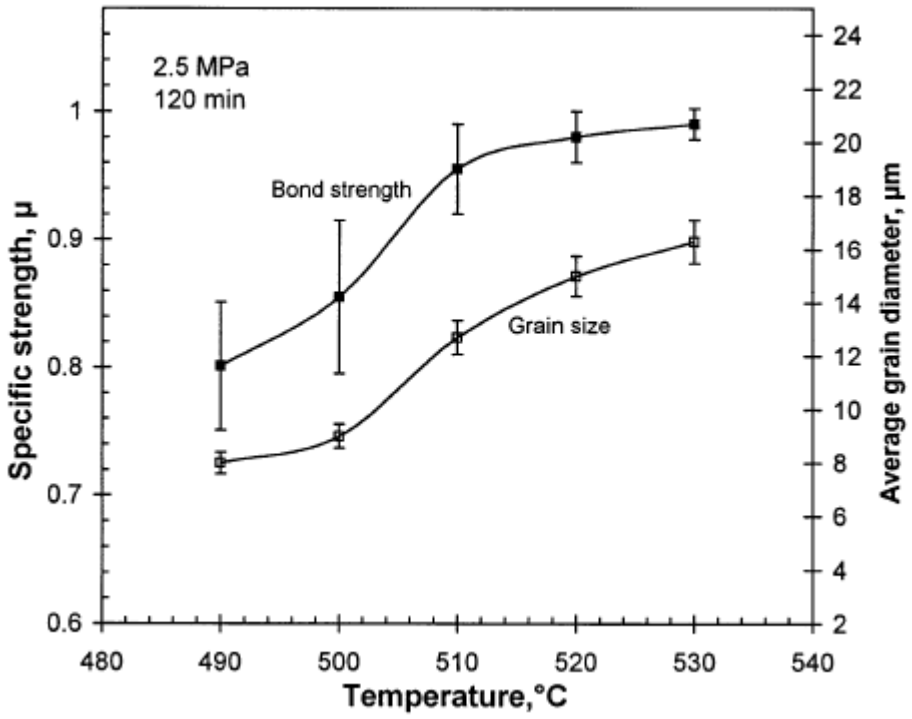

Figure 2. 12. Effect of bonding temperature on bond strength and grain size of diffusion bonded Al 7075 alloy [41].

2.5.3.4. Bonding Time

During the second and third stages of the DB void closure and a solid bond formation occurs. Time is required for atomic diffusion during these stages. Required time changes depending on the bonding temperature and pressure applied. Closure of the voids is followed by recrystallization and grain growth. That is to say there is an optimum time for bonding, and exceeding this time only results in degradation of the properties of the base materials [32].

Li et. al. studied the size and geometry of the voids at the bond interface of a Ti-17 alloy. Results shown in Figure 2.13. reveals that the main mechanism for bond formation is the void closure which appears to occur at the very beginning of the bonding process. Although amount of voids continues to decrease with further increase in time, bond strength exhibits a slight increase [43].

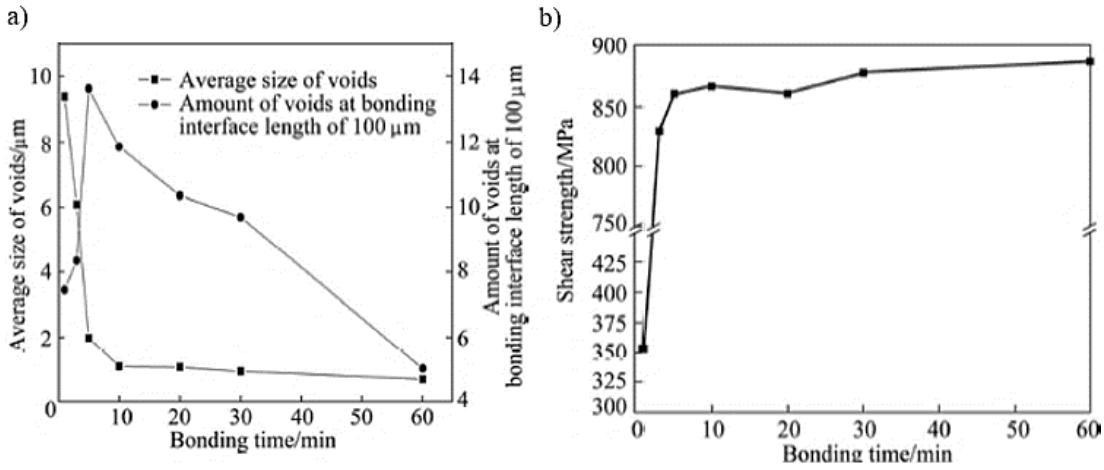

Figure 2. 13. Variation of a) average size and amount of voids, b) shear strength of the joints with time in Ti-17 alloy [43].

2.6. Introduction to Aluminum and Its Applications

Aluminum (Al) and its alloys have widespread applications in variety of engineering applications in manufacturing, aerospace and automotive industry due to their good combination of mechanical and physical properties including high specific strength, high wear, corrosion and creep resistance along with controlled thermal expansion coefficient [44]. The shiny finished surface of Al alloys makes them available for decorative applications, and since Al is non-toxic, they can be used in contact with the foods [45]. One of the most important physical properties of aluminum alloys is their high specific strength (ρ=2.7 g/cm^3) which makes these alloys a promising candidate for construction of strong lightweight structural parts like cylinders and pistons as well as machine parts and spacecraft and automotive components [46].

Aluminum alloys can resist corrosion by salt water and other environmental factors and by a wide range of other chemical agents when properly alloyed and heat treated. Thus, they are also suitable for the production of structural parts to work in corrosive environments like pressure vessels, tanks, chemical equipment containers, medical equipment and marine components [47], [48].

Solid solution strengthened Al alloys maintain their physical and mechanical properties at elevated temperatures, while they also maintain their toughness at cryogenic temperatures. Therefore, they can be used in a wide range of service temperatures [49].

Al alloys are known to be excellent conductors of heat and electricity. Electrical conductivity of the aluminum is twice that of the copper's, and thermal conductivity of Al can be reach to 60% that of the copper's when measured through identical cross-sectional area. Consequently, Al alloys are advantageous for applications such as heat exchangers, electrically heated appliances, radiators, evaporators and automotive cylinder heads [50].

Excellent formability and machinability are the two most important characteristics of Al alloys in terms of their widespread applicability and availability. Complex shaped

parts can be produced in various sizes. Variety of methods including welding, brazing, soldering and abrasive bonding are available to join the produced aluminum parts [46].

2.7. Aluminum Alloys

Aluminum alloys are divided mainly into two categories as cast compositions and wrought compositions. A more detailed categorization can be made according to the strengthening mechanism of the alloys as work hardening alloys and age hardening alloys [50]. Figure 2.14 shows the principle alloy categories.

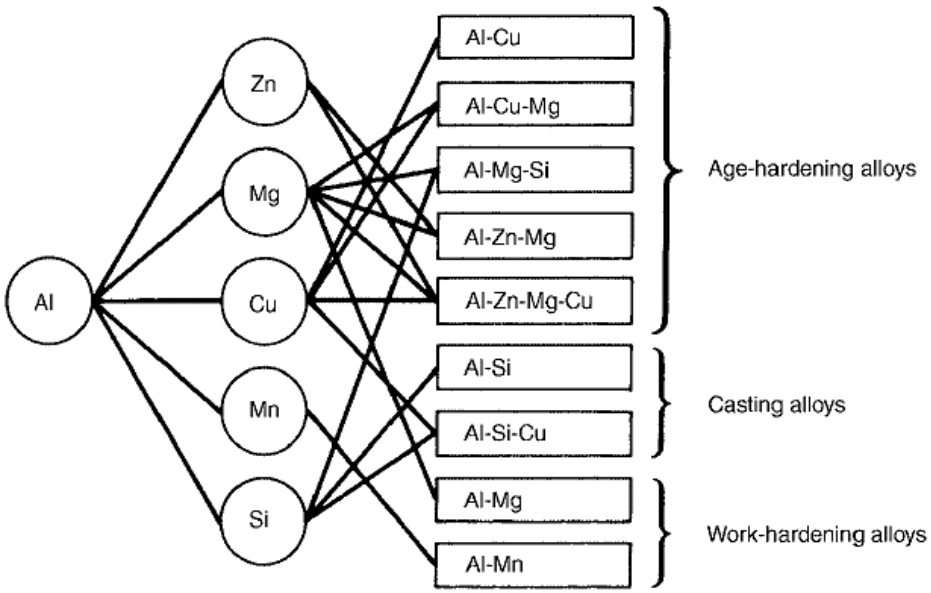

Figure 2. 14. Categories of principal aluminum alloys [46].

2.7.1. Wrought Alloys

Wrought alloys are divided into 8 categories according to the major alloying element in the alloy [50]. The major alloying elements and strengthening mechanism of the wrought alloys are summarized in Table 2.2.

Table 2. 2. Classification of Wrought Al Alloys.

Alloy Group	Principle Alloying Element	Strengthening Method
1xxx	Al	Cold Work
2xxx	Al-Cu	Heat Treatment
3xxx	Al-Mn	Cold Work
4xxx	Al-Si	Cold Work
5xxx	Al-Mg	Cold Work
6xxx	Al-Mg-Si	Heat Treatment
7xxx	Al-Zn	Heat Treatment
8xxx	Al-Li	Heat Treatment

2.7. 2. Cast Alloys

There is no single designation system for the cast Al alloys. The most widely used system for cast alloys is the three-digit Aluminum Association (AA) system. There are both heat treatable and non-heat treatable compositions of the cast Al alloys. Non-heat treatable alloys are used in as-cast condition [50]. Classification of the cast Al alloys are summarized in Table 2.3.

Table 2. 3. Classification of the Cast Al Alloys.

Alloy Group	Principle Alloying Element
1xx	Al
2xx	Al- Cu
3xx	Al-Si-Mg, Al-Si-Cu, Al-Si-Cu-Mg
4xx	Al-Si
5xx	Al-Mg
7xx	Al-Zn
8xx	Al-Sn

2.8. 6xxx Series Wrought Aluminum Alloys

Wrought Al-Mg-Si containing alloys are known as 6xxx series Al alloys. These alloys are heat treatable, moderate strength Al alloys. Mg is added to the Al-Si alloys to favor Mg_2Si precipitate formation; hence, to utilize precipitation hardening of the alloys [51]. 6xxx series Al alloys are strengthened via solutionizing, quenching and artificial aging following the phase regions in the Al-Mg_2Si phase diagram (Fig.2.15) [52]. The precipitation sequence of the Al-Mg-Si alloys after quenching can be described as follows: supersaturated solid solution - Mg-/Si- (co-) clusters - GP zones - β″ - β′ - Mg_2Si [53]. Formation of Fe_3SiAl_{12} and $Fe_2Si_2Al_9$ intermetallic compounds is also observed depending on the Al, Si and Fe content of the alloy [50].

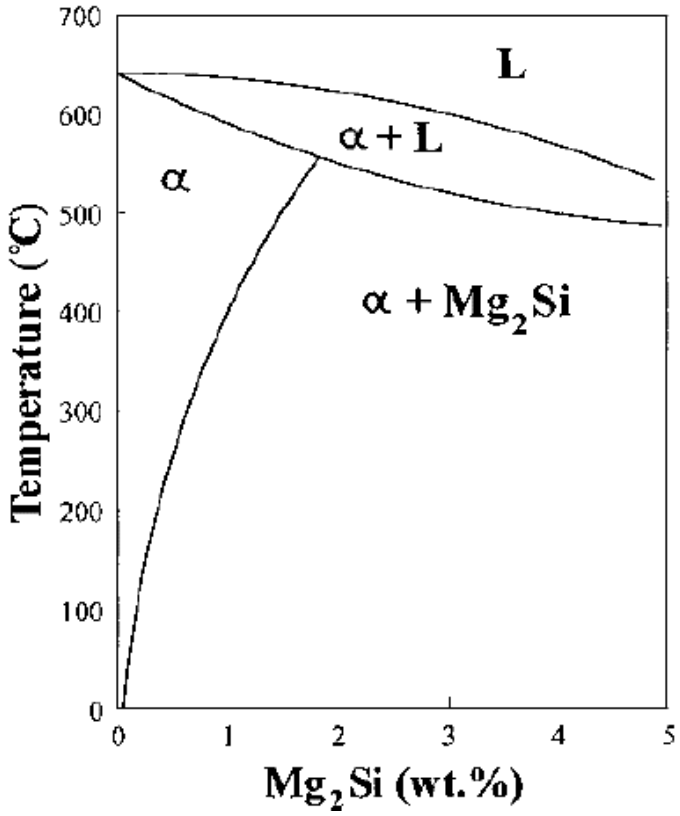

Figure 2. 15. Al- Mg_2Si phase diagram [52].

6xxx series alloys can be divided into three groups depending on the Mg and Si content. Various application areas of these alloys are summarized in Figure 2.16 [46]. Typical example of the first group is 6063 alloy in which total amount of magnesium and silicon does not exceed 1.5 wt%, and both elements are in nearly balanced ratio [52]. In the second group, the amount of magnesium and silicon is 1.5 wt% or more and other alloying elements such as 0.3 wt% Cu to provide additional strength during aging treatment and as manganese, chromium and zirconium to control the grain structure are used. Structural 6061 alloy is the one of the examples of this group [46]. The amount of Mg_2Si phase in the third group is overlapping with the first two with excess silicon in the structure. Excess Si increases the strength of an alloy up to 0.2 wt% Si; however, higher amounts of excess silicon are not beneficial due to segregation of silicon to the grain boundaries resulting in grain-boundary fracture. Common examples of this group are 6009, 6010, and 6351 type Al alloys [52].

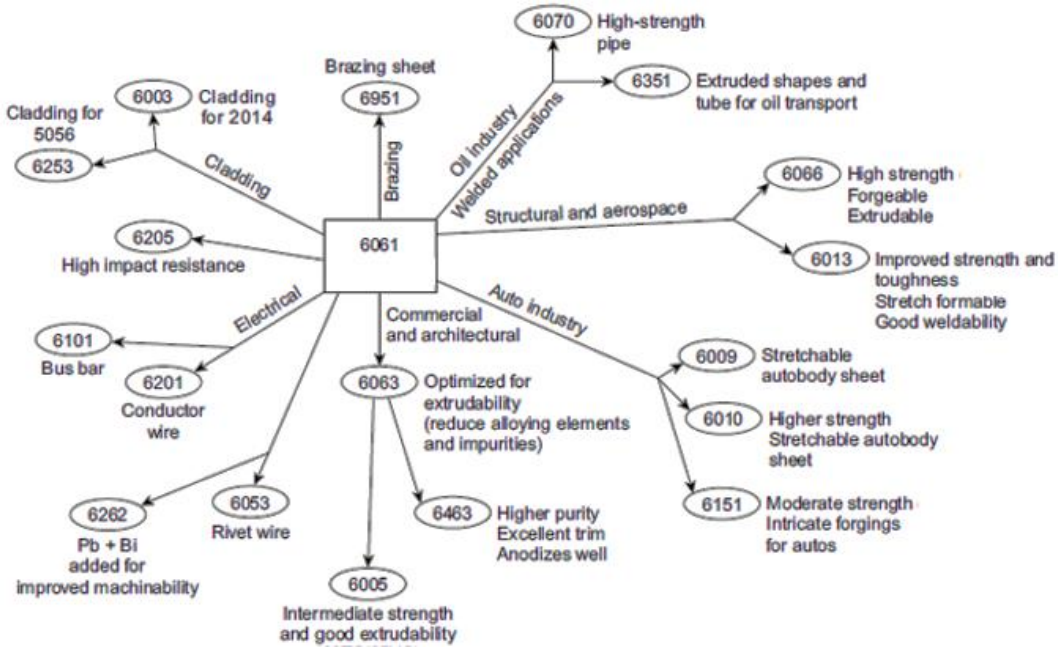

Figure 2. 16. Commonly used Al-Mg-Si alloys and their application [46].

2.9. Al 6063 Alloy

6063 is one of the most widely used alloys among 6xxx series Al alloys. Chemical composition limit of the alloy is given in Table 2.4 [54]. It is a medium strength aluminum alloy available in various shapes such as bar, rod, wire and tube. This alloy is widely used in architectural applications, extrusions, window frames, irrigation tubing along with hydro formed tubes for chassis and heatsinks [55].

Table 2. 4. Chemical composition limits of Al 6063.

Component	**Wt. %**	**Component**	**Wt. %**	**Component**	**Wt. %**
Al	Max 97.5	Mg	0.45 - 0.9	Si	0.2 - 0.6
Cr	Max 0.1	Mn	Max 0.1	Ti	Max 0.1
Cu	Max 0.1	Zn	Max 0.1	Fe	Max 0.35
Other, each	Max 0.05	Other, total	Max 0.15		

2.9.1. Physical Properties

Physical properties of the Al 6063 Alloy is shown in the Table 2.5 [56]. Density and melting point of this alloy is close to the that of pure Al. It is frequently used to produce parts which work at high temperatures like heatsinks due to its relatively low thermal expansion coefficient and high thermal conductivity.

Table 2. 5. General physical properties of Al 6063 alloy.

Property	**Value**
Density	2.70 g/cm³
Melting Point	655 °C
Thermal Expansion	23.5 x10-6 /K
Thermal Conductivity	201 W/m.K
Electrical Conductivity	52 % IACS
Electrical Resistivity	0.033 x10-6 Ω .m
Modulus of Elasticity	69.5 GPa

Al 6063 is highly resistant to all types of corrosion and stress corrosion cracking. It has a good formability and machinability. Thus, complex parts can be easily produced and machined using this alloy. Weldability and brazability of the alloy are also excellent for all commercial processes [54].

2.9.2. Mechanical Properties

Mechanical properties of the Al 6063 alloy depend on the heat treatment applied. Most commonly used heat treatments for this alloy and their designations are as follows:

O- Annealed

T1- Cooled from an elevated temperature shaping process and naturally aged to a stable condition

T4- Solution heat treated and substantially aged to a stable condition

T5- Cooled from an elevated temperature shaping process and artificially aged

T6- Solution heat treated and artificially aged.

Change in the mechanical properties with respect to applied heat treatment process is summarized in Table 2.5 [54]. As seen in the table, the alloy is softest in the annealed condition and gains moderate strength when cooled from an elevated temperature shaping process without any additional heat treatment. Highest strength and hardness is obtained with T6 treatment at the expense of ductility.

Table 2. 6. Typical mechanical properties of Al 6063 for varying heat treatments.

Temper	σ_{UTS} (MPa)	σ_y (MPa)	Elongation %	Hardness (HB)	τ (MPa)
O	90	48	-	25	69
T1	152	90	20	42	97
T4	172	90	22	-	-
T5	186	145	12	60	117
T6	241	214	12	73	152

2.9.3. Precipitation Process

To obtain desired properties above-mentioned heat treatments are applied to the Al 6063. Change in the properties are obtained via precipitation of Mg2Si phase. Precipitation behavior of Al-Mg-Si alloy system has been studied extensively, and the precipitation sequence is simplified as supersaturated solid solution - Mg-/Si- (co) clusters - GP zones - β″ - β′ - β(Mg_2Si) [57], [58]. However, it should be noted that this sequence is not valid for all temperatures and cooling rates [59]. Some of the phases might not form or some of them might coexist in the same temperature range depending on cooling rate and possible presence of additional alloying elements [60].

6063 alloys generally aged at around 170 °C, and formation of three distinct types of precipitates are observed [38]. First stage of precipitation involves formation of Mg and Si clusters. The excess Si present in the system enhances the precipitation process by reducing the solubility of Mg_2Si, and semi-coherent GP zones starts to precipitate from co-clusters of Mg and Si [61]. It is stated that after pre-precipitation reactions monoclinic β″ phase forms without dissolution of the GP zones [59]. After that rod like β′ precipitates form prior to equilibrium precipitates with a different crystal structure. Finally, coherent plate like β(Mg_2Si) with FCC crystal structure forms [62]. The alloy gains its strength by the formation of GP zones and β″ - β′ precipitates, as the equilibrium precipitate has little contribution on the strength of the alloy [63].

Three distinct temperature ranges of precipitation is determined by Milkereit et. al.; first one is from 450 to 430 °C, the second is from 430 to 300 °C and the third is from 300 to 250 °C. It has been found out that the high temperature reaction is the precipitation of β-Mg_2Si, intermediate temperature reaction is the precipitation of β′ phase and low temperature reaction belongs to the β″ precipitation [53].

According to the study conducted by Doan et.al there are six exothermic and two endothermic reactions observed during aging of an Al-Mg-Si alloy with a constant heating rate of 10 $K.min^{-1}$ (Figure 2.17) [62]. The low temperature exothermic peaks indicate the formation of individual or co-clustering of Mg and Si, and low temperature endothermic peaks indicate dissolution of these clusters. The exothermic peaks denoted as E and G are due to the formation of β″ and β′ precipitates, respectively.

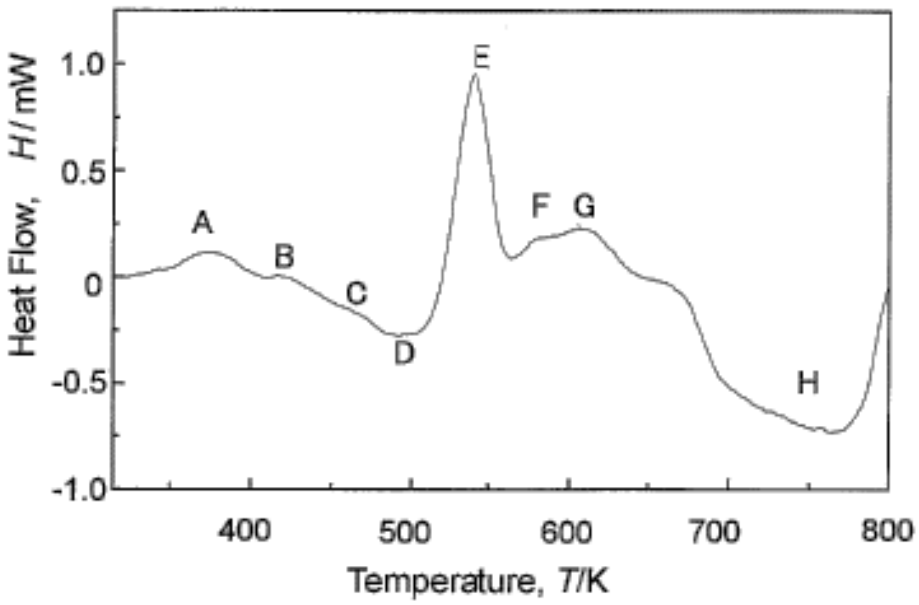

Figure 2. 17. Typical DSC thermogram of an Al-Mg-Si alloy at a constant heating rate of 10$K.min^{-1}$ [62].

2.9.4. Control of Grain Size

Control of grain size is essential to control the mechanical properties of the aluminum alloys. Generally fine, equiaxed grains are required for improved properties like higher strength and better corrosion resistance [52].

These microstructural features can be maintained for all aluminum alloys with the use of grain refiner additions during casting [64]. Master alloys of Al-Ti-Br system are the most widely used grain refiners. TiB_2, AlB_2 and $(Ti-Al)B_2$ particles are formed with the addition of these grain refiners, and formed particles act as a nucleation sites for α-Al. Addition of other alloying elements further increase the solute content, hence, segregation in the alloy [65]. Segregated elements restrict the growth of the solid/liquid interface during solidification leading to the formation of small, equiaxed grains [66]. Although grain refinement efficiency depends both on the segregation ability of the solute atoms and the amount of the nucleating particles, it is found out that addition of solutes decreases the grain size drastically [66].

Grain growth is also observed during high temperature processing of aluminum alloys. Thus, loss in the strength of the alloys has been observed after high temperature processing. Preventing rapid heating of the alloy to the processing temperature is a solution for this. In the case of joining of the alloys minimizing the time that the alloy is being held at elevated temperatures should be minimized [52].

2.9.5. Effect of Cu Alloying

Cu alloying is used to increase the strength and hardness of the aluminum alloys both at ambient and elevated temperatures [51]. When Cu is added to the Al-Mg-Si system, an intermetallic compound forms during solidification either as blocky $CuAl_2$ or as alternating lamellae of α-Al and $CuAl_2$ (Figure 2.18) [67]. Blocky $CuAl_2$ phase is hard to dissolve during solution heat treatment before aging.

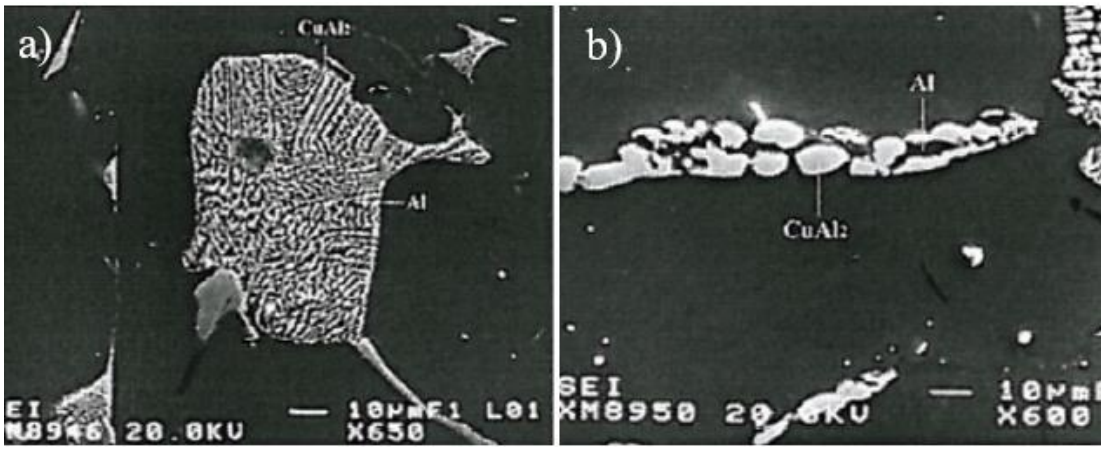

Figure 2. 18. a) Eutectic $CuAl_2$ and b) blocky $CuAl_2$ in as cast Al-Mg-Si-Cu alloy [68].

Cecares et.al. proved that increasing the Cu and Mg content increases the strength and hardness of the Al-Mg-Si alloy [69]. Strengthening effect of Cu in these alloys depends directly on the Mg:Cu ratio in the alloy. For lower values of precipitation S($CuMgAl_2$) phase is observed, while θ($CuAl_2$) precipitates form at higher values [70]. Mg_2Si or Q($Al_4CuMg_5Si_4$) precipitates are also observed for some compositions, yet they do not have much contribution on the strength of the alloy [50].

The precipitation sequence for S precipitates is found as α_{sss}- GPB zones-S″-S′-S($CuMgAl_2$) [71], where SSS stands for the supersaturated solid solution, and GPB are the Guiner-Preston-Bagaryatsky zones. Precipitation of the θ phase follows the sequence of α_{sss}- GP zones- θ″- θ′- θ($CuAl_2$) [70].

All of these precipitates may be formed during casting and aging of the alloy. It has been shown that Si containing phases only form upon artificial aging where hardening is achieved by presence of the GP and GPB zones [72].

2.9.6. Effect of Sn Alloying

Tin (Sn) alloying is commonly used in aluminum alloys to improve the antifriction characteristics [51]. Although there has been little work on the Sn addition to the Al-

Mg-Si alloy system, conducted studies proved that Sn alloying reduces the hardness and yield strength of the alloy and increases its elongation, while it does not have a significant effect on its UTS value [49]. When Sn is present in the alloy, formation of liquid phase at low temperatures is also expected. According to the Mg-Sn phase diagram in Figure 2.19 a eutectic reaction occurs between Mg_2Sn and (Sn) phases at 203˚C.

Grebenkin et. al. studied the effect of Sn alloying on the solidification characteristics of Al-Mg-Si alloys and determined that formation of (Sn) phase and Mg_2Sn intermetallic compound during solidification. Mg_2Sn and Mg_2Si has similar cubic crystal structures and similar heats of formations. Therefore, when Sn is present in the alloy, it replaces Si in Mg_2Si and increases the amount of free Si [73]. Unlike Mg_2Si, Mg_2Sn forms during solidification, and it is present in as-quenched condition before aging [74]. As a result, Sn may reduce the hardness of the alloy by preventing the Mg_2Si precipitation.

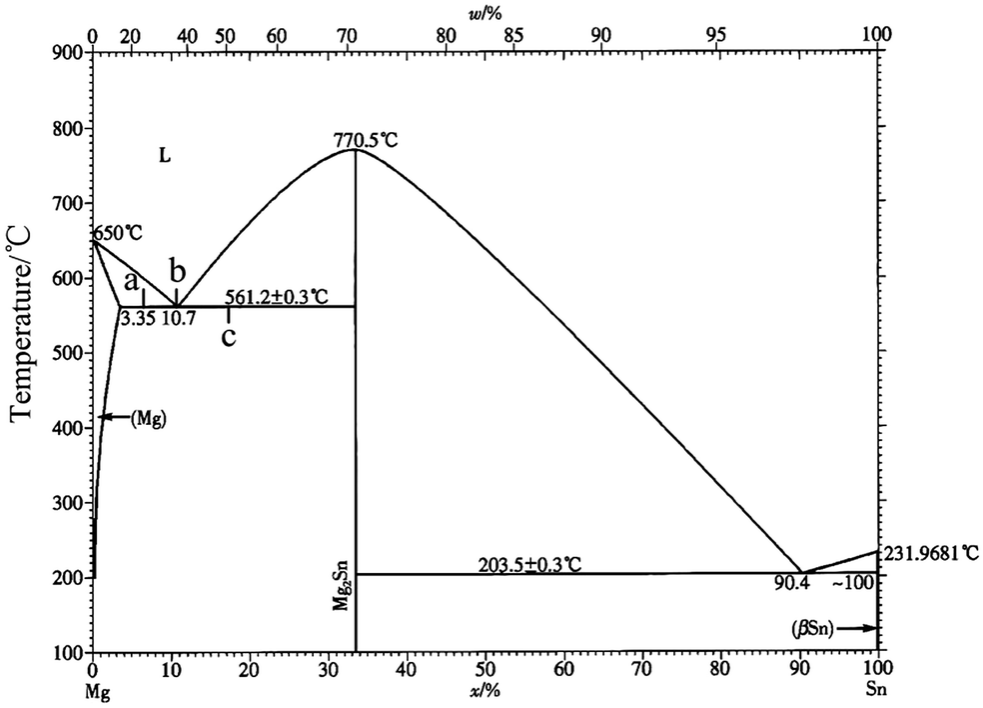

Figure 2. 19. Magnesium-Tin phase diagram[75].

2.10. Joining of Aluminum Alloys

Joining methods used to produce aluminum structural parts can be classified as liquid phase and solid state joining methods. The former (fusion welding, brazing) involves the formation followed by the solidification of a liquid phase at the bond interface, while in the latter case (friction stir welding, solid state diffusion bonding) the applied pressure has a key role in joint formation [38].

Fusion welding of aluminum and its alloys is used to produce variety of engineering products such as frames, pressure vessels, automotive components etc. [76]. Brazing is used for the production and repair of aluminum heat exchangers as well as aerospace and automotive components [77]. Bonding is achieved via melting and solidification of a filler material for both fusion welding and brazing, where the base metal does not melt in brazing unlike fusion welding. Presence of a different material at the interface for both methods generally reduces the thermal conductivity and affects the mechanical properties of the base metal. Both methods are also limited by the solidification defects like porosity and cracking during joining. These defects result in poor mechanical and thermal properties in the finished part [76]. Another problem associated with welding is the presence of heat affected zone (HAZ) and residual stress along with necessity of preheating treatment for large components [43].

In the case of brazing an inhomogeneous bond interface can be observed, if wetting of the component surfaces by the molten filler material is not achieved. Depending on the composition of the filler material an excessive erosion of the base material or embrittlement in the joint can occur. During brazing of complex parts it is hard to produce well-rounded fillets due to presence of liquid metal under pressure [78].

To prevent the problems arising from the formation of liquid phase development of a liquid-free solid state joining method is required. Friction stir welding is one of the most commonly used solid state joining methods [79]. However, large deformations involved during this type of joining makes it impossible to be use for complex parts with low dimensional tolerances [76]. Although heat input is less compared to fusion

welding, HAZ and residual stress formation are still observed in the friction stir welded parts [43].

Therefore, to produce complex parts a solid state bonding process applied at low pressures is required in order to avoid undesired phase transformations and large deformations during bonding [80]. Diffusion bonding (DB) is the most suitable candidate for these purposes.

2.11. Diffusion Bonding of Aluminum Alloys

Presence of a native surface oxide layer affects the diffusion bonding behavior of all materials. It is possible for the oxide film to dissolve or decompose at the bonding temperature for many steels, copper, titanium and zirconium alloys. However, in the case of aluminum and aluminum alloys the surface oxide film is chemically stable, and this makes the metal-to-metal contact necessary for the bond formation difficult.

Diffusion bonding of pure aluminum and multiple aluminum alloys have been studied by many researchers where variety of bonding parameters have been investigated. Usually diffusion bonding of aluminum alloys is conducted at temperatures ranging between 420 to 530 °C under pressures 2 to 30 MPa with bonding times changing from 30 seconds to 6 hours. Optimum temperature, pressure and time values were determined experimentally for each alloy to obtain the highest bond strength [81]. However, currently there are no commercially applied diffusion bonding processes due to the presence of a tenacious and chemically stable oxide film at the alloy surfaces. Numerous approaches have been developed to overcome the difficulties associated with the oxide layer during bonding of aluminum alloys.

One of the many approaches applied to reduce the effects of the oxide film is to impose plastic deformation on the base metals for local disruption of the surface oxide film on both faying surfaces. In the early work on diffusion bonding conducted by Urena et. al. it is suggested that at least 25% reduction in thickness is required to form joints with reasonable strengths, where bond strength increases along with increased level of

deformation [82]. Nevertheless, development of surface preparation methods is still required to join parts successfully without a significant reduction in the thickness.

As an alternative approach roughening of the base metal surfaces has been proposed to overcome the oxide film problem on the aluminum and aluminum alloy surfaces. When surface roughness is increased, excessive plastic deformation of the surface asperities occurs, as a result of which the oxide layer fractures at these local deformation zones leading to a higher contact area between two metal surfaces. Zuruzi et.al. studied the effect of surface roughness on the bond strength of Al 6061 alloy. It was concluded that grinding the base metal surfaces with P180 grit SiC paper yields a higher bond shear strength compared grinding them with P1000 SiC emery paper. Joints produced on surfaces with higher roughness values have a bond ratio of 76% compared to the strength of the base metal. Therefore, it may be possible to obtain joints with strengths reaching up to those of the base metals' by adjusting the initial surface roughness [40].

Introducing chemical reagents into the surface preparation process is an another approach to remove the surface oxide film. Anodizing the aluminum surface with an alkali (NaOH) solution and then neutralizing it with an acid (HNO_3) solution applied after the fracture of the oxide film by grinding is the most commonly used chemical cleaning technique for variety of aluminum alloys. Depending on the other bonding parameters (temperature, pressure and time) many successful joining operations were reported for variety of aluminum alloys with the use of this method [30], [83], [84].

Huang et. al. used an organic solution of acetone, styrene and polystyrene to protect the surface of the Al-7075 superplastic alloy after mechanical and electrolytic polishing. Main characteristic of the organic solution is that it could be easily coated to the faying surfaces to protect them from oxidation, while it is possible for it to volatilize completely before bonding under vacuum in the bonding chamber. They did not only obtain joints with reasonable strengths but also found out that this strength was achieved at temperatures where alloy shows optimum superplastic behavior. That

is to say grain boundary migration and grain growth at the interface are the main mechanisms for the removal of initial bond interface [41].

Ion beam cleaning is also an accepted technique for the removal of the surface oxide film of aluminum and aluminum alloys. Chen et. al. used ion beam cleaning to decrease the diffusion bonding temperature of pure aluminum. Results revealed that it is possible to remove the oxide film effectively by ion beam cleaning making joint formation achievable at lower temperatures. Residue of the surface oxide film is apparently diminishing as the ion beam cleaning time increases. Moreover, tensile strengths of the joints were determined to be increasing with decreasing the amount of the residual oxide film [85].

Enjo and Ikeuchi studied an unorthodox way of diffusion bonding of Al-2017 alloy in a temperature range between solidus and liquidus temperature of the alloy. Despite the formation of a liquid phase this technique still referred as solid state diffusion bonding. The idea was to disrupt the oxide film via formation of a liquid phase at the bond interface due to preferential melting. Successful bonding was achieved by this method. However, obtained bond strengths were found to be strictly dependent on the fraction of the liquid phase formed. Due to the cracking and porosity occurred during the solidification of the melt lower bond strengths were obtained when the fraction of the liquid phase has increased [86].

After the removal of the oxide film, bonding is usually carried out in a protective atmosphere (vacuum or an inert gas) to prevent the regeneration of the oxide film during bonding. To reduce the cost of the process several diffusion bonding studies were also conducted in ambient air atmosphere.

Wu and Lo has studied the use of liquid film protection to prevent the surface oxidation and preserve the clean surface for joining. This method involves chemical cleaning of the surfaces using alkali and acid solutions after grinding. After that faying surfaces are brought together in dehydrated alcohol to form a protective film at the surface. Use of this method for both 8090 and 7075 aluminum alloys have led to similar results.

Although removal of the liquid film without vacuum and interfacial reactions caused by the presence of a liquid film need further investigation, solid bonds were obtained where the bondline between two surfaces vanished [87], [88].

Zuruzi et. al. developed an interfacial treatment method for diffusion bonding of Al-6061 alloy in air. Specimens were ground and cleaned in acetone prior to bonding. Interface treatment technique involves creation of relative motion at the bond interface by rotating the parts 360^{o} perpendicular to the axis of applied pressure. Joint formation has been established by this method; however, unbonded regions were observed through the interface due to the entrapment of air. Therefore, conducting the DB studies in air still requires further work to achieve complete closure of the voids at the interface [89].

2.12. Use of Interlayers and Effect of Alloying Elements

Use of interlayers has been studied by Barta et.al. for solid state diffusion bonding of Al-7075 alloy. Electroplated, vacuum deposited, plasma sprayed and clad Al-7075 along with loose foils of silver, gold, nickel, aluminum, tin, zinc, iron, copper and magnesium have been used in this study for low temperature diffusion bonding of that alloy. Although, low temperature joining has its advantages in terms of mechanical properties of the base metal, the use of most of the mentioned interlayers yielded either no bonding or formation of bonds which have very poor mechanical properties [90].

Alloying elements also play an important role on the behavior of the oxide film and bond characteristics. Madrell et.al. conducted a study to understand the effect of magnesium and lithium addition on the morphology and high temperature behavior of the surface oxide film of aluminum alloys. It was concluded that these alloying elements cause disruption of the surface oxide film resulting in higher joint strengths for bonded parts. Increase in the amount of these elements was also determined to increase the amount of the fractured oxide film, and hence the ratio of the bond formation [91].

Work of Dunford, Partridge and Gilmore has yielded results which are in agreement with those of Madrell's. It has been proven that lithium reacts with the oxide layer and results in the formation of a discontinuous film. TEM studies of the bond interface proved the absence of a continuous oxide layer for Al-8090 alloys studied [92].

Ricks et.al. used thin foil interlayers of aluminum containing gallium, lithium and magnesium to investigate the effect of alloying element on bond strengths of Al-8090 alloy. Thicknesses of the used interlayers was 100 μm. For all interlayers an increase in the bond strength of the alloys was observed. TEM studies proved that this increase was caused by the disruption of the stable oxide film due to formation of oxides more stable than Al_2O_3 [93].

CHAPTER 3

EXPERIMENTAL PROCEDURE

3.1. Starting Materials

Wrought aluminum 6063 alloy sheets (Figure 3.1) were used for diffusion bonding in this study. Wrought samples of 9 mm thickness and with nominal composition given in Table 3.1 were supplied by ASELSAN A.Ş. T6 heat treatment (solution heat treatment and artificial aging to a substantially stable condition) was applied to all of the samples after rolling to desired dimensions, and surfaces of all of the samples were machined after heat treatment.

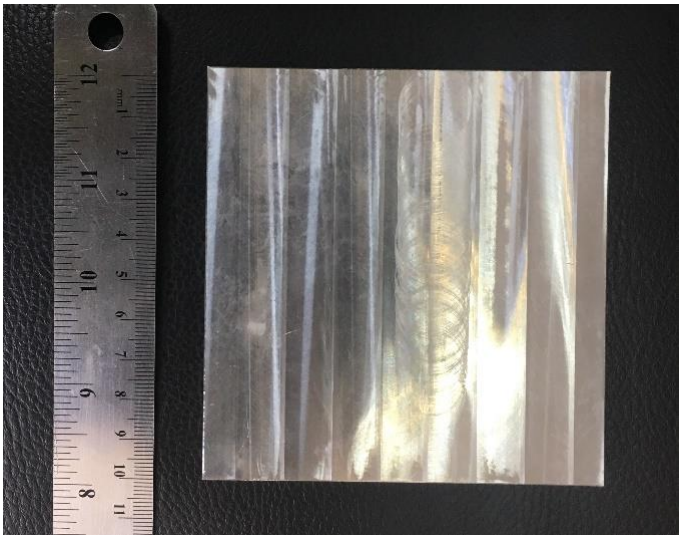

Figure 3. 1. As received Al 6063 alloy sheet used in this study.

Table 3. 1. Chemical composition of the Al 6063 alloy used in the study.

Chemical Composition (wt%)			
Si	Mg	Fe	Al
0.489	0.553	0.100	balance

3.2. Diffusion Bonding Experiments

3.2.1. Surface Preparation

Surface preparation for diffusion bonding includes rupture of the native oxide film on the surface of the as-received aluminum 6063 alloy sheets via grinding and then further removal of this film via chemical cleaning with acid and alkali solutions. In this study, surfaces of all specimens were ground with #600 grit SiC paper until a completely smooth surface is obtained. Ground specimens were immersed into 6% NaOH solution at room temperature for 2 minutes, then immediately immersed into 40% HNO_3 solution for another 2 minutes. Prepared surfaces of two samples were then brought together for diffusion bonding.

3.2.2. Load Adjustment

Pressure is applied by bolting the two base materials between two stainless steel blocks (Figure 3.2). Two pairs of samples were pressurized in each experiment. Strain gauges were used to measure the pressure applied to the samples prior to bonding. For this purpose, a strain gauge was bonded to one of the four sides of the base metal, which is not in contact with the steel blocks. Torque wrench was used to measure the applied torque to each bolt, and compressive microstrain values was measured as a function of torque applied to the bolts.

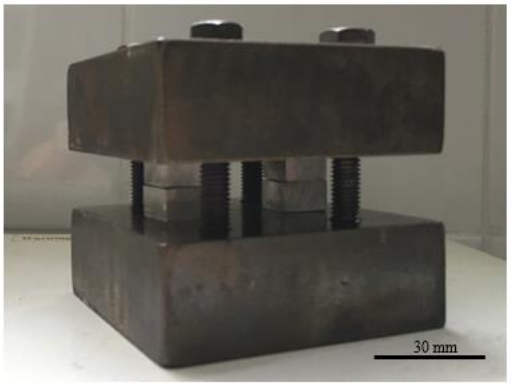

Figure 3. 2. Stainless steel die assembly used to apply pressure for diffusion bonding.

Elastic modulus of the as-received aluminum 6063 alloy was determined as 62.8 GPa using the standard tensile testing method ASTM B557M−15 [94]. Since all of the stresses applied by bolting in the stainless steel die assembly were in the elastic deformation region, Hooke's law was used to determine the applied stress as a function of torque (Figure 3.3).

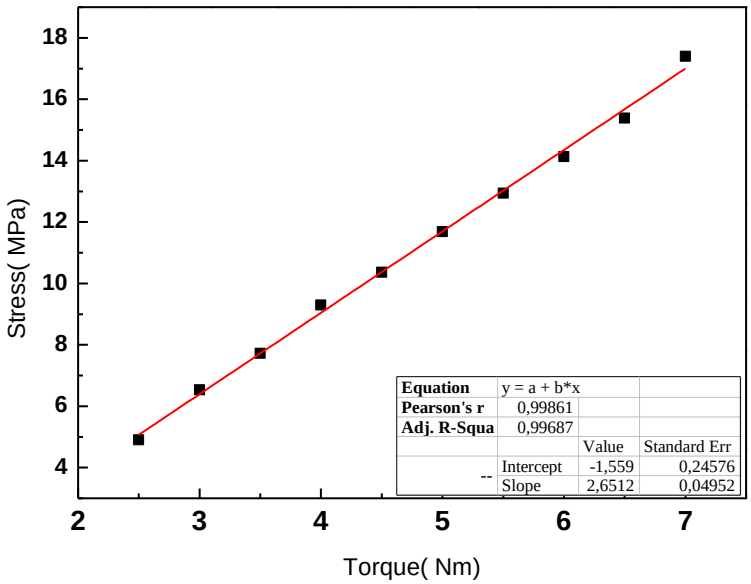

Figure 3. 3. Applied stress during diffusion bonding as a function of torque applied to the bolts for Al6063 alloy.

3.2.3. Experimental Setup

Due to fast oxidizing nature of aluminum alloys a top loading muffle furnace which is working under high purity argon atmosphere was custom-built to produce diffusion bonded Al 6063 joints in this study (Figure 3.4). Alumina refractory bricks were used as the internal lining of a steel box for heat insulation. Kanthal resistance wires were coiled around alumina bars and connected to the mains electricity for heat generation. Three holes were drilled inside the furnace for vacuum/gas inlet and outlet as well as for installation of the K-type thermocouple. Glass wools were used at the top of the furnace to reduce the heat conducted to the furnace door. O-rings and vacuum sealing tapes were used to seal the furnace atmosphere from external environment during the experiments.

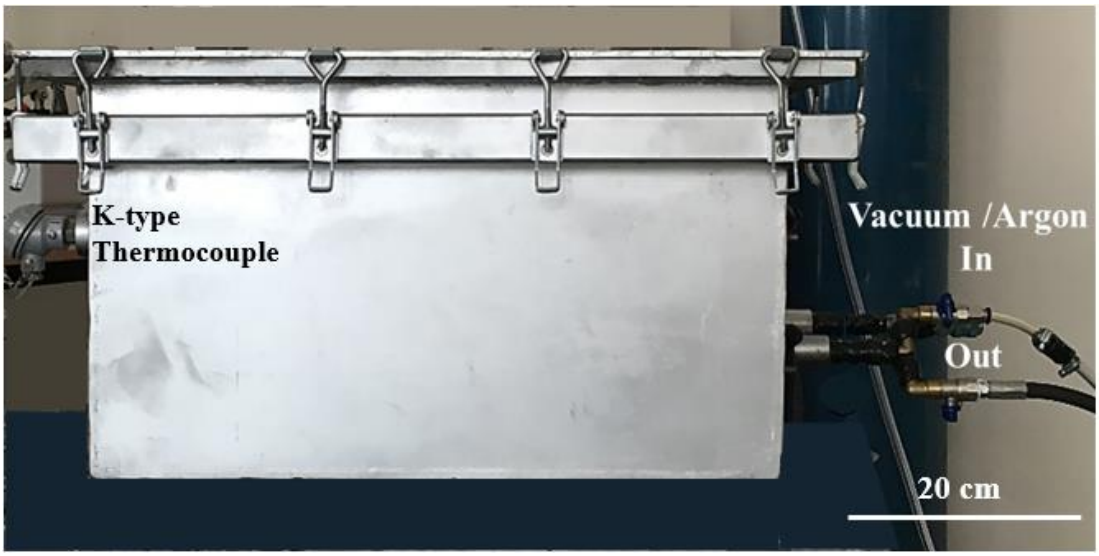

Figure 3. 4. Muffle furnace used for DB.

3.2.4. Bonding Procedure

After surface preparation, base materials were immediately bolted in the steel die assembly, and torque was applied to the bolts according to the desired stress value. Two pairs of the surface prepared base metals pressurized in the steel die assembly were then placed into the homemade muffle furnace. Furnace is vacuumed to 10^{-3} mbar and then flushed with argon two times to free the furnace chamber from air before the heating procedure. Following this, furnace was heated to the desired temperature value with a heating rate of 20 K/min and held at that temperature for required bonding time under argon atmosphere.

Several set of experiments were conducted using the above mentioned surface preparation method followed by the bonding procedure. Experiments were divided into 3 groups for lucidity according to the initial material and the presence of an interlayer. Samples produced by applying various bonding parameters were summarized in Table 3.3.

3.2. Optimization of the Diffusion Bonding Parameters

Square shaped pieces of 15 mm side length were cut from the wrought Al 6063 alloy sheets via precision abrasive cutting machine to be used in the diffusion bonding experiments. Prepared surfaces of these square shaped pieces were then brought in contact, and pressure was applied in the steel die assembly.

Temperature, pressure and time values were optimized for diffusion bonding of wrought Al 6063 alloy. Used temperature values were 450, 500 and 520°C, pressure values were 5, 10, 13 and 17 MPa and holding times at the applied temperature were 1, 2 and 3 hours. Each parameter was tested by keeping the other two constant. After bonding under argon atmosphere, power of the furnace was turned off, and the samples were left to cool down in the furnace under argon atmosphere for the optimization experiments.

To understand the effect of cooling rate on the properties of the joint and the base material air cooled samples were produced using the optimum bonding parameters (temperature, pressure and time) obtained from previous experiments. These samples were removed from the furnace after the completion of the bonding time. Since cooling rate of the steel die assembly would be much lower than the aluminum samples pressurized inside of it, the samples were removed from the steel die assembly and left to cool in air.

3.3. Investigation of the Effect of Interlayer Materials

3.3.1. Interlayer Materials

In the present study Silver, Nickel and Gold were used as interlayer materials in variety of forms to investigate their effect on the diffusion bonding behavior.

3.3.1.2. Nickel Flakes

First material used as interlayer was nickel flakes (99.8% purity) supplied by Alfa Aesar (Figure 3.5). Average diameter and thickness of the flakes were 44 and 0.37 μm, respectively.

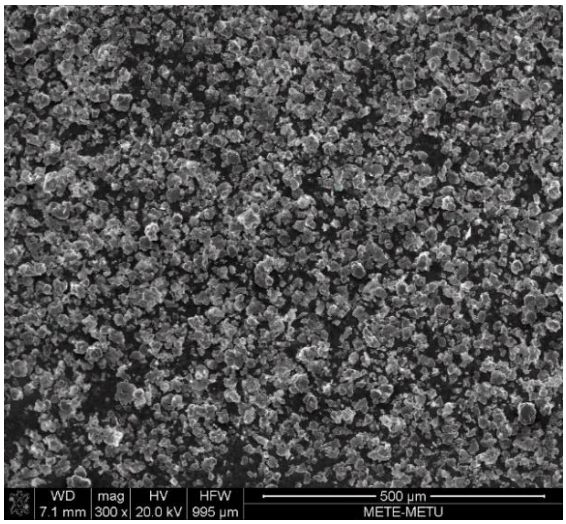

Figure 3. 5. SEM image of the nickel flakes used as interlayer material.

3.3.1.3. Silver Nanowires

As an alternative interlayer material two different forms of silver nanowires were used in this study. The first one was in the form of a self-standing film, which was 0.3 μm thick. The film could be cut into desired dimensions to fit it in the bond interface. The second one was in the form of a silver nanowire suspension. 1, 0.5 and 0.25 mg/ml silver nanowire and ethanol suspension was prepared by a magnetic stirrer and applied on the prepared surfaces of the base materials.

3.3.1.4. Gold Coating

Final material used as interlayer was gold. Gold was deposited on to the surfaces of the Al 6063 alloys by sputter coating (SC7640, Quorum Technologies, Ashford, UK). Thickness of the gold coating was controlled using the instrumental parameters.

3.3.2. Bonding Procedure

Surfaces of the square shaped base materials of a side length of 15mm were prepared by using the above-mentioned surface preparation method. Interlayer materials were then applied to one side of the bond interface to act as a diffusion source, and the effect of different interlayer materials on the diffusion bonding behavior was investigated. Different methods were used to apply interlayer materials depending on their forms.

To see the effect of nickel as the interlayer material prepared surface of one of the two base materials was immersed into the nickel flakes and excess of the flakes were blown off from the surface.

Self-standing silver nanowire film was cut with scissors to fit it into the bond interface and directly placed between two base materials (Figure 3.6.a). As an alternative method 1, 0.5 and 0.25mg/ml silver nanowire and ethanol solutions were dripped on to the prepared surfaces of one of the base materials (Figure 3.6.b). Five drops of the suspension were applied for all of the specimens, four of which were applied to the corners and one of which to the center. A hot plate was used during the dripping procedure to volatilize the ethanol from the surface before bonding.

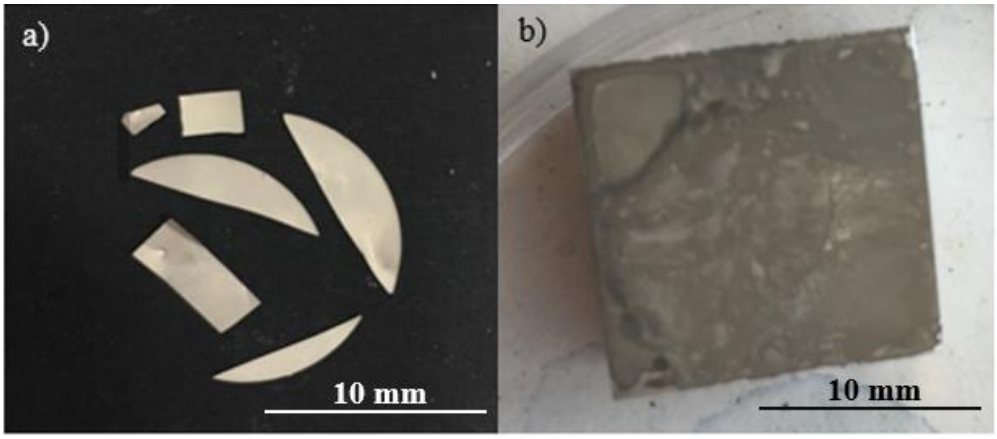

Figure 3. 6. Silver nanowires a) shaped self-standing film b) dripped in solution with ethanol.

Gold was applied to the bond interface by a commercial sputter coating apparatus. (Figure 3.7.a). A homogeneous gold film having 200, 400 and 800 nm thickness was obtained on the surface of the aluminum after sputter coating (Figure 3.7.b).

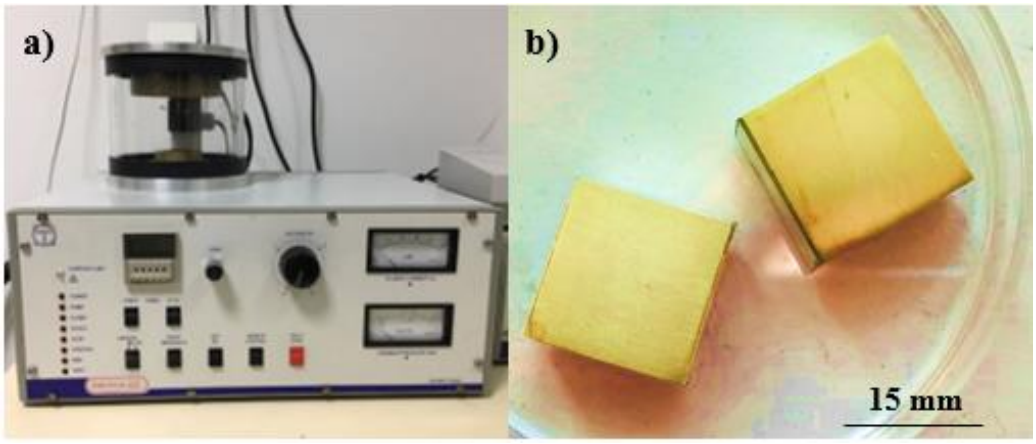

Figure 3. 7. a) Sputter coating apparatus used in the study and b) gold sputter coated Al 6063 sample surfaces.

After placement of the interlayer materials at the bond interface two surfaces were brought together for bonding. Bonding process conditions used for all of the samples

containing an interlayer material were 520°C of maximum temperature, 13 MPa of pressure and 3 h of holding time at the maximum temperature. Specimens bonded under argon atmosphere were then cooled in air after bonding was completed.

3.4. Investigation of the Effect of Alloying Element Addition

Cast alloys were produced and diffusion bonded to investigate the effect of alloying element addition on the properties of the base material and bond formation. Cu and Sn were used as the alloying elements. Either Cu or Sn was added into the Al 6063 base composition in three different amounts.

3.4.1. Production of the Cast Alloys

Alloys with compositions given in Table 3.2 were cast for diffusion bonding using a lab scale induction melting and casting setup (MC 15+, Indutherm GmbH, Wössingen, Germany) shown in Figure 3.8.a and b under argon atmosphere. Among these compositions 0 wt% refers to the as-cast Al 6063 without further alloying element addition. Alloying was done by adding high purity Cu (99.9 wt%) and Sn (99.9 wt%)to Al-6063 alloy. All compositions were cast into copper molds seen in Figure 3.8.a, and rods having 12 mm diameter were obtained (Figure 3.8.c).

Table 3. 2. Compositions of the cast alloys.

Alloying Element	**Amount (wt %)**			
Cu	0	0.5	2.5	5.0
Sn	0	0.5	2.5	5.0

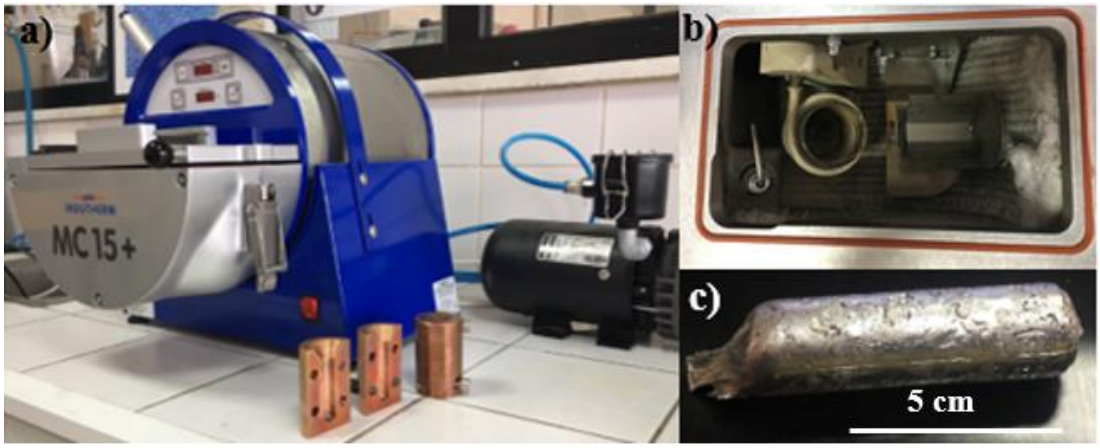

Figure 3. 8. a) Induction melting and casting setup with copper molds used in this study, b) inside view of the setup and c) rod produced via casting.

3.4.2. Bonding Procedure

10 mm thick discs were cut from the cast rods via precision abrasive cutting machine to be used in diffusion bonding experiments. Similar to the previously mentioned specimens grinding was carried out on the sliced discs with #600 grit SiC paper in order to break the native surface oxide layer. Ground specimens were immersed into 6% NaOH solution for 2 minutes and then neutralized in 40% HNO_3 solution for another 2 minutes at room temperature. Prepared surfaces of the disc shaped specimens were brought together in the stainless steel die assembly and compressive stress was applied. Bonding was achieved by holding the specimens at 520°C for 3 h under 6.5 MPa pressure. Bonding was carried out under argon atmosphere, and bonded samples were cooled in air.

Table 3. 3. Summary of diffusion bonded joints produced under varying conditions.

Al-6063	Temperature (ºC)	Pressure (MPa)	Time (Hours)	Cooling Medium	Interlayer	Alloying Element
Wrought	450	5,10,13,17	3	Furnace	-	-
Wrought	500, 520	13	3	Furnace	-	-
Wrought	520	13	1,2	Furnace	-	-
Wrought	520	13	3	Air	-	-
Wrought	520	13	3	Air	Gold Sputter	-
Wrought	520	13	3	Air	Nickel flakes	-
Wrought	520	13	3	Air	Silver nanowires	-
Cast	520	6	3	Air	-	-
Cast	520	6	3	Air	-	Sn-0.5,2.5,5 wt %
Cast	520	6	3	Air	-	Cu-0.5,2.5,5 wt %

3.5. Characterization Studies

Following the bonding procedure diffusion bonded samples were cut into two halves using a precision abrasive cutting machine. Both sides of the diffusion bonded samples were ground until a 5×20 mm^2 smooth surface area is obtained for metallographic examination and mechanical characterization studies.

3.5.1. Microstructural Characterization

Microstructural characterization was conducted for both base materials and bonded interfaces. A scanning electron microscope (SEM) (Nova NanoSEM 430, FEI Company, Eindhoven, The Netherlands) equipped with an energy dispersive X-ray spectroscopy (EDS) analyzer along with a high capacity digital microscope (HDS-5800, Huvitz Corp., Gyeonggi-do, Republic of Korea) equipped with a polarization filter were used for microstructural characterization studies.

Diffusion bonded samples were examined under SEM in as polished condition to investigate the integrity of the bond through the bond line.

In order to understand the microstructural changes during diffusion bonding, wrought Al-6063 parts were examined using digital microscope under polarized light before and after the bonding procedure. After standard metallographic sample preparation steps (grinding, polishing etc.) electrolytic etching was applied for polarized microscopy examinations. Samples were anodized with Barker's reagent (5 ml HBF_4 (48vol.%) in 200 ml distilled water) under 20 V voltage for 1 minute for electrolytic etching.

As-cast samples were also investigated under SEM both before and after the diffusion bonding to comment on the microstructural changes caused by the alloying element addition and high temperature diffusion bonding process. Cast samples were etched with Keller's reagent (5ml HNO_3, 3ml HCl, 3ml HF in 190ml distilled water) following the metallographic surface preparation steps.

3.5.2. Structural Analysis by X-ray Diffraction (XRD)

XRD analyses were conducted with Bruker D8 Advance x-ray diffractometer (Bruker Corporation, MA, USA) using Cu-Kα ($\lambda = 1.5406$ Å) radiation to determine the phases present in the as-received sample as well as the phases formed during casting and the subsequent diffusion bonding process applied. Grinding was carried out, and sample surfaces were cleaned with ethanol before XRD measurements. Scanning was conducted between 2θ angles of 10-100° with a fixed scan speed of 1°/min, and the diffractometer was operated at 40 kV and 30 mA.

3.5.3. Thermal Analysis by Differential Scanning Calorimetry (DSC)

Thermal analysis was conducted for the cast samples using differential scanning calorimetry (DSC) (X-DSC 7000, Seiko Instruments Inc., Chiba, Japan) to understand the phase transformations occurring under the applied bonding process conditions.

Samples of 10-20 mg weight were cut and cleaned before the thermal analysis. These samples were then placed into aluminum pans and encapsulated with aluminum covers. The pan containing the sample is placed onto one holder of the DSC instrument and reference sample is placed onto the other one. Samples were heated up to 500°C under a protective N_2 atmosphere. This temperature value is lower than some of the chosen diffusion bonding temperatures, which was dictated by the limitations of the DSC apparatus utilized. During the DSC experiments, heating and cooling rates were kept at 20 and 60 K/min, respectively, which are comparable to those achieved during the heating and cooling cycles of the diffusion bonding process.

3.5.4. Mechanical Characterization

3.3.4.1. Microhardness Measurements

Microhardness measurements were conducted with 100 g load for 10 seconds using a standard microhardness tester (HMV-2, Shimadzu Scientific Instruments, Kyoto, Japan) before and after the DB process. Microhardness measurements were carried out on the polished cross-sections of the specimens. 5 measurements with 2 mm intervals were conducted before the bonding and results were averaged. For diffusion bonded samples measurements were carried out across the interface and on the base metal. One of the measurements was taken just on the interface, and the others were taken on both sides of the bond line along a line perpendicular to the interface with 5 mm intervals. Five measurements were carried out on each base metal side, and the results were averaged.

3.5.4.2. Shear Test

Shear strength of the joints were tested under quasi-static loading condition using Instron 5582 mechanical testing equipment with max. 100 kN force. Shear strength tests were performed by using the fixture arrangement schematically shown in Figure3.9 at a strain rate of 10^{-4} s^{-1}. One side of the bonded specimens was fixed in the fixture and compressive load was applied to the other side of the bond. All of the specimens were fractured in shear mode, and shear strengths were calculated by using the bonded area. Two tests were conducted for each specimen processed under identical conditions, and results were averaged.

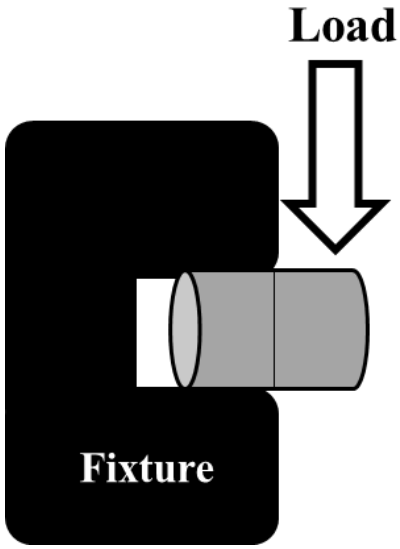

Figure 3. 9. Mechanical testing arrangement used for the measurement of shear strength of the bonded joints.

3.5.5. Fractography Analysis

After mechanical testing fracture surfaces of the joints were examined under SEM with 20 kV accelerating voltage to understand the mechanical behavior of the joints and to comment on the fracture mode.

CHAPTER 4

RESULT AND DISCUSSION

4.1. Optimization of the Diffusion Bonding Parameters

Solid state diffusion bonding is a complex phenomenon controlled mainly by 3 important parameters, namely, temperature, pressure and bonding time. Optimization of these parameters is essential to obtain a solid bond that has properties close to those of the parent material. Cooling rate after bonding is also effective on the post-bonded properties of the base metal and bond strength. In the following section selection of the optimum process parameters for diffusion bonding of aluminum 6063 alloy will be discussed with the aid of obtained experimental results.

4.1.1. Pressure Optimization

Aluminum 6063 alloys were diffusion bonded under argon atmosphere at 450°C for 3 hours. Four different pressure values (5, 10, 13 and 17 MPa) were used to determine the optimum pressure value.

Cross-sections of the bond interfaces were examined under SEM to comment on the integrity of the bonds. Figure 4.1 shows the variation in the cross-sectional appearance of the bonds with pressure. Bond interface was visible for the specimens bonded under 5 and 10 MPa pressure. The thickness of the bond line was found to be decreasing with increasing pressure, which should be accompanied with an increase in the bond strength. Bondline was almost invisible for the sample bonded under 17 MPa pressure.

Since selection of the optimum bond structure based on the SEM micrographs would be misleading, mechanical characterization of the bonds is crucial. These specimens

were subjected to shear tests and no measurable strength was obtained for the first three specimens bonded under 5, 10 and 13 MPa. On the other hand, maximum shear strength of 7.5 MPa was obtained for the specimen bonded under 17 MPa pressure (Figure 4.4).

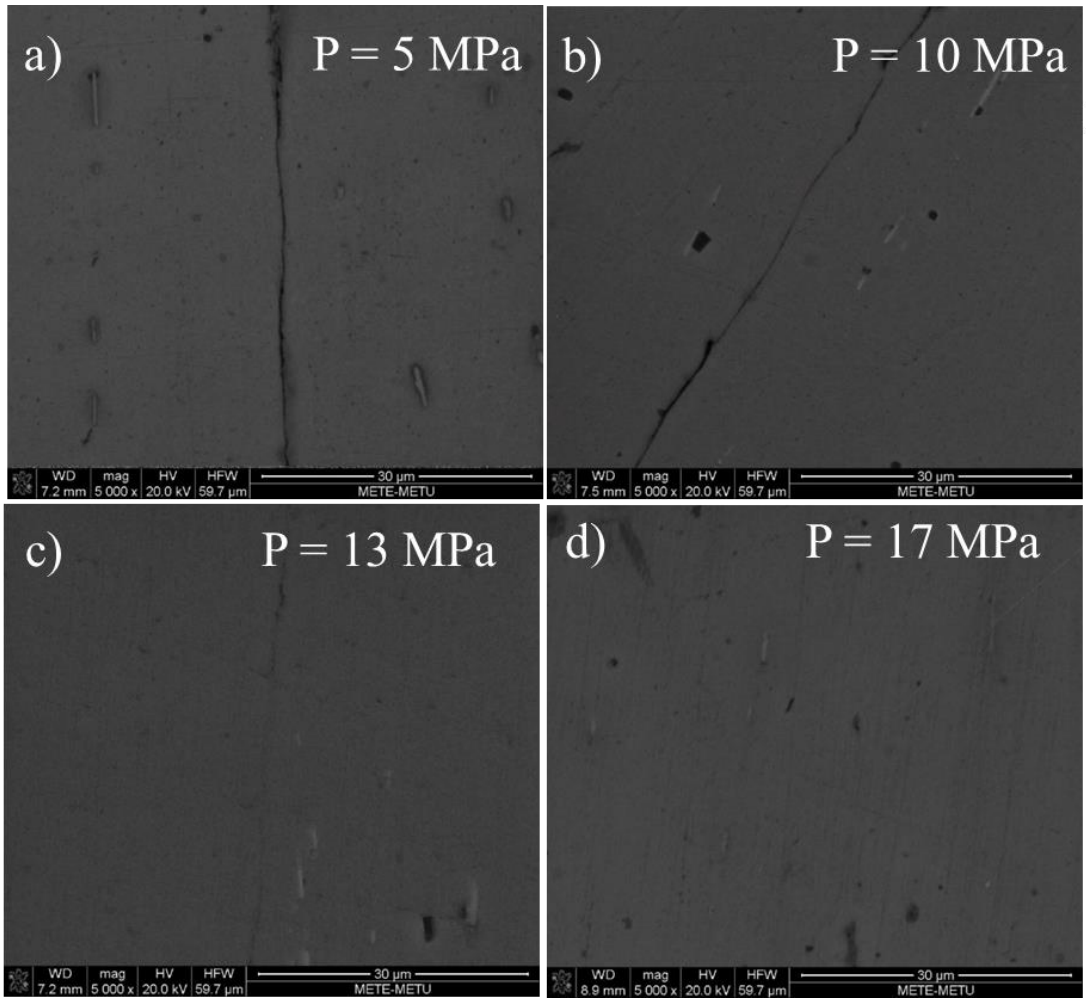

Figure 4. 1. Cross-sectional views of the interfaces diffusion bonded under a) 5 MPa, b) 10 MPa, c) 13 MPa and d) 17 MPa at 450˚C for 3 h. and cooled in furnace.

Both microstructural and mechanical characterization results proved that the bond strength was increasing with increasing bonding pressure. To verify these results fracture surfaces of these specimens were also investigated under SEM (Figure 4.2).

Fracture surface of the bond should show similar characteristics to fracture surface of the base aluminum alloy to be able to speak of bond formation. Therefore, in the case of the diffusion bonded samples cross-sectional fracture surfaces should include dimples proving that fracture has occurred in a ductile manner.

Investigation on the fracture surfaces proved that for 5 and 10 MPa bonding pressure at 450°C bond formation could not be achieved. Fracture surfaces of these samples are completely flat and grinding scratches remaining from the surface preparation step are still visible (Figure 4.2.a and b). For the specimen bonded under 13 MPa pressure signs of mechanical impingement are present on the fracture surface (Figure 4.2 c). This is to say initial contact was maintained by deformation of surface asperities, yet bond formation by grain boundary migration could not be achieved. Specimen bonded under 17 MPa pressure shows traces of dimples (Figure 4.2 d) which explains the higher bond strengths achieved at this bonding pressure.

Preservation of the initial dimensions is also a concern during the diffusion bonding process. Therefore, plastic deformation of the base metals, in this case aluminum samples, should be prevented. For this purpose, bonding pressure should be kept as low as possible considering the fact that the yield strength of the metals decrease with increasing temperature. Thicknesses of all of the samples were measured before and after the diffusion bonding to comment on the plastic deformation behavior. For the applied pressure values of 5, 10 and 13 MPa thicknesses of the samples were maintained during the bonding. However, for 17 MPa bonding pressure reduction in the thickness of the samples was observed indicating plastic deformation under this pressure condition. To prevent this 13 MPa was chosen as the optimum pressure value which was sufficient to maintain an initial contact and formation of mechanical impingement.

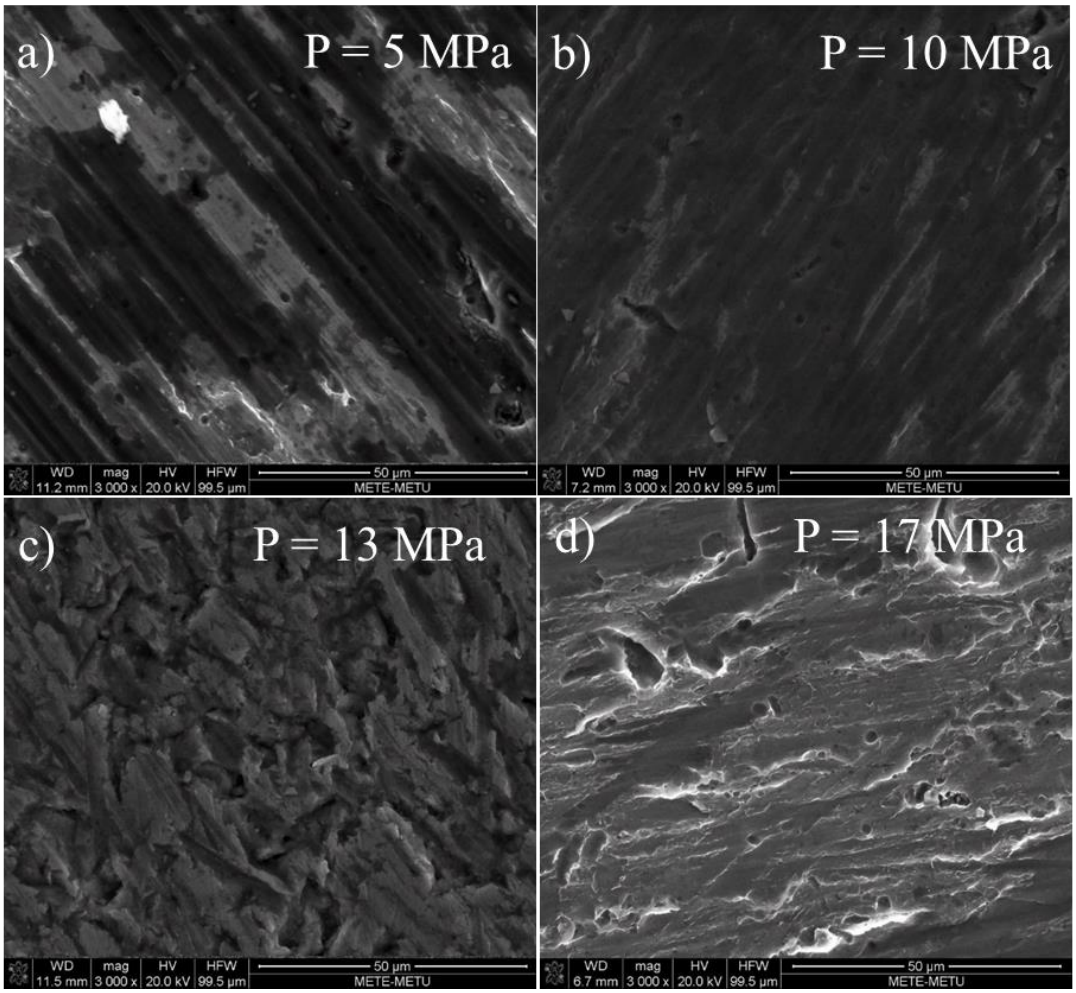

Figure 4. 2. Fracture surfaces of the specimens diffusion bonded under a) 5 MPa, b) 10 MPa, c) 13 MPa and d) 17 MPa at 450°C for 3 h. and cooled in furnace.

4.1.2. Temperature Optimization

After choosing the 13 MPa as optimum bonding pressure at 450°C , diffusion bonding experiments were conducted at higher temperature values to determine the optimum bond strength. Experiments were conducted at 500 and 520°C under 13 MPa for 3 hours under argon atmosphere.

SEM micrographs of the cross-sections of the bond interfaces are shown in Figure 4.3. It is clearly seen that there is a reduction in the thickness of the bond interface for higher bonding temperatures compared to the sample bonded at 450 °C. Bond line was almost invisible for both 500 and 520°C temperature values.

Shear tests were also conducted for these samples and results were shown in Figure 4.4. Since, no measurable strength was obtained for the sample diffusion bonded at 450°C under 13 MPa pressure for 3 hours, shear strength value obtained from the sample bonded under 17 MPa pressure was used for comparison. Shear test results proved that bond strength increases as the bonding temperature was increased. Obtained shear strength values were summarized in Table 4.1. Maximum bond strength of 32.3 MPa was obtained when diffusion bonding was conducted at 520ºC.

It can be said that temperature is more effective on bond strength compared to pressure. This can be explained by the exponential increase in diffusivity with increasing temperature.

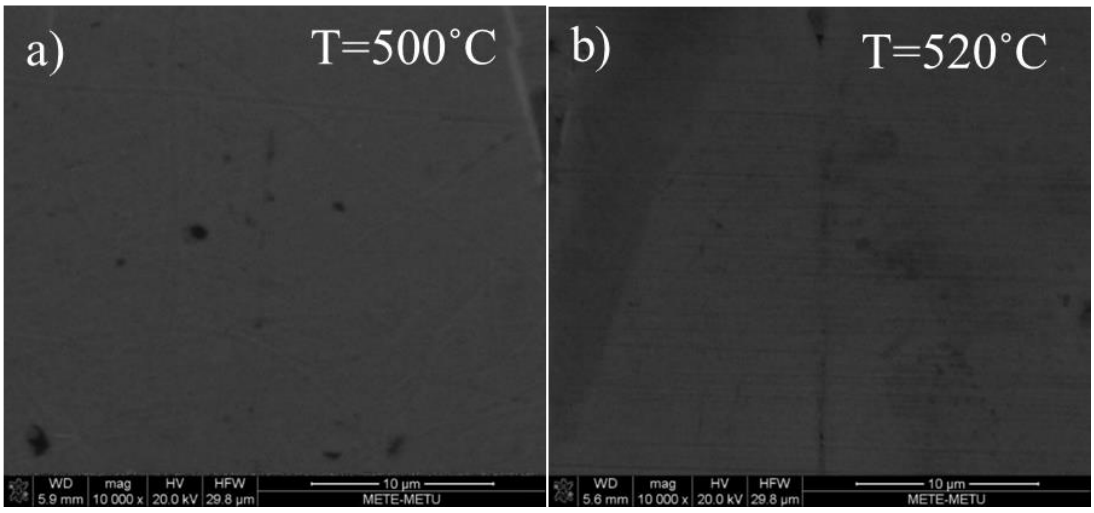

Figure 4. 3. Cross-sectional views of the bond interfaces of the specimens, diffusion bonded at a) 500°C, b) 520°C under 13 MPa, pressure for 3 h. cooled in furnace.

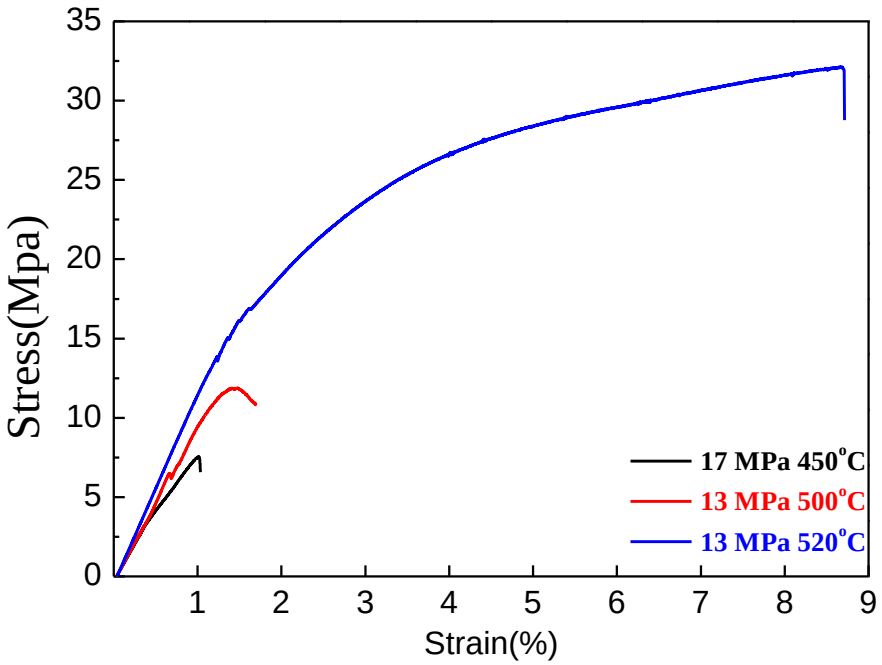

Figure 4. 4. Change in the shear strengths of the bonds with temperature.

Table 4. 1. Summary of the shear test results for different diffusion bonding temperature values.

P, T	σ_{UTS} (MPa)
17 MPa, 450°C	7.5
13 MPa, 500°C	12
13 MPa, 520°C	32.3

Fracture surfaces of these two samples were also verified the bond formation (Figure 4.5). Traces of dimples were observed on the fracture surface of the specimen bonded at 500°C. Oval shaped dimples were clearly visible on the fracture surface of the sample bonded at 520°C which proves that bonding was achieved for this sample and fracture occurred under shear mode. Thus 520°C was chosen as the optimum diffusion bonding temperature.

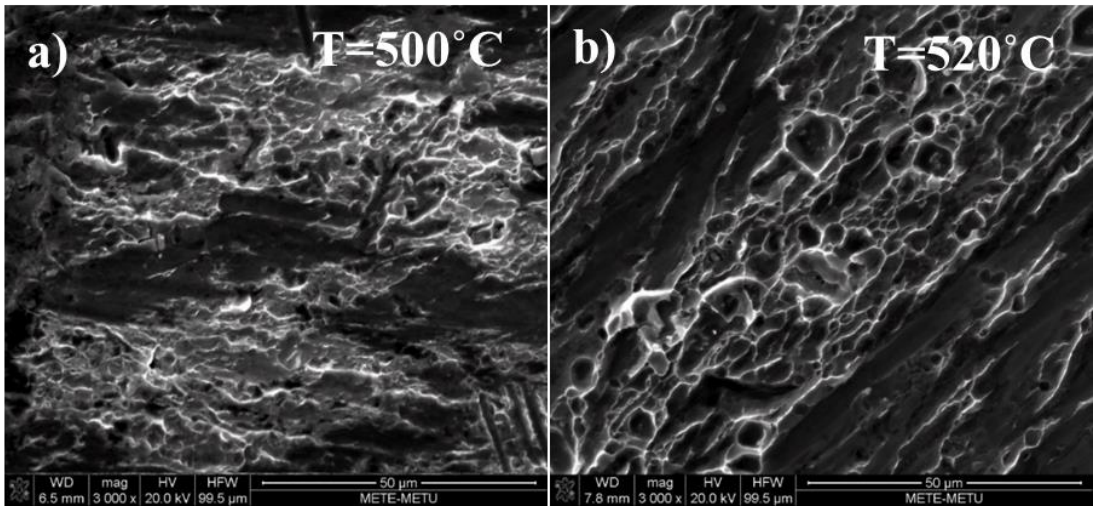

Figure 4. 5. Fracture surfaces of the specimens, diffusion bonded at a) 500°C, b) 520°C under 13 MPa pressure, for 3 h. cooled in furnace.

4.1.3. Time Optimization

After determination of the optimum pressure and temperature values as 13 MPa and 520˚C, time of bonding was optimized. For this purpose, specimens were diffusion bonded for 1 hour and 2 hours and characterized. Shorter bonding times were tested for efficiency of the process.

Cross-sectional views of the bond interfaces showed that certain parts of the bond interface were invisible while it is clearly visible in some parts (Figure 4.6). When two micrographs were compared change in the thickness of the bond line was observed. It gets thicker for shorter bonding time.

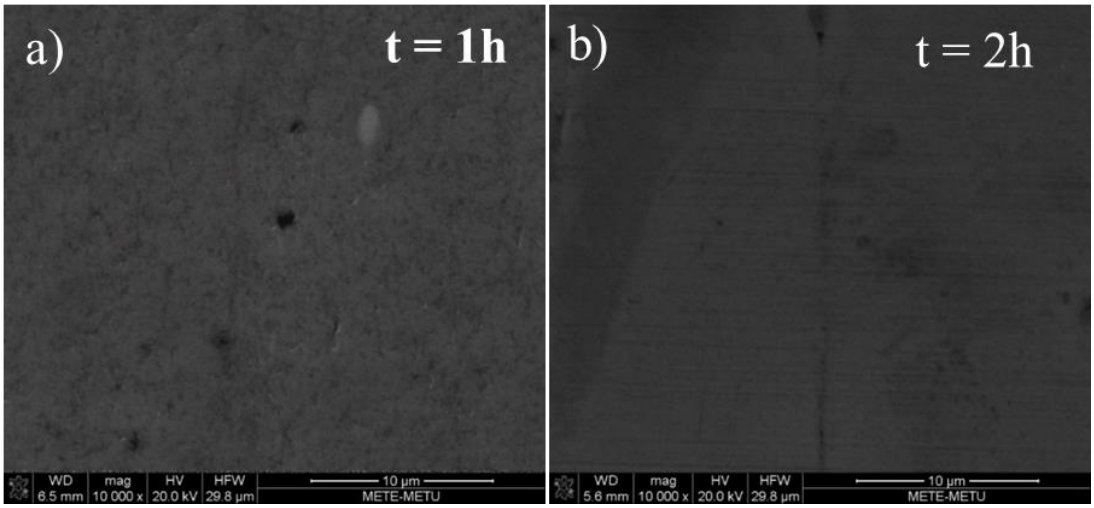

Figure 4. 6. Cross-sectional views of the bond interfaces of the specimens, diffusion bonded for a) 2 hours, b) 1 hour under 13 MPa pressure, at 520°C cooled in furnace.

Shear strengths of the specimens were again measured to determine the optimum bonding time. Figure 4.7 shows that shear strength of the bonds was decreasing with decreasing bonding time. As it is seen in the Table 4.2 highest shear strength was obtained for the specimen bonded under 13 MPa pressure at 520°C for 3 hours and it decreases significantly for shorter times. Bond strengths of the specimens bonded for 1 hour and 2 hours were close to each other, proving that formation of a solid joint by grain boundary diffusion takes place after 2 hours.

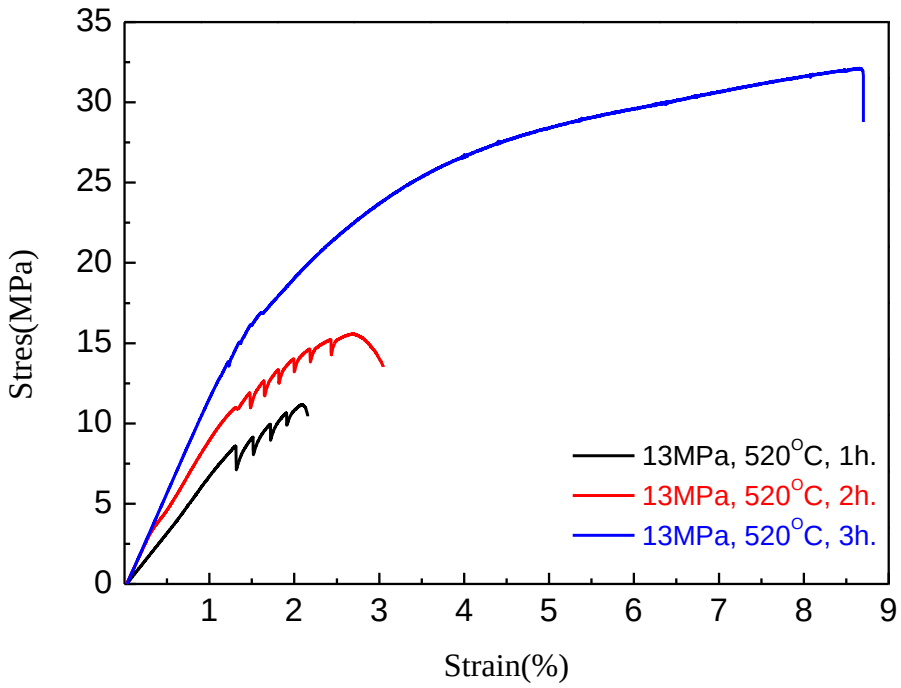

Figure 4. 7. Change in the shear strengths of the bonds with bonding time.

Table 4. 2. Summary of the shear test results for different diffusion bonding times.

T,t	σ_{UTS} (MPa)
520°C, 1hr	11.2
520°C, 2hrs	15.6
520°C, 3hrs	32.3

Shear strength diagrams of the 1 and 2 hours bonded samples showed a serrated behavior. This behavior can be explained with the presence of bonded and unbonded regions on the fracture surfaces of this specimens. Sudden drop in the strength was observed when these unbonded regions were fractured. Dimples were again visible on the remaining parts of the fracture surfaces verifying the formation and ductile fraction of a diffusion bond on these regions. Fraction of the area covered by bonded regions

found to be decreasing with decreasing bonding time which is in consistence with the shear test results.

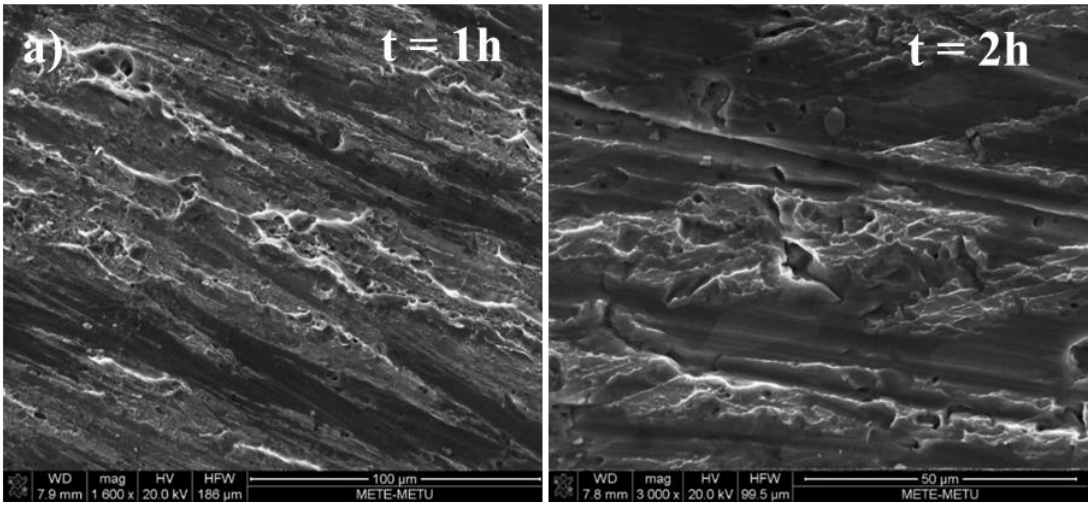

Figure 4. 8. Fracture surfaces of the specimens, diffusion bonded for a) 2 hours, b) 1 hour under 13 MPa pressure, at 520°C and cooled in furnace.

4.1.4. Cooling Rate Optimization

Furnace was shut down after bonding and samples were left to cool in it during the experiments conducted to determine the optimum pressure, temperature and time parameter for DB. To understand the effect of cooling rate air cooled samples were also produced. Air cooled samples were bonded at 520°C, under 13 MPa pressure for 3 hours since, those are the parameters that gives the highest bond strength.

Observations of the cross-section of the bond line showed that the interface was disappeared, meaning that diffusion bonding is achieved for the air cooled sample similar to the furnace cooled one (Figure 4.9.a).

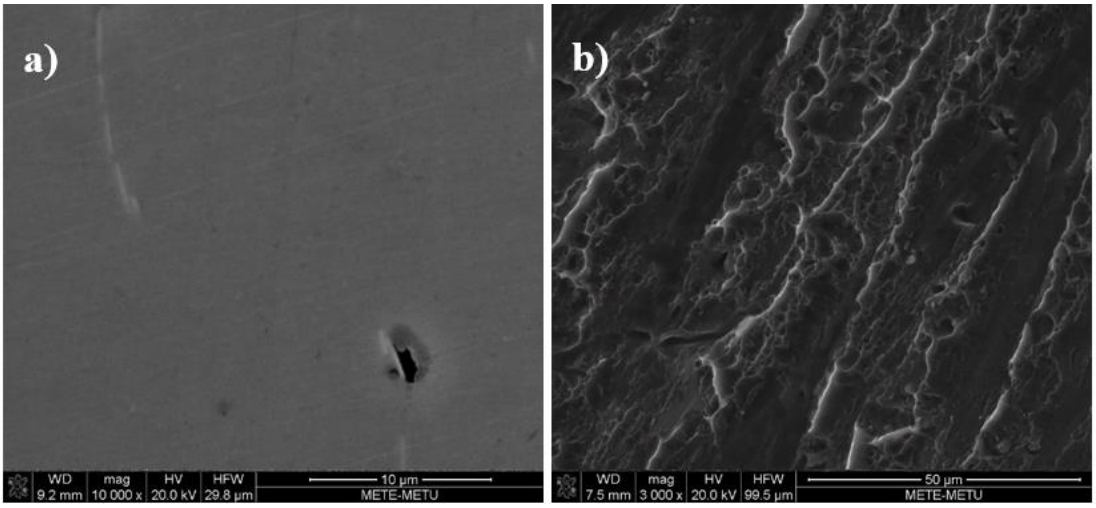

Figure 4. 9. a) Cross-sectional view of the bond interface, b) fracture surface of the specimen, diffusion bonded under 13 MPa pressure, at 520°C, for 3 h. and cooled in air.

Shear test were conducted to understand the effect of cooling rate on bond strength and it is found that increase in the cooling rate results in an increase in the shear strength of the bonds (Figure 4.10). Among the specimens bonded with same parameters shear strength of the bonds were increased from 32.3 to 39.9 MPa when samples were cooled in air instead of furnace (Table 4.3).

Fracture surface of the air cooled sample proved that bonding was achieved and fracture occurred on the bond interface. It is evident that the fracture mode was ductile and oval shape of the dimples showed that fracture occurred under shear stress.

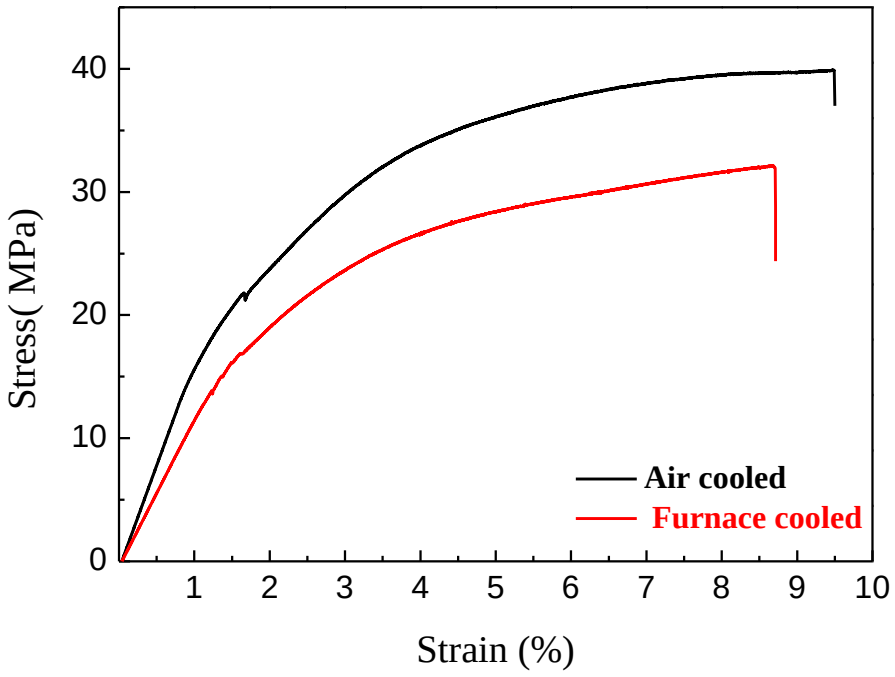

Figure 4. 10. Change in the shear strengths of the bonds with cooling rate.

Table 4. 3. Summary of the shear test results for different cooling rate after diffusion bonding.

From 520°C	**σ_{UTS} (MPa)**
Furnace cooling	32.3
Air Cooling	39.9

4.1.5. Change in the Base Metal Properties During Diffusion Bonding

Maintaining the base metal properties during diffusion bonding is as important as achieving a high bond strength. Therefore, change in the properties of Al6063 alloy during DB were also examined.

XRD analysis were conducted both before and after the diffusion bonding at 520°C for 3 hours to comment on the phase transformations occurred during bonding. XRD

results in Figure 4.10 proved presence of FCC-(Al) phase and Mg_2Si and β-AlFeSi intermetallic phases before the bonding. After diffusion bonding (Al) peaks were remained unchanged and intensity of Mg_2Si peaks were increased slightly meaning that the size or the amount of Mg_2Si precipitates present in the alloy would be increased after diffusion bonding. α- AlFeSi peaks were appeared instead of β-AlFeSi peaks after bonding showing the dissolution of orthorhombic β-AlFeSi (Al_5FeSi) intermetallic phase and formation of BCC, α-AlFeSi (Al_8Fe_2Si) intermetallic phase during the diffusion bonding process [95]. All of the peaks that belong to intermetallic phases were at low intensity due to their trace amount in the (Al) phase. Since the alloy was in T4 condition presence of Mg_2Si phase as the age hardening precipitates was expected before the bonding. Dissolution or coarsening of these precipitates is also a commonly observed phenomenon during high temperature processing of Al 6063 alloy, which would explain the slight increase in the intensity of the Mg_2Si peaks [96].

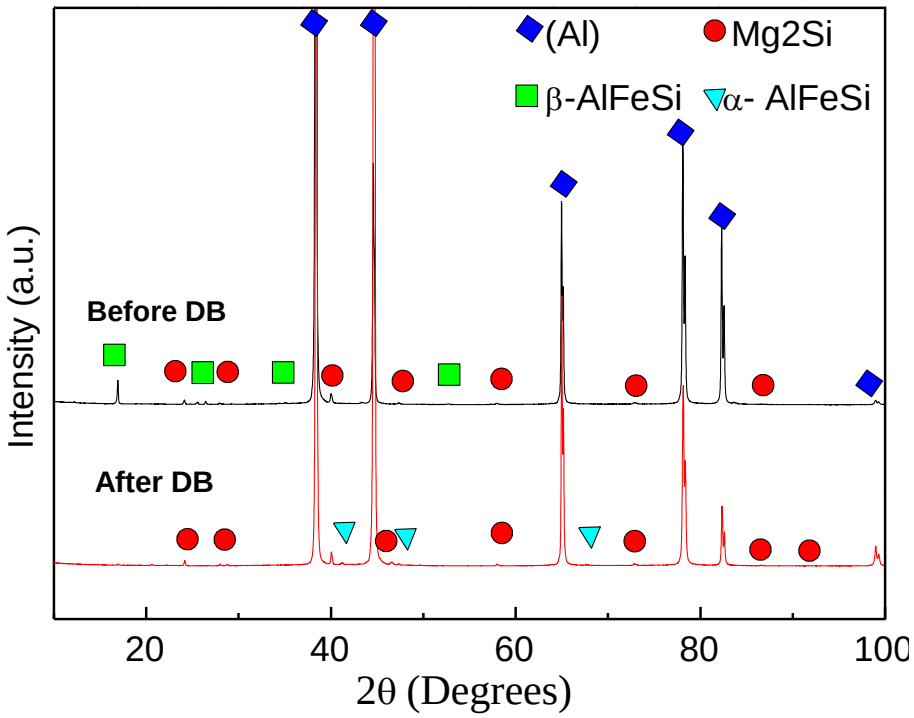

Figure 4. 11. XRD analysis of the Al6063 alloy before and after the diffusion bonding process.

Metallographic observations were also conducted to observe the changes during diffusion bonding and compared with the XRD analysis results. Both Mg_2Si and β-AlFeSi intermetallic phases were observed in the optical micrograph of the Al6063 sample taken before the bonding (Figure 4.12.a). Two different types of Mg_2Si precipitates was observed in this sample. One of them was appeared as small black dots and other one was the larger black particles in the micrograph. Among these two larger particles does not contribute to the strength much while small ones are the age hardening precipitates. AlFeSi intermetallic phase has two distinct morphologies observed in the literature. β-AlFeSi phase has needle like morphology while α-AlFeSi is observed as chinese script [97]. Therefore, the gray needle like particles observed in the optical image are the β-AlFeSi intermetallic phase which were also present in the XRD analysis. After diffusion bonding of the alloy at 520˚C, Mg_2Si precipitates formed after age hardening, were not appear and an increase in the amount of the large Mg_2Si precipitates was observed. It can be said that the age hardening precipitates were either dissolved in the aluminum matrix or coarsened during the bonding. As it was also observed in the XRD analysis α-AlFeSi phase in chinese script morphology was also observed instead of β-AlFeSi in the image taken after DB Figure (4.12.b).

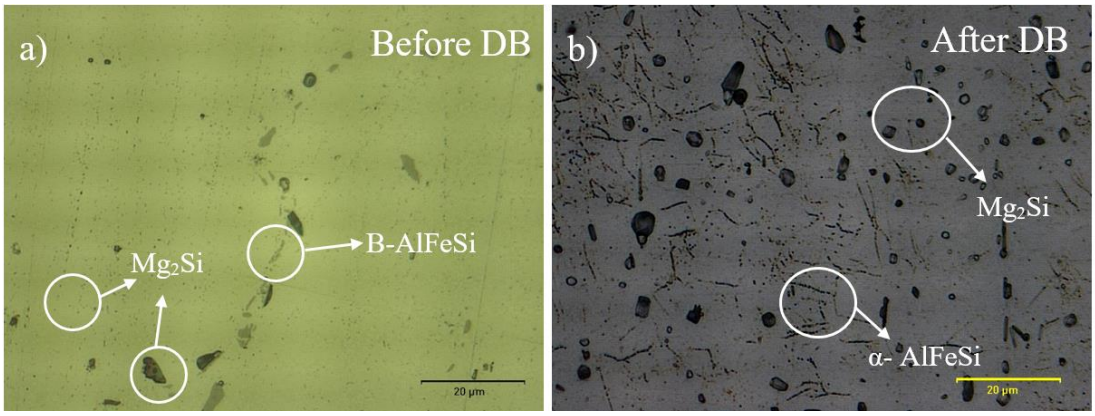

Figure 4. 12. Optical micrographs of the Al6063 alloys a) before, b) after the diffusion bonding process.

Optical images taken under polarized light in Figure 4.13 shows that a significant increase in grain size was observed after bonding at 520°C for 3 hours. Grain growth was an expected consequence of a high temperature joining process which would result in degradation of the mechanical properties of the base metal [52].

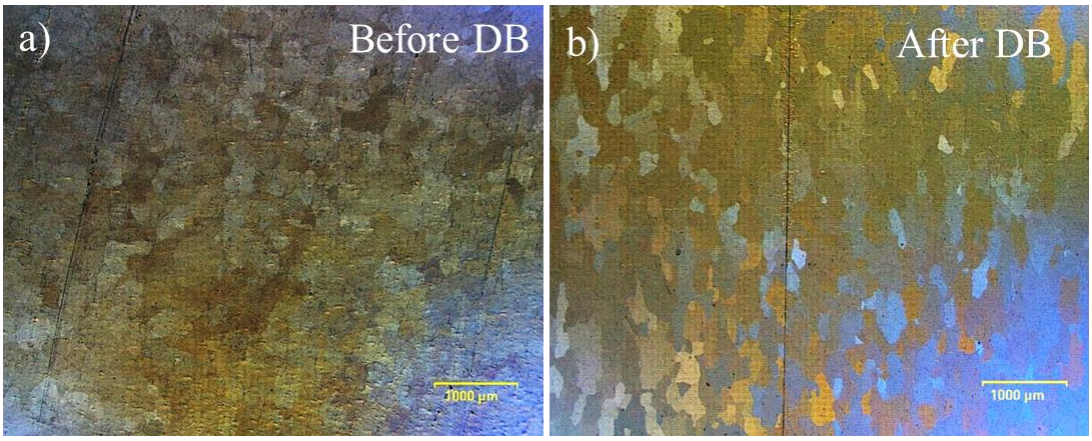

Figure 4. 13. Optical micrographs of Al-6063 alloy a) before b) after DB under polarized light.

Microhardness measurements were conducted to understand the changes in the mechanical properties of the base metal during bonding. The average hardness value of the aluminum alloys was measured as 106 HV before the bonding. Hardness measurements were also conducted for the alloys diffusion bonded at 450, 500, and 520°C and then cooled in the furnace. Microhardness values of all the furnace cooled specimens were close to each other and changing around 40 HV which is less than the half of the initial microhardness value before the bonding. As it was seen both in XRD and metallographic analysis, age hardening precipitates were either dissolved or coarsened during the bonding meaning that they do not contribute to the strength of the base metal after the diffusion bonding. Therefore, a significant decrease in the hardness was observed for these alloys. Microhardness value of the air cooled sample was higher compared to furnace cooled ones. 6000 series aluminum alloys does not require an additional aging process to achieve a moderate strength value when they are

quenched from a high temperature shaping or a joining process [98]. Difference in the Microhardness values of the furnace cooled and air cooled samples can be explained by this phenomenon. Decrease in the grain boundary area due to grain growth also causes a loss in the strength of the base metal for all specimens. Although effect of both grain growth and coarsening and dissolution of the precipitates were less in the air cooled specimen the Microhardness value is still less than the as received sample (Figure 4.14).

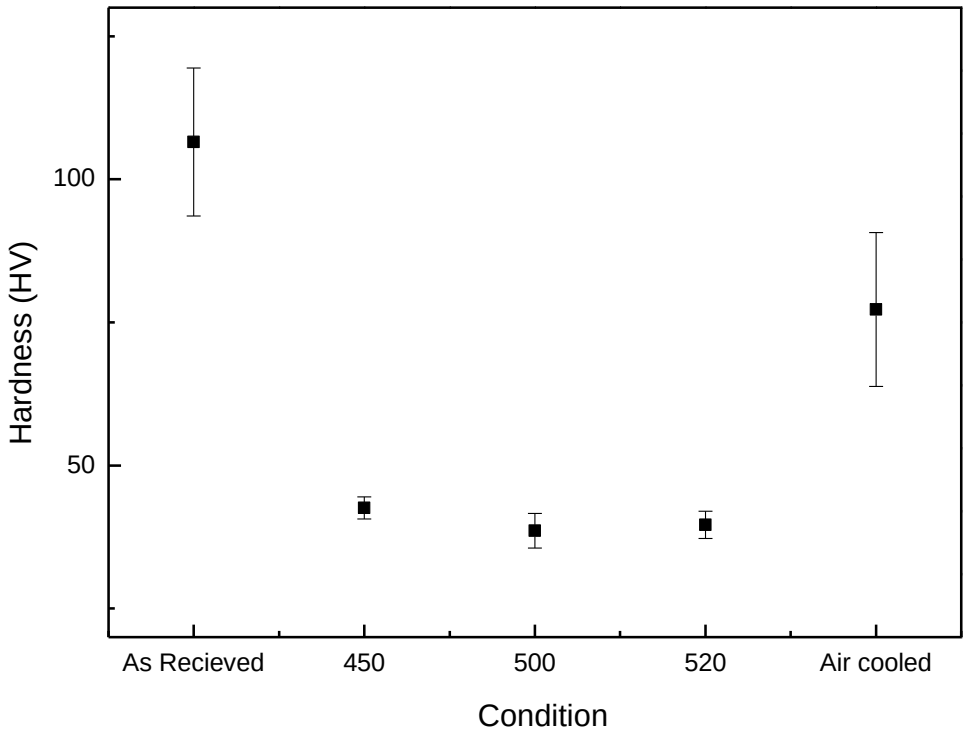

Figure 4. 14. Change in the microhardness value of Al-6063 alloy during different diffusion bonding conditions.

While choosing the optimum bonding parameters the most important concern was to obtain a high bond strength without causing a major degradation in the properties of the base metal. For this study, bonding under 13 MPa pressure at 520°C for 3 hours and air cooling after the bonding not only gives the highest bond strength of 39.9 MPa but also causes the least degradation in mechanical properties. However, further

studies were required to minimize the grain growth during bonding and these studies would be conducted under these determined optimum bonding conditions.

4.2. Investigation of the Effect of Interlayer Materials

Diffusion bonding of aluminum 6063 alloy was achieved and optimum bonding parameters were determined in the previous experiments yet a decrease was observed in the microhardness value of the base metal due to grain growth during bonding. To maintain the initial mechanical properties grain growth should be minimized. Bonding time and temperature should be decreased to minimize the grain growth without altering the composition of the alloy. To obtain a bond at lower temperatures and in shorter times faster bonding kinetics is required.

In this part of the study variety of interlayer materials were placed on to the bond interface to see their effect on the diffusion bonding kinetics and obtained bond strength.

4.2.1. Silver as Interlayer Material

Silver nanowires were the first material that was used as interlayer. Nanowires were placed on to the interface by two different methods. First method was to drop a solution of ethanol and silver nanowires on to the surface of the aluminum alloys. Solutions containing 1, 0.5, 0.25mg/ml nanowires were used in these experiments and diffusion bonding was conducted at 520˚C, under 13 MPa pressure and for 3 hours. When samples were removed from the furnace for air cooling, no bond formation was observed for any composition of the applied interlayer.

These specimens were examined under SEM after the application of the interlayer and nonhomogeneous distribution of the silver nanowires were observed (Figure 4.15). Silver nanowires were accumulated at the certain parts of the base metal surface causing irregularities in the initial surface contact of the surfaces and it is impossible to form a bond with atomic diffusion unless this initial contact is established [32].

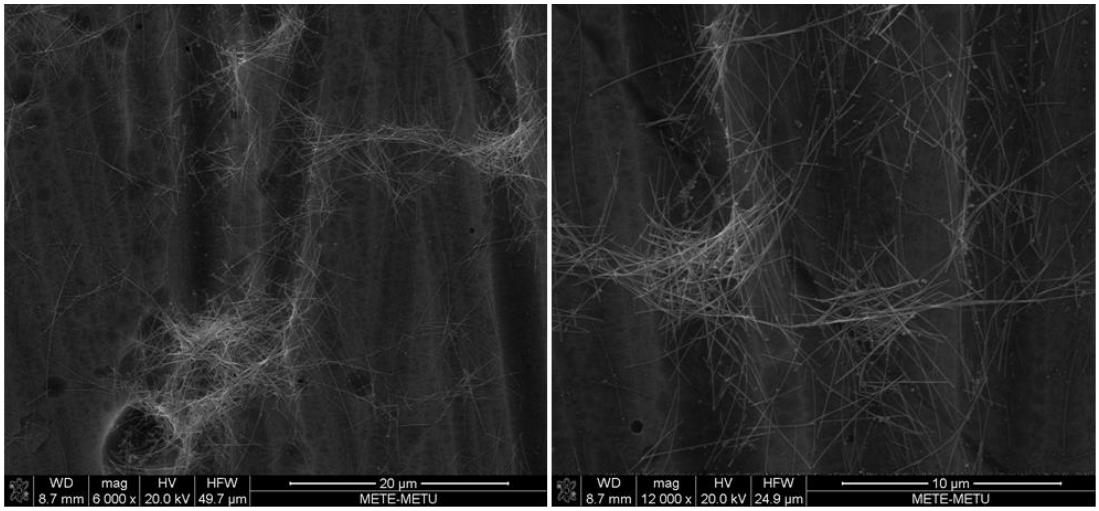

Figure 4. 15. SEM images of the aluminum surface after silver nanowire, ethanol solution was applied as interlayer.

Second method was to use of a self-standing film of silver nanowires as interlayer material. Surface of the Al6063 alloys were prepared than a self-standing film of silver nanowires were placed in between them. Diffusion bonding parameters were kept constant and bonding was again unsuccessful for these samples. Diffusion bonding would occur between the film and aluminum alloy in this condition. Therefore, investigation of the film surface was important to understand the failure of the bonding procedure. Investigation of the self-standing silver nanowire films under SEM revealed a wavy pattern (Figure 4.16). Although nanowires seemed to be homogeneously distributed in higher magnifications, presence of irregularities were observed at lower magnifications. Waviness of the material surface should be kept minimum to form a better initial contact for diffusion bonding[32]. Bond formation could not be achieved when silver nanowire film was used due to the presence of gaps and high waviness of the film surface.

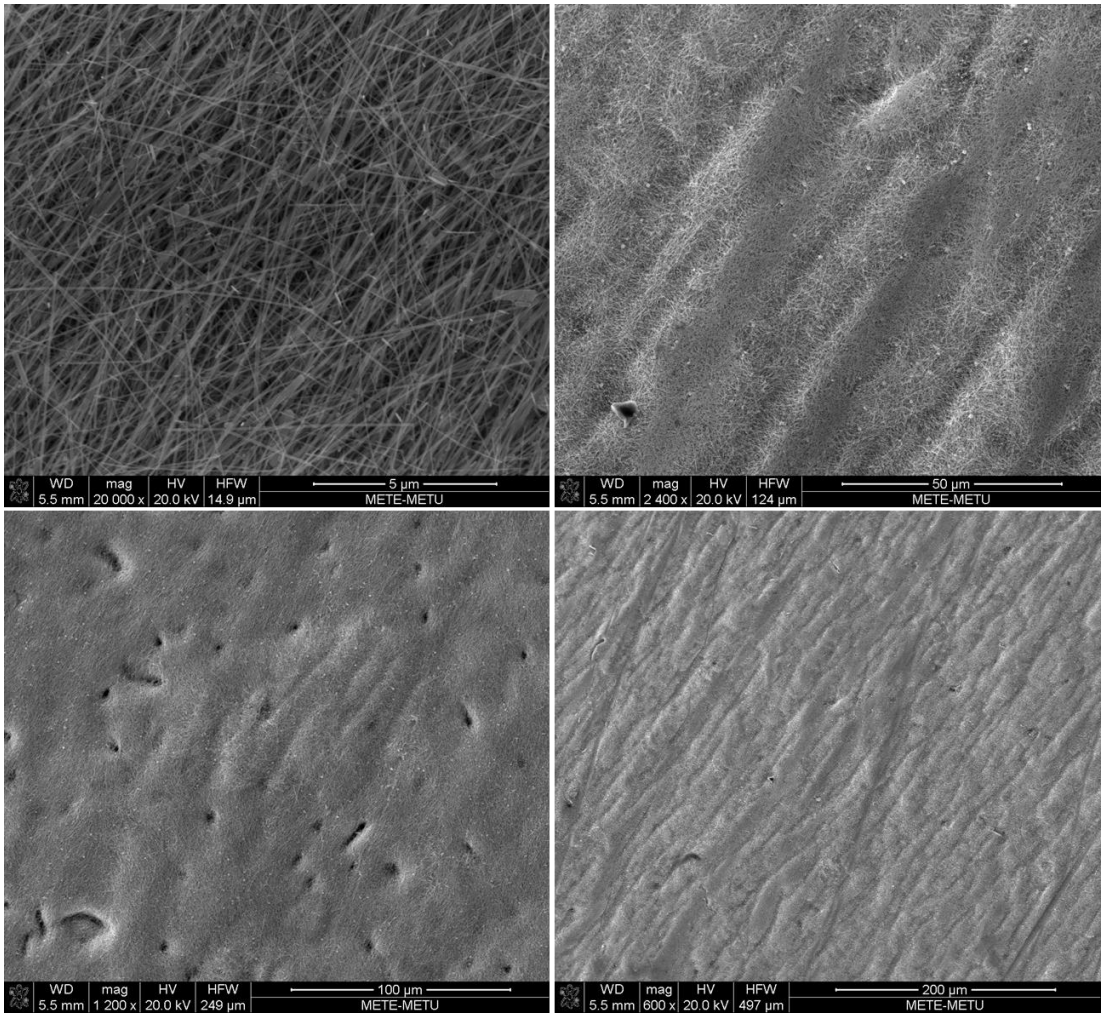

Figure 4. 16. SEM images of the surface on the self-standing silver nanowire film used as interlayer material.

Use of silver nanowires as interlayer material either in solution with ethanol or as self-standing films resulted in failure of the bond formation between two Al6063 alloys. It can be concluded that interlayer material should cover the surface of the base metal homogeneously and surface of the applied interlayer material should be smooth and free from irregularities.

4.2.2. Nickel as Interlayer Material

Second material to be used as an interlayer were the nickel flakes. Flakes were placed on to the aluminum surface by dipping the parts in to the flakes. Initial observations of the nickel coated samples revealed that flakes were homogeneously distributed on the surface of the base metal (Figure 4.17.a). After coating diffusion bonding was carried out again at 520˚C, under 13 MPa pressure and for 3 hours. Specimens were than cooled in air and cross-sections of the bond interfaces were examined under SEM. The average thickness of the nickel interface was measured as 14.5 μm and shown in Figure 4.17.b. Elongation of the nickel flakes along the bond interface was also observed at higher magnifications. Air gaps were also observed in between the elongated nickel flakes (Figure 4.17.c).

Flattened nickel flakes were observed on the fracture surface of the specimen with nickel interlayer (Figure 4.17.d). The elongated view of the flakes on the cross-sectional observations of the interface could be explained by this flattening. The failure was occurred at the nickel interface but not at the base metal. Fracture surface proved that failure occurred in between the nickel flakes which can be explained the presence of the air gaps seen in the cross-sectional view. The fracture occurred due to widening of these gaps under shear force.

Shear tests were conducted and bond strength of 21.8 MPa was measured (Figure 4.18). Use of nickel as interlayer material lead to bond formation yet the measured bond strength was still lower compared to the sample bonded without the use of any interlayer material.

Homogeneous distribution of the flakes was lead to a solid bond formation but achieved bond strengths were low due to presence of the air gaps in between the flakes. Therefore, use of an interlayer material with a more intact structure could be beneficial for higher bond strengths.

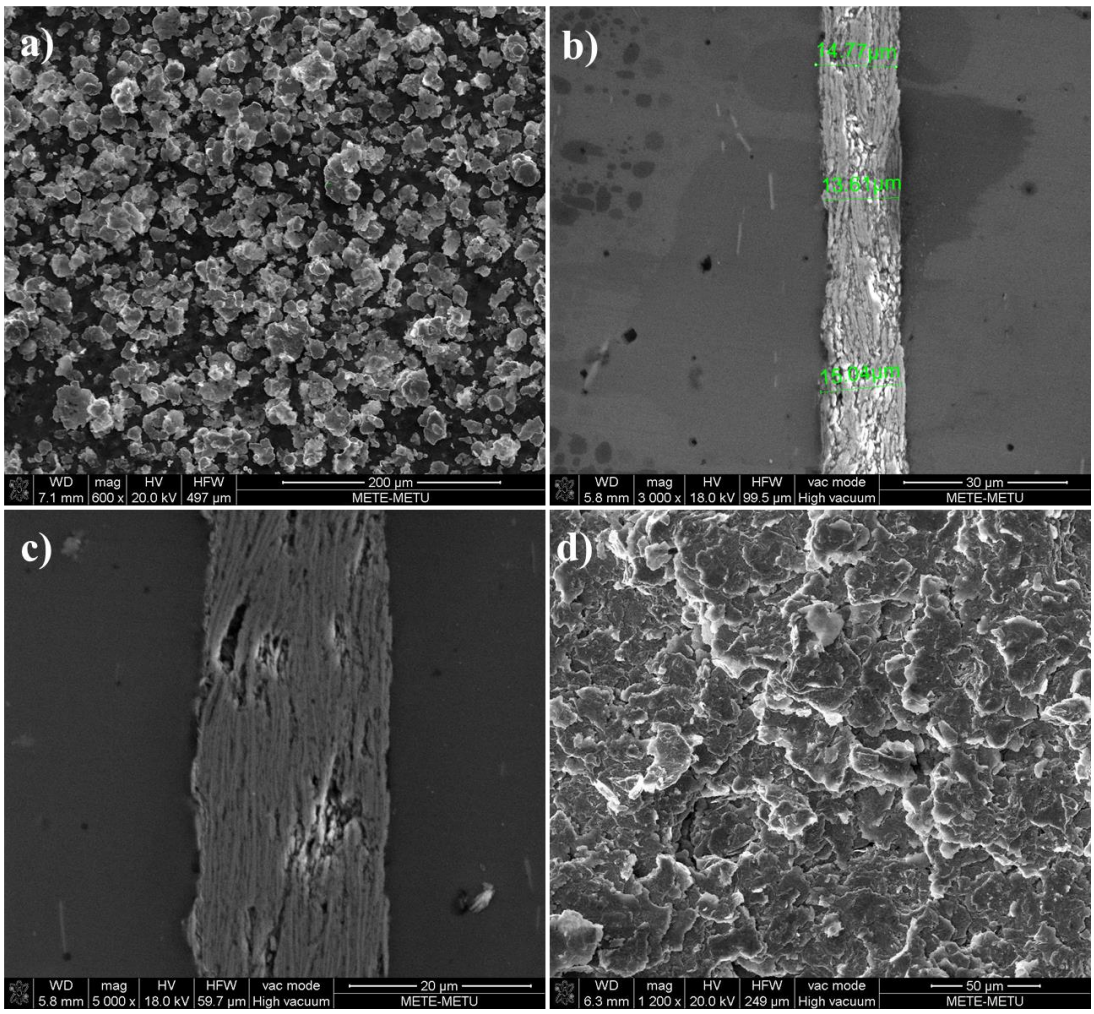

Figure 4. 17. SEM images of a) aluminum surface after nickel flakes were placed b), c) cross-sectional view of the bond interface including nickel flakes as interlayer material, d) fracture surface of the sample that has nickel as interlayer material.

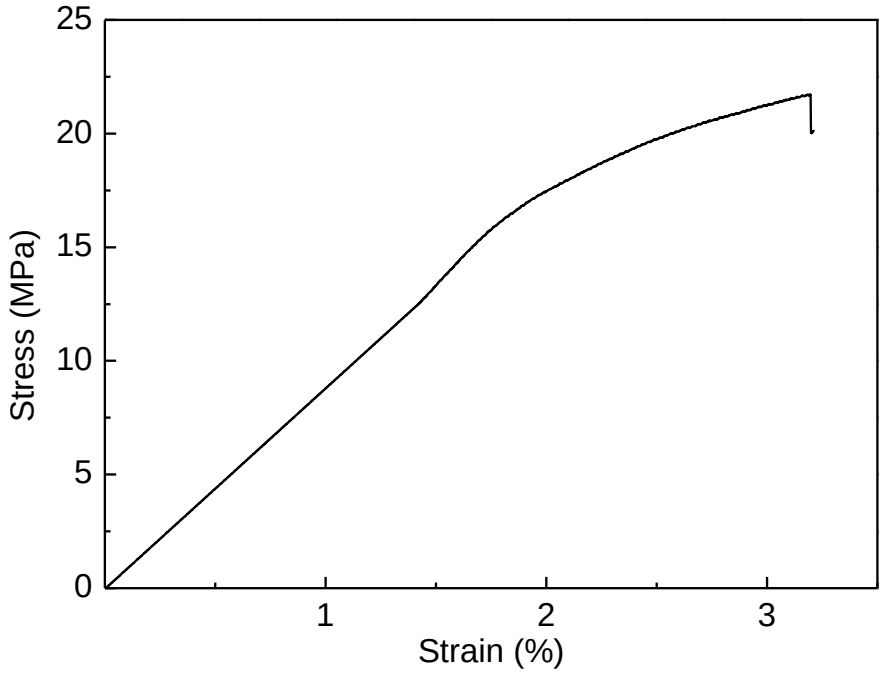

Figure 4. 18. Shear test results of the sample prepared with a nickel interlayer.

4.2.3. Gold as Interlayer Material

Gold layers having 200 nm, 400 nm and 800 nm thicknesses were sputter coated to the aluminum alloy surface as the third interlayer material. Gold coated samples were diffusion bonded at 520˚C, under 13 MPa pressure for 3 hours and cooled in air. Presence of an interlayer was observed on the cross-section of the bond interface in Figure 4.19.a, b, c and thickness of this interlayer found to be increasing with increasing coating thickness. The interlayer was disappeared by diffusion of gold in aluminum at certain parts of the interface indicating a solid diffusion bond formation. EDS elemental mapping was conducted from the part of the interface in Figure 4.19.d to confirm that the observed interlayer was gold. It was clearly seen that the composition of the aluminum decreases and composition of gold increases at the interface where the interlayer was present (Figure 4.19.e, f). Meaning that the contact between two base metals were prevented due to the presence of the gold coating at the interface.

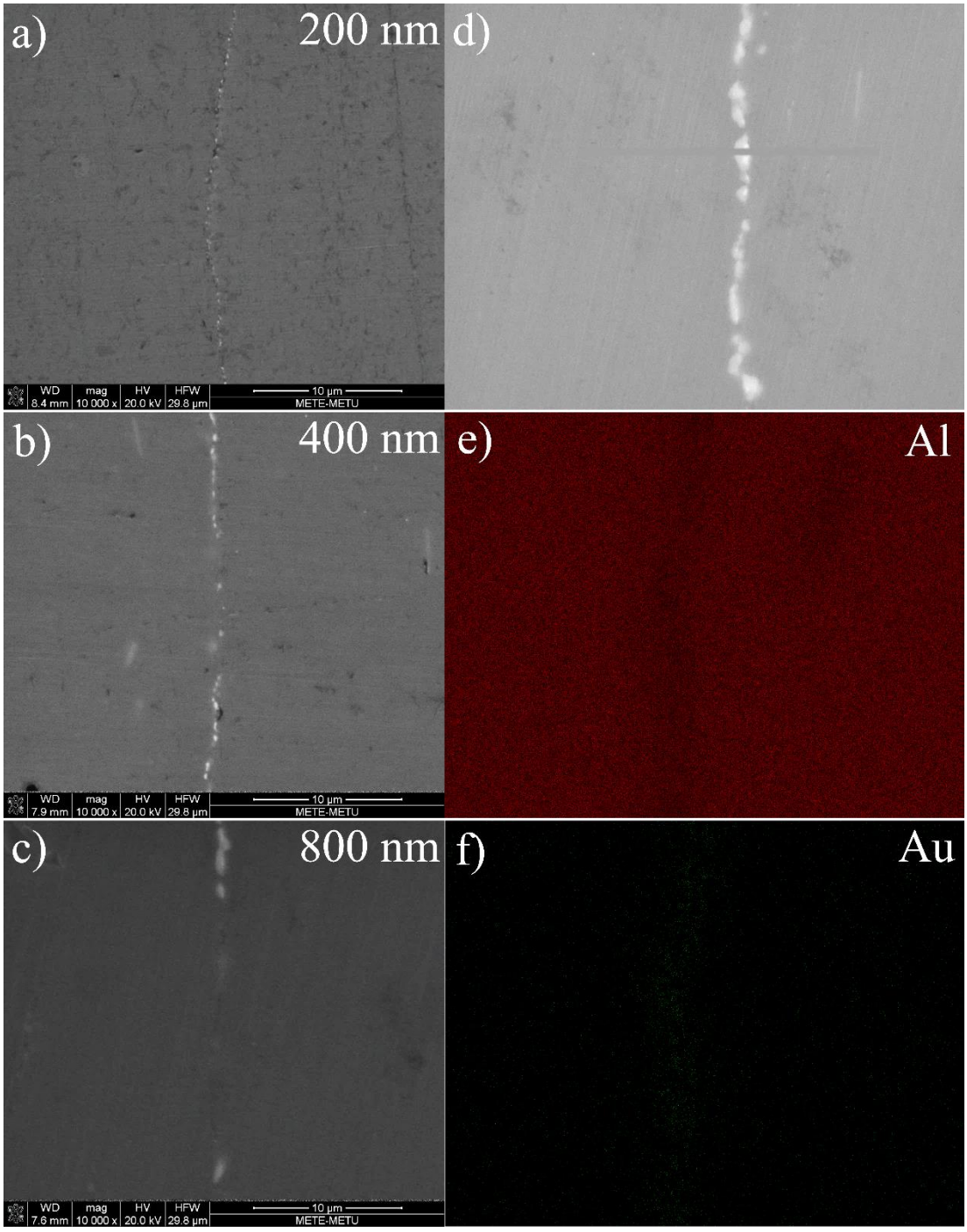

Figure 4. 19. Cross-sectional view for the interface of the diffusion bonded samples with a)200 nm, b) 400 nm, c), d) 800 nm thick gold interlayer along with spatial elemental distribution of e) aluminum, f) gold at the interface.

EDS line scan analysis were also conducted to see the elemental distribution of gold and aluminum along with the major alloying elements magnesium and silicon at the diffusion bond interface. Line scan analysis results in Figure 4.20 were in consistence with the results obtained by elemental mapping. Composition on aluminum was decreased at the bond interface while composition of gold as increasing. The decrease in the aluminum composition gets larger as the gold interlayer gets thicker. Therefore, it can be said that as the initial thickness of the gold interlayer was increased the contact between the aluminum surfaces was decreased.

In the EDS line scan results of the sample having 800 nm gold interlayer, an increase in the magnesium and silicon composition was also observed. Therefore, both major alloying elements of the Al6063 alloy were diffused toward the bond interface during the diffusion bonding. In the case of thinner gold interlayers composition of the silicon remained constant at the bond interface whereas an increase in magnesium composition was still observed but in lower quantities compared to the alloy with 800 nm gold interlayer. It can be said that no silicon diffusion towards to interface was observed in the detection limits of EDS while magnesium diffusion was still observable for alloys with 400 nm and 200 nm gold interlayers. Therefore, presence of a gold interlayer not only impedes the initial contact between two base metals but also causes the diffusion of the alloying elements in this metals towards to bond interface during bonding. The most probable explanation to the diffusion of alloying elements is the formation of an intermetallic phase or phases containing Au, Mg and Si. However, due to their low amount it is impossible to detect these phases with conventional XRD.

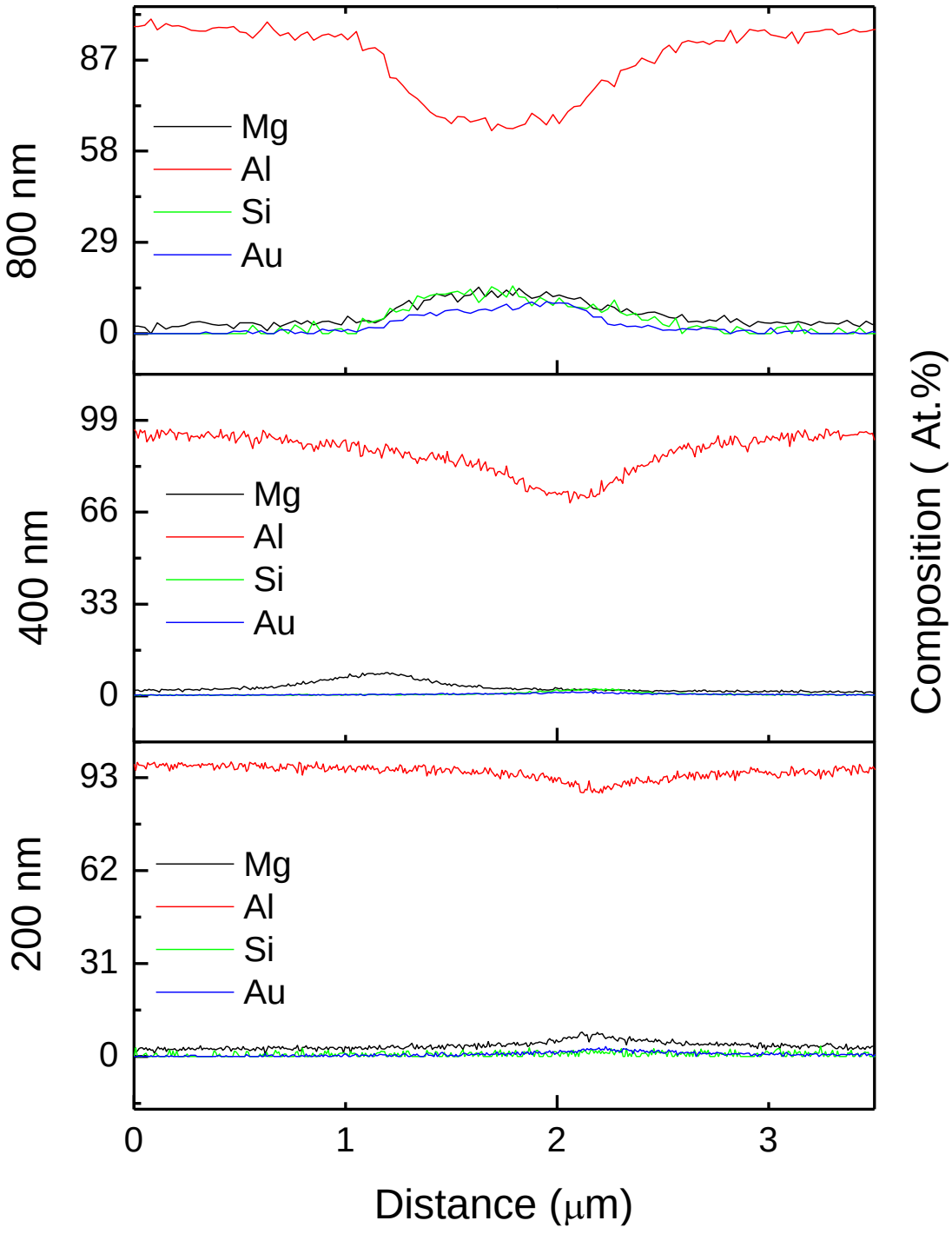

Figure 4. 20. Change in the elemental distributions of Al, Au, Mg and Si through the diffusion bond interface with thickness of the gold interlayer.

Bond strengths of the samples bearing gold interlayers were also measured by shear testing and results were shown in Figure 4.21. Highest bond strength measured was 13.6 MPa for the alloy with 200 nm gold interlayer and decrease in this value was observed as the interlayer thickness increased (Table 4.4). Even the highest obtained strength was very low compared to the strength of the bond without any interlayers. Therefore, presence of a gold interlayer resulted in poor bond strengths due to the prevention of the initial contact between the base metals hence the grain boundary diffusion leading to bond formation. Since the initial contact area decreased as the interlayer thickness was increased, further loss in the bond strengths was observed for the samples prepared with thicker interlayers.

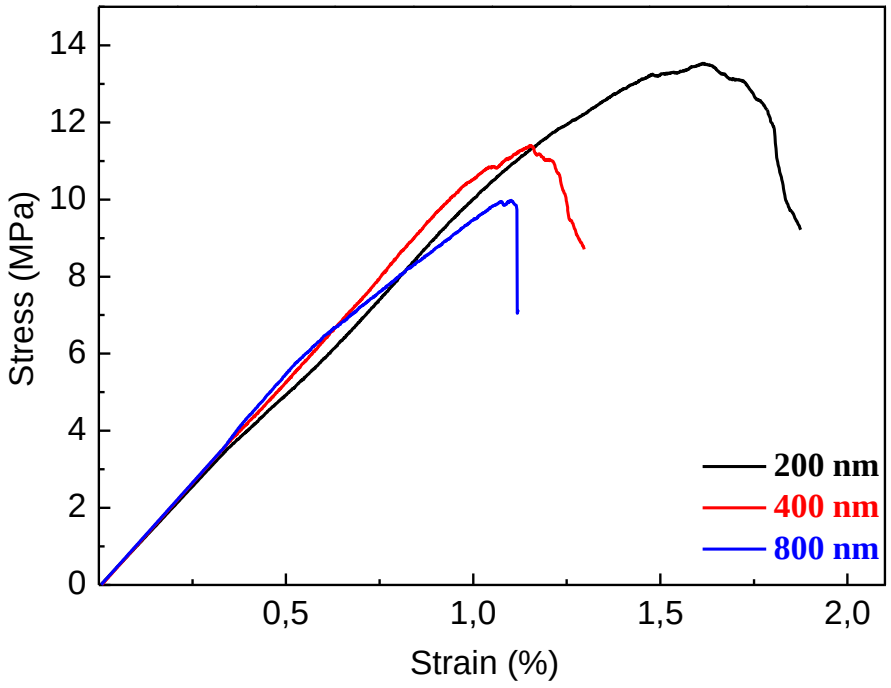

Figure 4. 21. Change in the shear strength of the diffusion bond with gold interlayer thickness.

Table 4. 4. Summary of the shear test results for the samples bearing gold interlayers.

Coating Thickness	σ_{UTS} (MPa)
200 nm	13.6
400 nm	11.5
800 nm	10

Different features were observed for each gold interlayer thickness when their fracture surface were examined. The fracture surface of the sample with 200 nm gold interlayer was similar to the fracture surfaces of the alloys bonded without interlayer. Oval dimples indicating ductile fracture under shear loading were observed along with smooth areas indicating no bonding was occurred at that regions. Small shiny particles were also observed at certain areas of the fracture surface proving the presence of the gold at the interface (Figure 4.22.a, b). Both bonded areas with dimples and unbonded areas were again observed when the interlayer thickness was 400 nm. However, the area covered by the dimples were less and dimples were more shallow compared to the sample with 200 nm gold interlayer. Gold agglomerates were observed on both bonded and unbonded parts of this alloy. The decrease in the bond strength due to the decrease in the bonded area could be explained by the significant increase in the size and amount of the gold particles observed on the bond interface (Figure 4.22.c, d). For the alloy with 800 nm thick gold interlayer grinding scratches from the surface preparation step were still visible in the unbonded regions and no sign of ductile fracture was observed. When the bonded region was examined at higher magnification it was seen that fracture occurred at the gold interlayer meaning that no contact was establishes between the aluminum surfaces through diffusion bonding (Figure 4.22.e, f). Therefore, amount of gold observed on the bond interface was increased as the interlayer thickness was increased resulting in a decrease in the bond strength since it prevents the bond formation between the aluminum alloys.

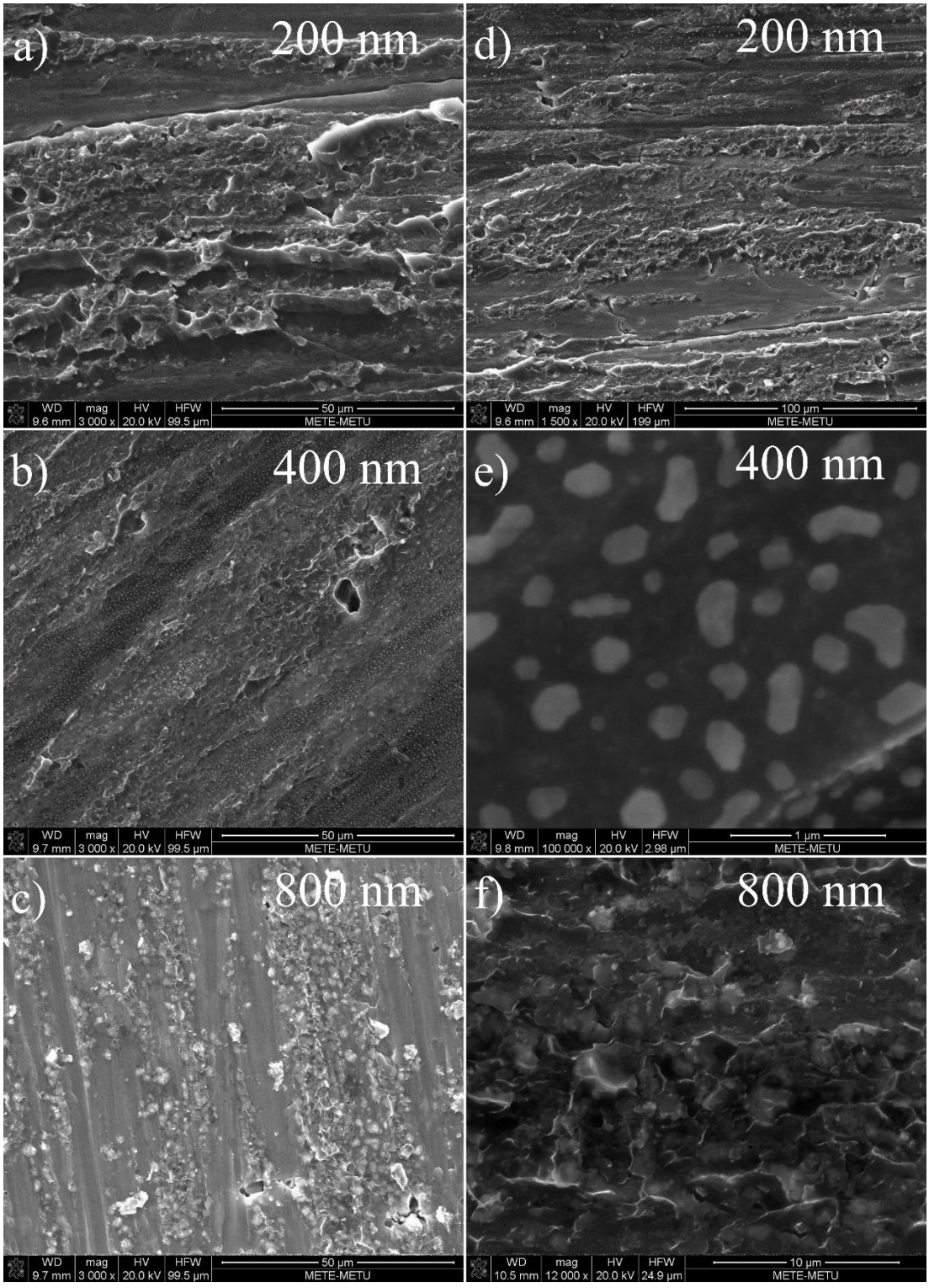

Figure 4. 22. Fracture surfaces of the diffusion bonded samples with a), b) 200 nm, c), d) 400 nm, e), f) 800 nm thick gold interlayers.

4.3. Investigation of the Effect of Alloying Elements

In this part of the study diffusion bonded parts were produced by using the cast alloys of Al6063 before further alloying element addition. Investigations on the as-cast aluminum 6063 sample under SEM revealed a dendritic solidification structure (Figure 4.23.a). Surface of the as-cast sample were prepared with the same method mentioned before and bonding was carried out at 520˚C, under 6 MPa pressure for 3 hours for all the cast samples. During bonding a more homogeneous equiaxed grain structure was formed.

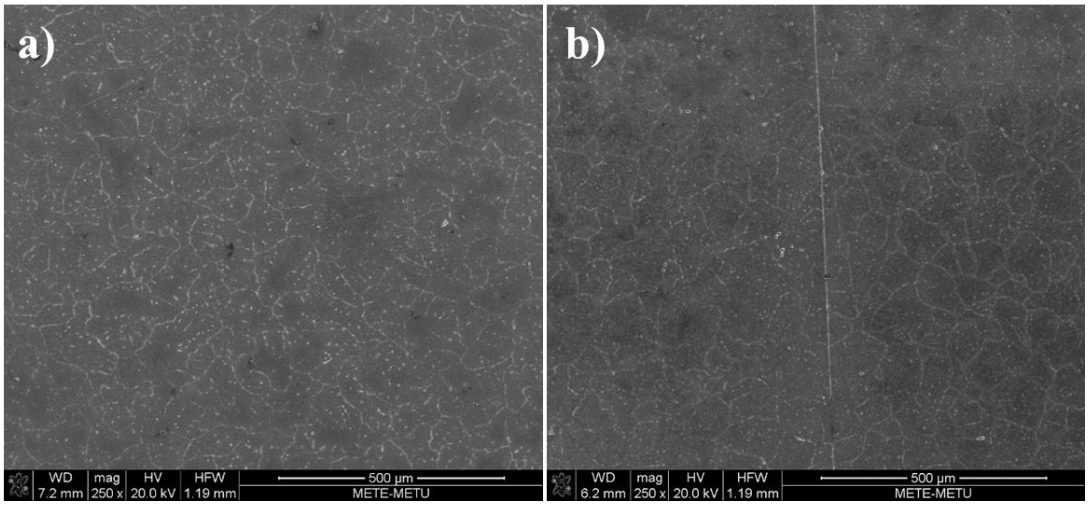

Figure 4. 23. SEM images of the a) as-cast b) diffusion bonded Al6063 alloy.

Average microhardness values were measured to see the effect of diffusion bonding on base metal properties and results were shown in Table 4.5. Due to homogenization and grain growth during DB grain boundary areas in the microstructure was decreased resulting a decrease in the microhardness value of the as-cast alloy.

Shear strength of the bond was also tested and found as 14.4 MPa. Obtained low bond shear strength could be explained by examination on the fracture surface of the diffusion bonded sample. Oval dimples were observed on the fracture surface in Figure 4.24 proving that bond formation has occurred and this bond has fractured in shear

mode. However, there were also some smooth regions in which grinding marks were still present instead of dimples meaning that bond formation has not occurred in these regions. The area covered by these smooth regions were almost the same as the area covered by the bonded regions for these samples which explains the obtained low bond shear strength.

Table 4. 5 Summary of the mechanical properties of cast Al 6063 alloy.

As-Cast Hardness (HV)	Diffusion Bonded Hardness (HV)	Bond Strength (MPa)
76.2	39.9	14.4

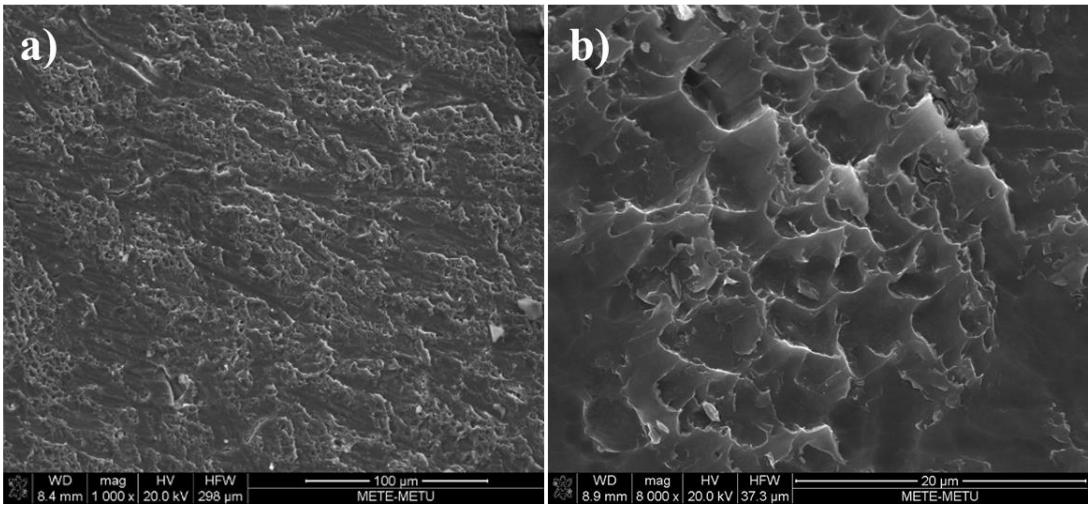

Figure 4. 24. Fracture surface of the diffusion bonded cast Al6063 alloy.

To prevent the loss in the mechanical properties of the base metal and to obtain higher bond strengths by eliminating the inhomogeneity of the bond interface alloying elements were added to the base alloy. Pure copper and tin were added separately as alloying elements and their effect on the properties of the base metal and the diffusion bonding behavior were investigated.

4.3.1. Effect of Copper as Alloying Element

Cast Al6063 alloys containing 0.5, 2.5 and 5 wt. % Cu were cast to investigate the effect of copper as alloying element. It was observed that addition of copper effects both the grain size and grain morphology of the as cast alloy. As cast microstructures of the alloys in Figure 4.25 revealed that grain size was smaller and grains solidified in a more dendritic fashion for the Cu containing alloys. The reduction in the grain size was increasing with increasing copper content due to an increase in the solute content of the alloy. Addition of alloying elements causes an increase in the solute content hence the amount of segregation in the alloy which results in formation of smaller grains by preventing the grain boundary motion [99].

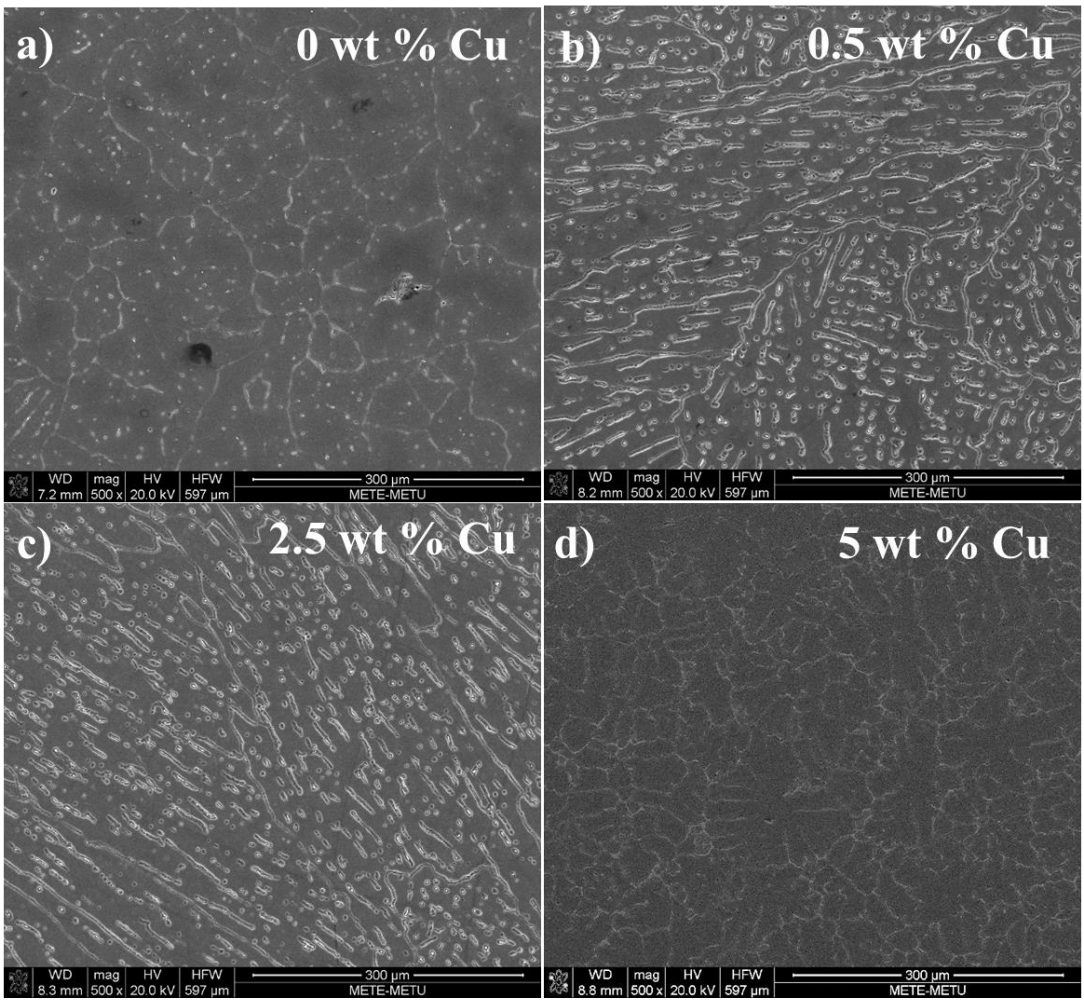

Figure 4. 25 As-cast microstructures of the alloys containing a) 0, b)0.5, c)2.5, d) 5 wt. % Cu.

XRD analysis of the as-cast copper containing samples were conducted to comment on the phases formed during solidification. Only FCC (Al) phase was observed in the detection limits of the XRD analysis of the sample containing 0.5 wt% Cu (Figure 4.26). When Cu composition was increased low intensity $CuAl_2$ peaks were appeared along with the (Al) phase. $CuAl_2$ phase was observed for both 2.5 and 5 wt% Cu containing alloys. Both intensity and number of the $CuAl_2$ peaks were increased as the copper content of the alloy was increased. Therefore, addition of Cu to the Al, Mg, Si

alloy system resulted the formation of $CuAl_2$ phase during solidification when the copper content of the alloy was higher than 0.5 wt%.

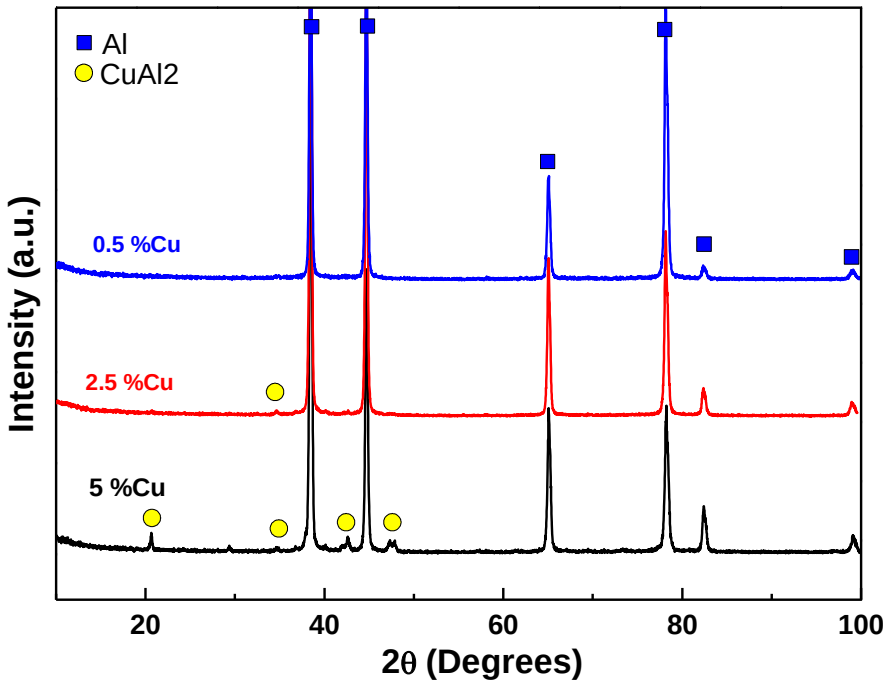

Figure 4. 26. XRD patterns of the 0.5, 2.5, 5 wt% Cu containing Al-Mg-Si alloy in as-cast condition.

The increase in the amount of $CuAl_2$ precipitates with increasing Cu content causes the reduction in the as-cast grain size of the copper containing alloys. As it was mentioned before presence of these precipitates impedes the grain boundary motion and yields formation of smaller grains during solidification.

After initial characterization of the alloys thermal analysis were conducted to investigate if there are any phase transformations during diffusion bonding. Samples were heated up to a temperature lower than the DB temperature due to the limitations forced by the DSC equipment. During the DSC analysis heating and cooling rates were kept as 20 K/min and 60 K/min respectively. Two exothermic peaks were observed in the DSC pattern of the cast Al6063 alloy before the Cu addition (Figure 4.27). For Al,

Mg, Si containing alloys precipitation sequence accepted in the literature was GP zones -β′′- β′- β(Mg2Si). The low temperature exothermic peak in the DSC corresponds to the formation of β′′ precipitate while high temperature peak corresponds to formation of β′ precipitate of Mg_2Si [62].

When Cu was introduced to the system the precipitation sequence of the alloy was altered. In literature formation of either one or both of the GP-θ′′-θ′-θ ($CuAl_2$) and GP-S′-S ($CuMgAl_2$) precipitates were reported for Cu containing Al-Mg-Si alloys [70]. In the DSC patterns of all copper containing samples an exothermic peak was observed at around 240°C corrresponding to the formation of S′ precipitates. Therefore, addition of Cu in to the Al6063 alloy system compeletely changes the age hardening behavior of the alloy by preventing the precipitation of Mg_2Si phases and causing the precipitaion of $CuMgAl_2$ phase instead, during high temperature processing. A low intensity endothermic peak followed by an exothermic one was observed for the 5 wt% Cu containing alloy at 200°C. The endothermic peak corresponds to the dissolution of the precipitates present after the casting and following low intensity endothermic peak accounts for the formation of either GP zones or θ′′ precipitates of $CuAl_2$. Hence, as the copper composition was increased further $CuAl_2$, which is the main age hardening precipitate of the Cu bearing aluminum alloys, starts to form during bonding.

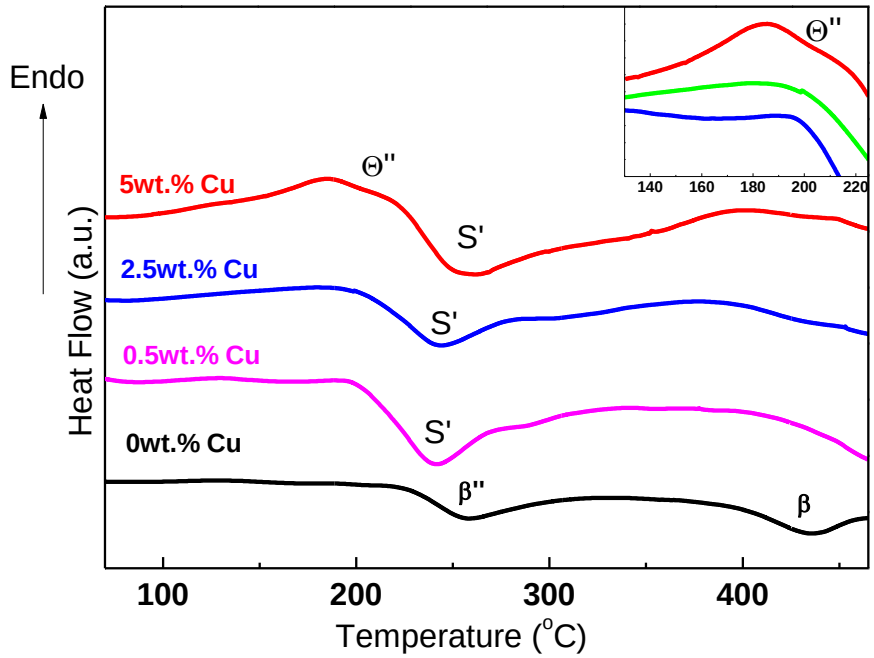

Figure 4. 27. Isochronal DSC curves of 0, 0.5, 2.5, 5wt% Cu containing Al-Mg-Si alloy at 20 K/min.

Microhardness value of the 0.5 wt% Cu containing alloy was lower compared to the copper free alloy but an increase in the microhardness value was observed as the Cu content increased (Figure 4.28). According to the XRD results $CuAl_2$ formation was observed for the 2.5 and 5 wt% Cu containing sample. Therefore, presence of $CuAl_2$ precipitates causes an increase in the microhardness value of the as-cast alloy. 5 wt% Cu containing alloy had higher hardness value than the Cu-free alloy meaning that hardness value continues to increase as the amount of $CuAl_2$ in the alloy increases. Another set of measurements were also conducted after the diffusion bonding to understand the changes on the mechanical properties of the base metal during bonding. A decrease was observed in the microhardness values of all the sample except the alloy containing 5 wt% Cu. As it was already accounted for the copper-free sample homogenization and grain growth causes this decrease in the hardness value. Most significant decrease was observed for the Cu-free sample the reason for that is the hindered grain boundary motion due increase in the solute content caused by the

alloying element addition. Thus, formation of β(Mg2Si), S′($CuMgAl_2$) precipitates did not caused any increase in the hardness of the alloy. When the precipitation sequence has proceeded up to the equilibrium precipitate, strengthening effect of the precipitates has decreases. The microhardness value of the 5 wt% Cu bearing alloy has increased from 88.7 HV to 119 HV (Table 4.6). For this alloy formation of the GP zones of the θ precipitates was observed along with the S′($CuMgAl_2$) precipitates in the DSC analysis. Therefore, GP zones of the θ precipitates resulted a significant increase in the hardness of the alloy during the bonding process. The hardening behavior of the alloy became similar to the that of age hardaneble Cu-bearing aluminum alloys.

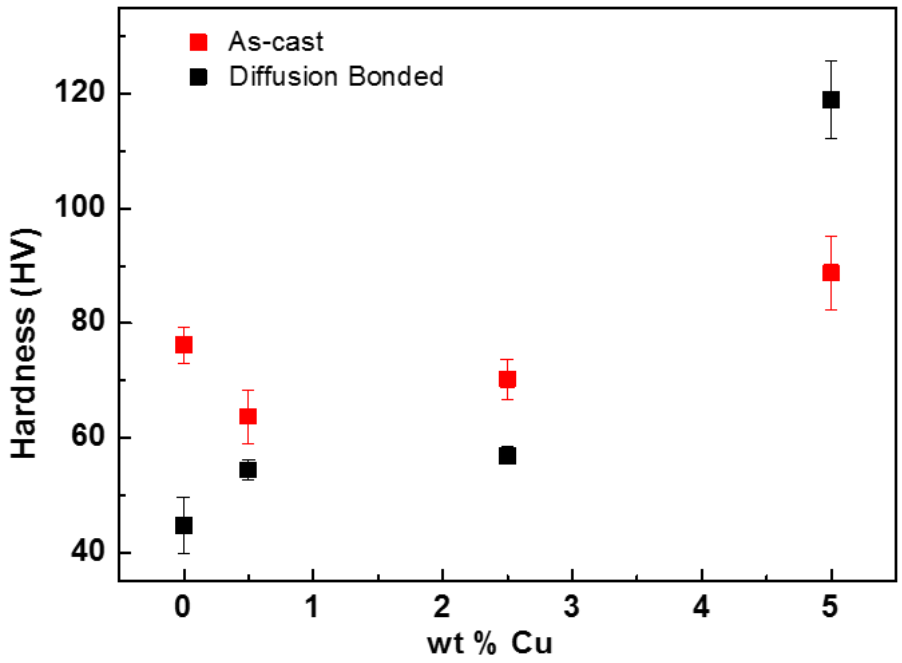

Figure 4. 28. Average microhardness values of the 0, 0.5, 2.5, 5 wt% Cu containing alloys before and after the diffusion bonding.

Bond shear strengths of the Cu alloyed Al-Mg-Si alloy joints were tested and showed in Figure 4.29. Two tests were conducted for each specimen and average was calculated. Bond strengths of the Cu containing alloys were close to the bond strength of the Cu-free alloy. Therefore, addition of copper does not seem to contribute to the

bond strength. Maximum bond strength of 22.6 MPa was obtained for the 2.5 wt% Cu containing sample which is slightly higher than the remaining samples (Table 4.6). Therefore, it can be said that addition of copper to the Al6063 alloy system does not yield any significant increase in case of bond shear strength.

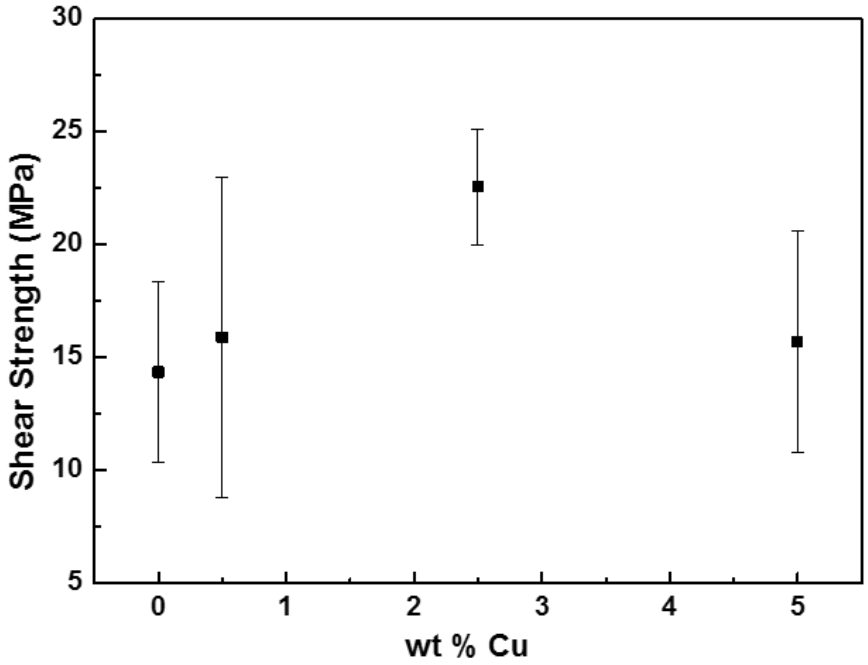

Figure 4. 29. Shear strength of the diffusion bonded joints of 0, 0.5, 2.5, 5 wt% Cu containing Al-Mg-Si alloys.

Table 4. 6 Summary of the mechanical properties of the base metal and diffusion bonded joints of Cu containing Al, Mg, Si alloy.

Alloy	**Microhardness (as-cast) (HV)**	**Microhardness (after DB) (HV)**	**Bond Shear Strength (MPa)**
Al 6063	76.2	44.	14.4
0.5 wt. % Cu	63.7	54.4	15.9
2.5 wt. % Cu	70.2	56.9	22.6
5 wt. % Cu	88.7	119.0	15.7

Fracture surfaces of the samples containing 0, 0.5, 2.5, 5 wt% Cu were shown in Figure 4.30. Similar features were observed on the fracture surfaces of the alloy which is in consistence with the shear test results. Since bond shear strengths were similar fracture surfaces was also expected to be similar. Both bonded and un-bonded regions were observed on the fracture surface of the Cu-free alloy. The unbonded regions remained unchanged when Cu is added to the system and area covered by these un-bonded regions were close to the area covered by the bonded region. Therefore, Cu addition did not prevent the formation of an inhomogeneous fracture surface. Dimples indicating the ductile fracture of the joint were also observed in the bonded areas of these alloys. When these dimples were examined at higher magnifications it was observed that, the size and depth of these dimples were also inhomogeneous for all of the alloys which explains the high deviations on the shear test results of these joints.

It can be concluded that it is possible to prevent the loss in the hardness of the base metal during bonding when it is alloyed with 5 wt% copper. However, it is not possible to obtain higher bond shear strengths for diffusion bonded joints of Al-Mg-Si alloy unless, the inhomogeneity on the bond interface were eliminated.

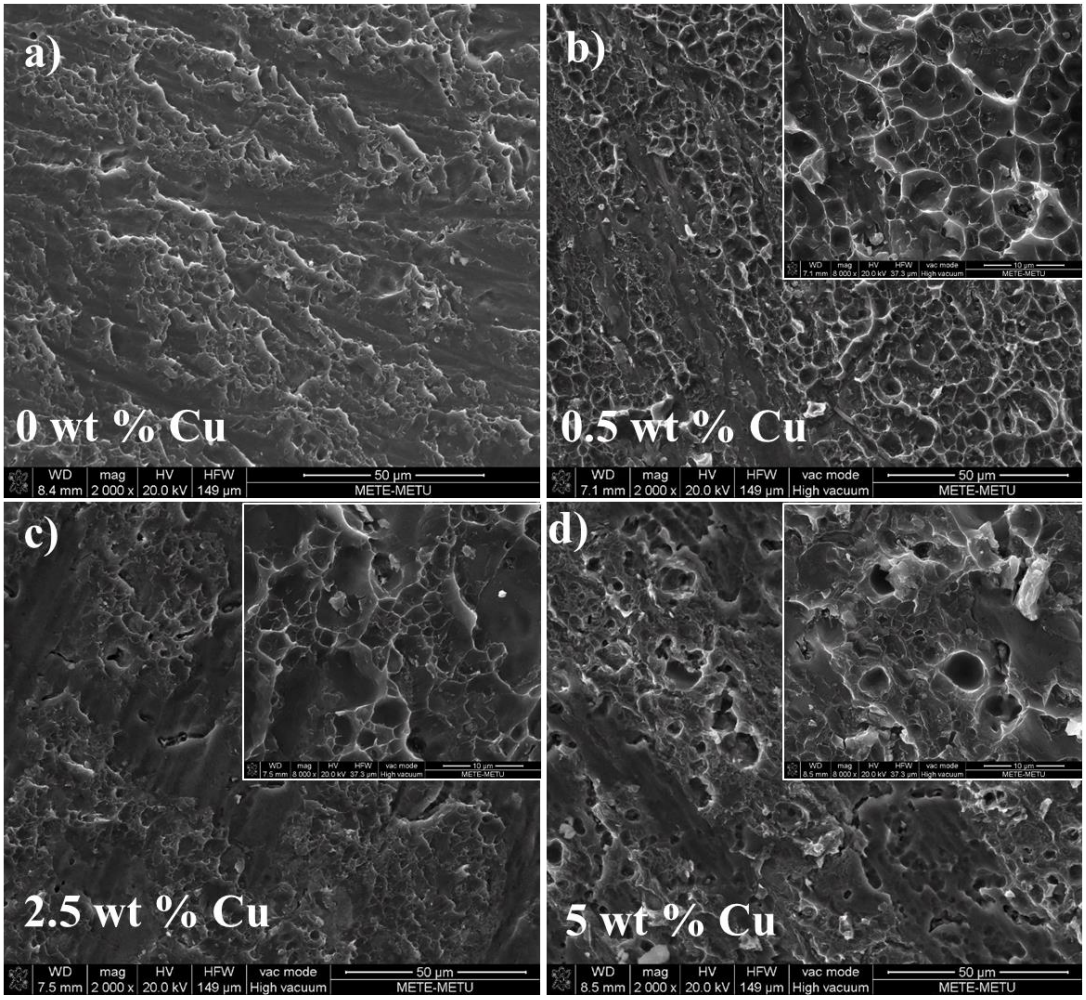

Figure 4. 30. Fracture surface of the diffusion bonded joint of a) 0, b) 0.5, c) 2.5, d) 5 wt% Cu bearing Al-Mg-Si alloy.

4.3.2. Effect of Sn as Alloying Element

As-cast microstructures of the 0, 0.5, 2.5, 5 wt% Sn containing Al, Mg, Si alloys were shown in Figure 4.31. As in the case of copper, addition of Sn also yielded the reduction of the as-cast grain size. Since, all the casting parameters were identical, the reason of this reduction was again the hindrance of the grain boundary motion due to the increase in the segregation of the solute atoms in the alloy. It was reported in the literature for many system introducing alloying elements causes an increase in the

solute content of the alloy. As a result, segregation at the grain boundaries increases [66].

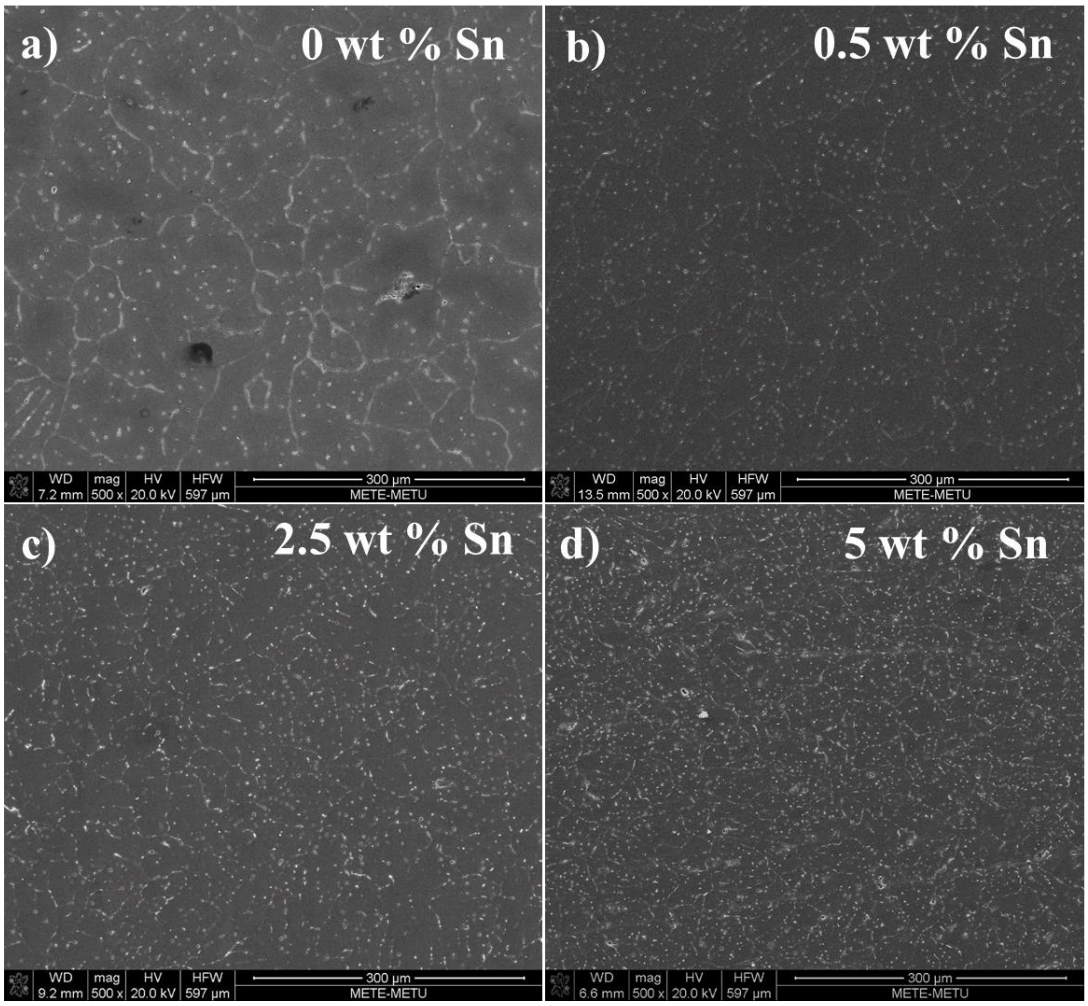

Figure 4. 31. As-cast microstructure of a) 0, b)0.5, c)2.5, d) 5 wt% Sn containing Al-Mg-Si alloy.

XRD analysis conducted on the as-cast samples are shown in Figure 4.32. Low intensity Mg_2Sn peaks were observed in the XRD pattern of the 0.5 wt% Sn containing alloy apart from the FCC-(Al) peaks indicating the formation of Mg_2Sn phase during solidification of this alloy. When the Sn composition was increased further amount and number of Sn bearing phases in the alloy also increased. (Sn) formation was also

observed along with FCC-(Al) and Mg_2Sn phases during solidification of both 2.5 and 5 wt% Sn containing alloys. Sn rich phases appear brighter in the as-cast microstructures of the alloys observed under SEM due to high atomic number of tin. Increase in the amount of these brighter phases were clearly observed in the microstructures for higher Sn compositions. This is accompanied by an increase in the intensity of the both (Sn) and Mg_2Sn peaks in the XRD pattern of the alloys. Mg_2Sn and Sn formation was reported in the literature when Sn is added as alloying element to the Al-Mg-Si system [73]. The data obtained in this study was also proved that the addition of Sn to the Al-Mg-Si alloy system triggers the formation of Mg_2Sn phase when Mg and Sn composition are close to each other and further increase in the tin composition yield to formation of (Sn) phase in addition to the Mg_2Sn.

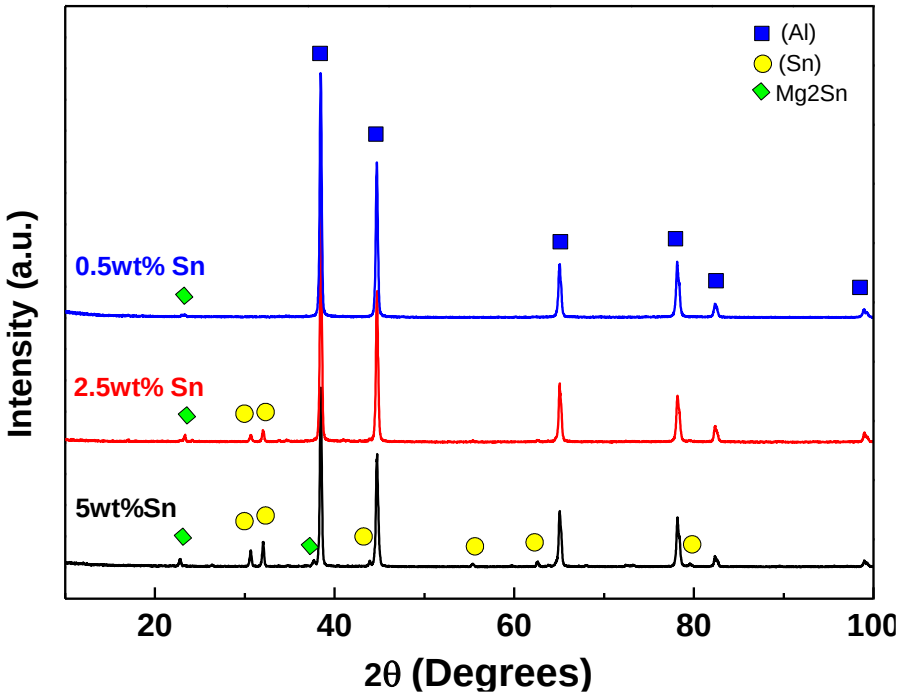

Figure 4. 32. XRD patterns of the 0.5, 2.5 and 5 wt% Sn containing Al-Mg-Si alloys in as-cast condition.

Average microhardness values of the alloys were measured in as cast condition and showed in Figure 4.33 Addition of Sn to the Al-Mg-Si system caused a decrease in the

hardness of the alloy in as-cast condition. Comparison among the Sn bearing alloys showed an increasing trend in the microhardness value with increasing Sn composition. This increase is caused by the increase in the amount of Mg_2Sn phase formed during solidification with increasing Sn content. Even though this is the case, microhardness values of the Sn containing samples were never reach up to the microhardness values of the Sn-free alloy.

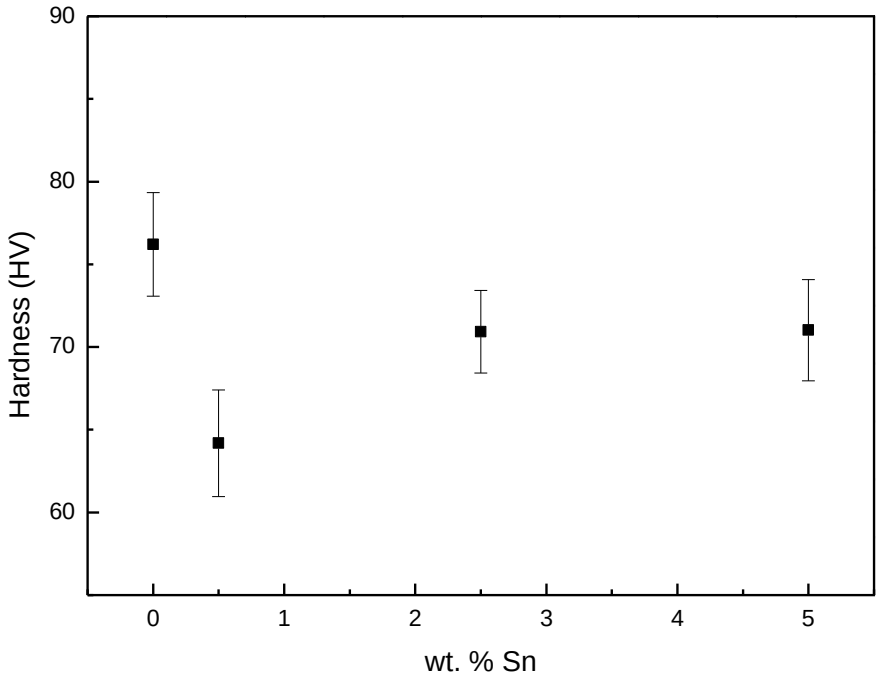

Figure 4. 33. Average microhardness values of the 0, 0.5, 2.5 and 5 wt% Sn containing Al-Mg-Si alloys in as-cast condition [100].

DSC analysis were conducted by heating the specimens up to 500°C at a rate of 20K/min to see the phase transformations occurring in the Sn containing alloys during the heating and cooling cycles of the DB process. In Figure 4.34 an endothermic reaction was observed in the DSC patterns of Sn bearing samples at 203°C corresponding to the eutectic transformation in the Mg-Sn phase diagram (Figure 2.19). Thus, formation of a local liquid phase due to melting of (Sn) phase was expected when Al-Mg-Si system is alloyed with Sn. Intensity of this melting signal

was higher for higher Sn compositions caused by the increase in the amount of (Sn) phase. Although very low in intensity, the endothermic peak was still seen for the 0.5 wt% Sn alloy indicating presence of (Sn) phase in this alloy at an amount that is below the detection limit of conventional XRD.

Two exothermic peaks were observed at around 250 and 435°C. As it was mentioned among them the low temperature peak belongs to β' precipitation, while the high temperature peak belongs to β (Mg_2Si) precipitation. In this study, these two peaks were observed in the DSC patterns of in 0 and 0.5 wt% Sn containing alloys and disappear with increasing Sn content. Due to similar crystal structures of Mg_2Sn and Mg_2Si, Sn is known to replace Si in Mg_2Si and results the formation of Mg_2Sn during solidification [73]. Therefore, increase in the amount of Mg_2Sn formed during solidification accompanied by the decrease in the amount of free Mg in the alloy. When all of the Mg present in the alloy is employed in the formation of Mg_2Sn, Mg_2Si cannot be formed during aging and alloy loses its precipitation hardening ability. That is to say, alloys cannot be precipitation strengthened after the applied diffusion bonding process. Therefore, a limiting composition was present to preserve the age hardening ability of the alloy and this composition was found to be approximately 2.5 wt% Sn due to low intensity of Mg_2Si exothermic precipitation signals.

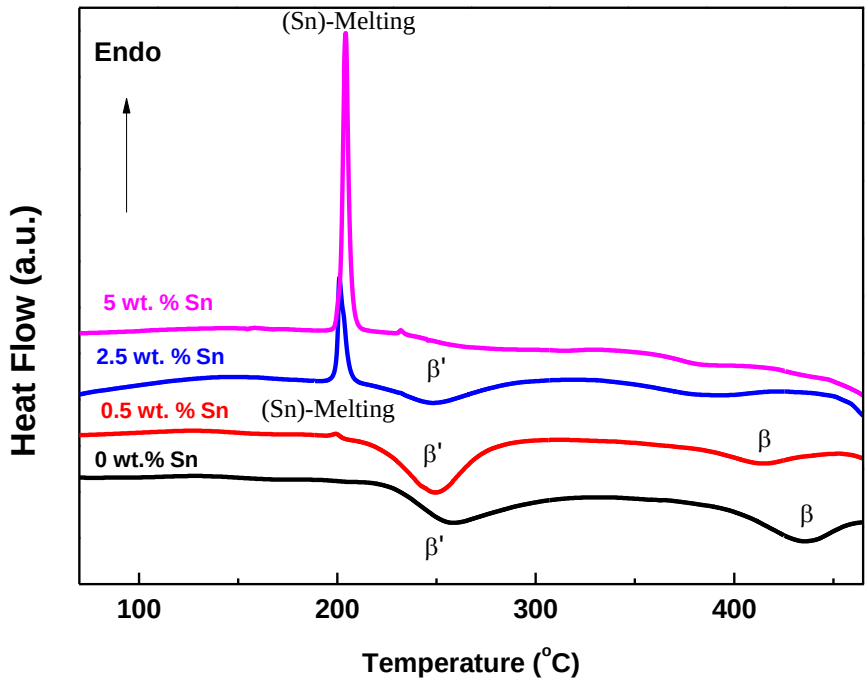

Figure 4. 34. Isochronal DSC traces of the 0, 0.5, 2.5 and 5 wt% Sn containing Al-Mg-Si alloys at 20 K/min [100].

After diffusion bonding process, both microstructural examination and microhardness measurements were conducted on the cross-section of the bond interface. The microstructural view of the Sn-free sample after bonding shows insufficient bonding with pore formation at the bond interface (Figure 4.35.a). However, for 5 wt% Sn containing alloy formation of a new phase was observed at the bond interface. A local liquid (Sn) phase formation was observed in the DSC analysis of the Sn containing samples. EDS analysis proved that the observed phase at the bond interface was a Sn rich phase spread through the interface (Figure 4.35.b).

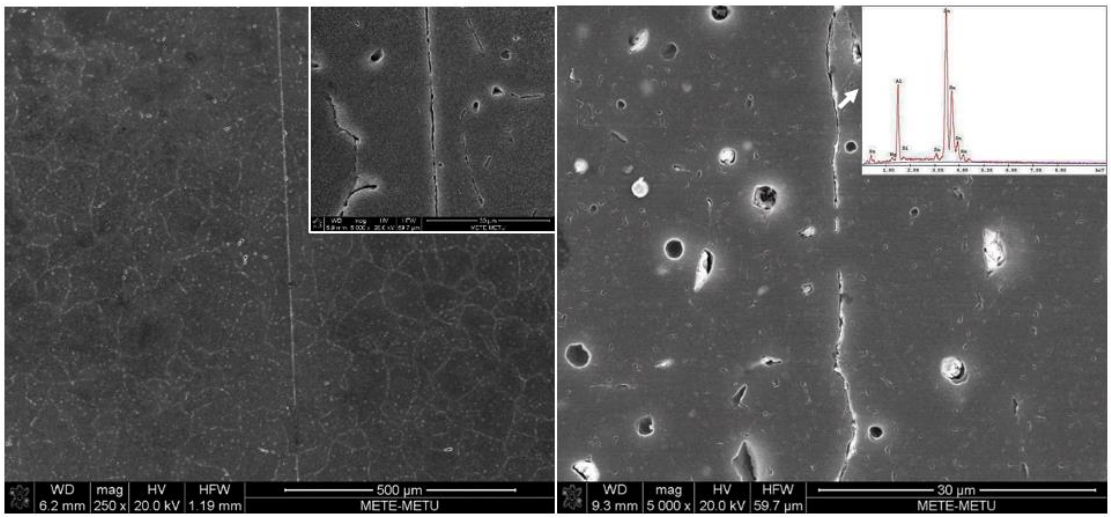

Figure 4. 35. Diffusion bonded microstructures of the a) 0 wt% and b) 5 wt% Sn containing Al-Mg-Si alloys [100].

Previous findings in the literature suggests that, as the mechanical properties of the diffusion bond approaches to the mechanical properties of the base metal it is possible to talk about the formation of a solid bond [37]. Microhardness measurements were conducted to the diffusion bonded samples and results were shown in Figure 4.36. Diffusion bonded microhardness profile of the Sn-free alloy revealed a significant decrease at the bond interface which can be attributed to the insufficient bond formation. This decrease in the hardness value can be explained by the pore formation observed in the cross-sectional view of the bond interface of this alloy. Microhardness profiles of the Sn containing alloys showed a constant trend throughout the sample. Hardness of the diffusion bonds were close to the hardness of base metal indicating the formation of a solid bond for these samples.

Microhardness values after the bonding were significantly lower compared to the hardness values of these alloys in as-cast condition (Table 4.7). Most significant decrease was observed for the Sn-free alloy due to homogenization of the grains during diffusion bonding cycle. Among the Sn-bearing samples the highest microhardness value after diffusion bonding was observed for the 0.5 wt% Sn containing alloy. The

hardness of this alloy after bonding was also close to the hardness value measured in as-cast condition. As it was mentioned in the DSC analysis as the Sn content of the alloy increases the exothermic signal indicating the precipitation of the Mg_2Si phase diminishes. That is to say, alloy loses its precipitation hardening ability since all Mg available was used to form Mg_2Sn during solidification. The loss of the precipitation hardening ability is accompanied by a significant decrease in the hardness of the base metal after the diffusion bonding process applied.

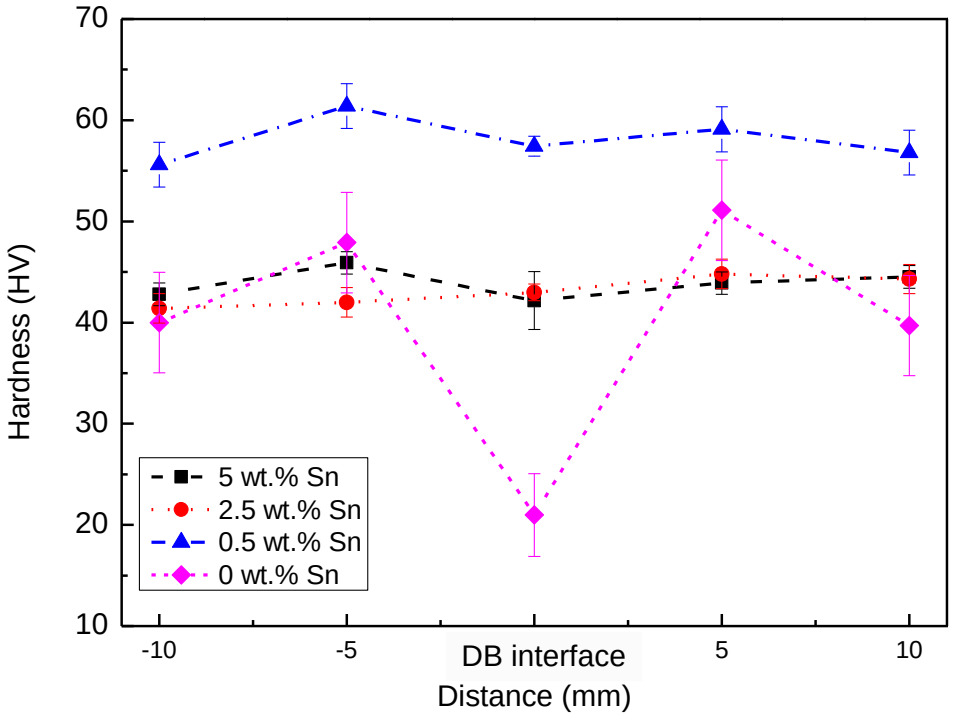

Figure 4. 36. Microhardness profiles of the 0, 0.5, 2.5 and 5 wt% Sn containing Al-Mg-Si alloys across the bonded interface after DB process [100].

Shear strengths of the bonds were measured and an increasing trend with increasing Sn content was observed (Figure 4.37). Bond strengths of the Sn bearing samples were almost two times higher compared to bond strength of the Sn-free sample. The low bond strength obtained for this alloy can be explained by both porous structure of the bond interface and the decrease in the microhardness profile. When 5 wt% Sn was

added to this alloy shear strength was increased from 14.4 to 29.0 MPa. Therefore, Sn rich phase observed at the bond interface causes an increase in the bond strength of the alloy. The difference between the bond strength values of the Sn containing alloy was not significant. Thus, addition of Sn to the Al-Mg-Si system yields to formation of bond with higher strengths.

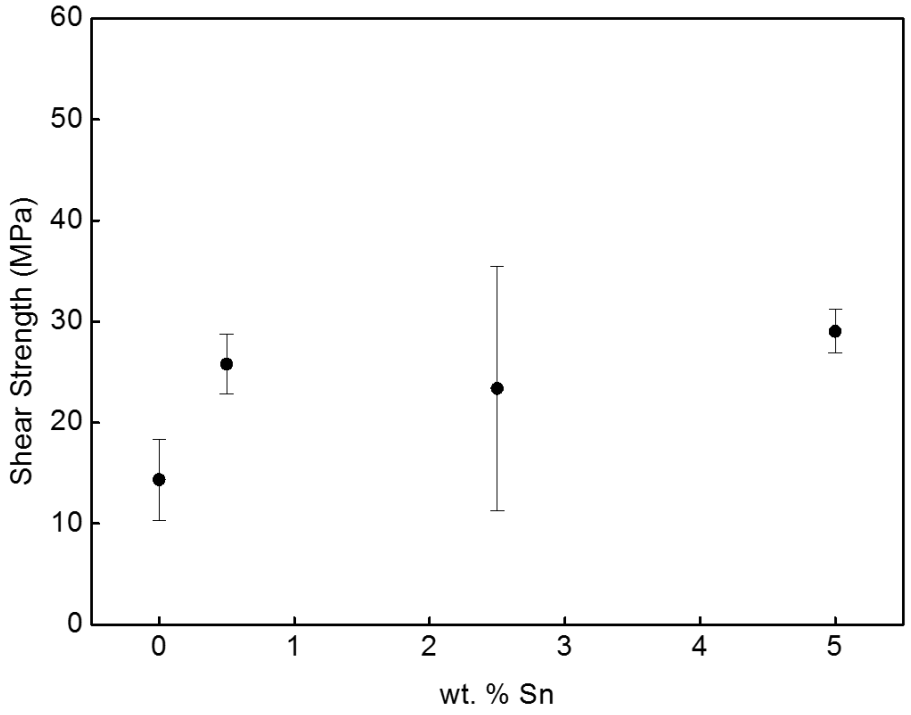

Figure 4. 37. Shear strengths of diffusion bonded joints of the 0, 0.5, 2.5 and 5 wt% Sn containing Al-Mg-Si alloys [100].

Table 4. 7 Summary of the mechanical properties obtained before and after DB of the 0, 0.5, 2.5 and 5 wt% Sn containing Al-Mg-Si alloys.

Alloy	Microhardness (as-cast) (HV)	Microhardness (after DB) (HV)	Bond Shear Strength (MPa)
0 wt. % Sn	76.2	44.7	14.4
0.5 wt. % Sn	64.2	58.2	25.8
2.5 wt. % Sn	71.0	43.1	23.4
5 wt. % Sn	71.0	44.3	29.0

Fracture surfaces of the Sn containing samples were examined after shear testing and SEM micrographs were shown in Figure 4.38. The unbonded regions causing poor bond shear strengths for both unalloyed and Cu containing samples were eliminated when Sn is added as alloying element to the Al-Mg-Si system. DSC results indicated formation of a local liquid phase during the bonding. This liquid phase was spread through the interface under the applied load and lead to a more uniform bond formation hence, a more homogeneous fracture surface.

Fracture surface of the 0.5 wt% Sn containing sample consists of homogeneously distributed oval dimples. Therefore, a solid uniform diffusion bond was obtained and fractured in a ductile manner under shear load for this sample. For higher Sn compositions cleavage planes starts to appear on the fracture surface along with the oval dimples. Therefore, a transition was observed in the fracture mode of the alloy when Sn content was higher than the 0.5 wt%. Both XRD and DSC results suggests that increase in the amount of local liquid phase was expected when the Sn content was increased. When, the amount of liquid phase was increased the Sn rich layer at the bond interface gets thicker. Relatively high cooling rate applied after the bonding caused rapid solidification of this (Sn) layer. As a result, cracks are also observed on the fracture surface of these two samples.

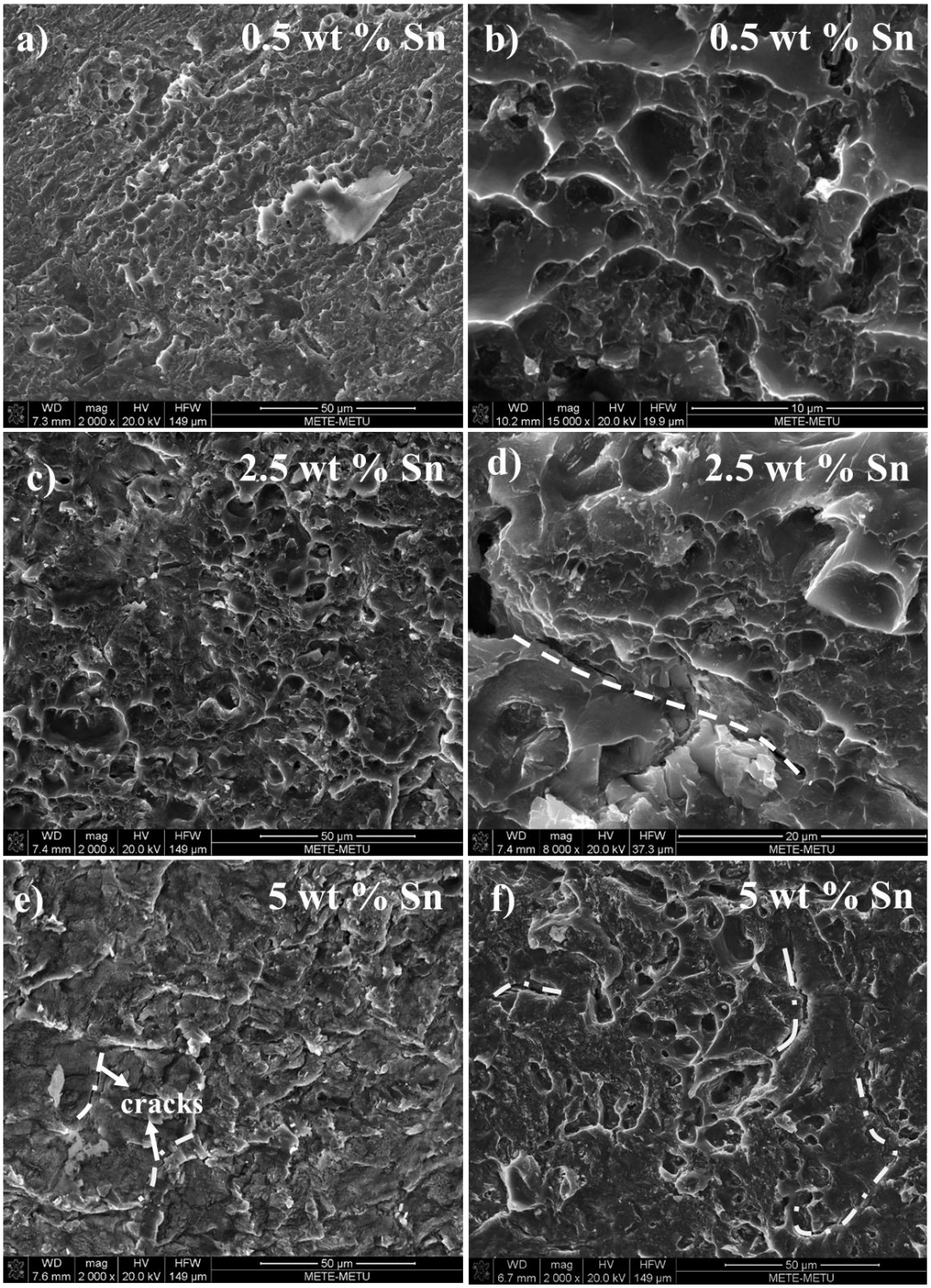

Figure 4. 38. Fracture surface of the diffusion bonded a), b) 0, c), d) 2.5 and e), f) 5 wt% Sn containing Al-Mg-Si alloy [100].

It can be concluded that 0.5 wt% Sn addition to the Al6063 alloy does not give the highest bond strength but maintaining the properties of the base material during the bonding is also as important as the bond strength. When the Sn content was higher than the 0.5 wt% loss in the precipitation hardening behavior and transition in the fracture mode were observed. Therefore, 0.5 wt% Sn containing alloy gives the optimum results in terms of bond strength and preservation of the properties during diffusion bonding.

CHAPTER 5

CONCLUSION

In this study, it has been shown that properties of the diffusion bonded joints are closely controlled by the applied bonding parameters. Wrought Al 6063 alloys were used for the optimization experiments, and the effect of pressure, temperature and time on the bond shear strength was investigated. Increasing the time, temperature and pressure during diffusion bonding was found to increase the shear strength of the produced joint. Pressure increase yields higher bond strengths due to larger initial contact area caused by the higher deformation of the surface asperities. Increase in the temperature was found to be more effective compared to the increase in pressure and time due to exponential dependence of the atomic diffusion to temperature. Maximum bond shear strength of 32.3 MPa was obtained when samples were diffusion bonded under 13 MPa pressure at 520°C for 3 hours and cooled in the furnace.

High temperature processing and furnace cooling applied during the optimization experiments resulted in changes in both the mechanical and structural properties of the alloy. Hardness of the base metal dropped from 106 HV to 40 HV after diffusion bonding due to dissolution and coarsening of the Mg_2Si precipitates and grain growth. To prevent this degradation air cooled specimens were produced with same bonding parameters. Bond strength of the air cooled specimen was found as 39.9 MPa and hardness of the base alloy after the bonding was measured as 77 HV. Therefore, higher cooling rates yield higher mechanical properties of both the base metal and the joint. Although, hardness of the air cooled samples were higher than that of the furnace cooled ones, they are still lower than the initial hardness of the base alloy. To minimize the deterioration of the properties of the base metal, both bonding time and temperature should be minimized.

To achieve this several interlayer materials were applied to the bond interface to act as a diffusion source, and their effect on the bond formation was investigated. Use of silver nanowires either in the form of self-standing films or in suspension with ethanol resulted in failure in the bond formation. Investigation of the samples prepared with ethanol-silver nanowire suspension as interlayer material was shown to form agglomeration of the silver nanowires at some parts creating irregularities at the bond interface. Use of self-standing films of silver nanowires was also not successful due to high waviness of the film surface. Therefore, bond formation via diffusion was suppressed due to low contact area. It was concluded that the interlayer material used in diffusion bonding should be smooth and free from irregularities.

Nickel flakes were also used as interlayer material, since they are expected to meet these criteria. Consequently, successful bonding with a bond shear strength of 21.8 MPa was achieved. After the bonding the observed interlayer consisted of elongated nickel flakes and air gaps in between them. Failure of the joints occurred due to widening of these air gaps and resulted in a low bond strength compared to interlayer material-free joint. Thus, to obtain higher bond strengths interlayer material should be more intact.

Lastly, gold was sputter coated in three different thickness as interlayer material. Although, joint formation was observed when gold is used as interlayer material, obtained bond shear strengths were very low. Maximum bond strength of 13.6 MPa was measured for the sample with 200 nm gold interlayer, and a decreasing trend in the bond strength was observed with increasing interlayer thickness. Elemental mapping and fractography analysis conducted on these samples revealed that presence of the gold interlayer prevented the contact between the two aluminum surfaces, and hence, retarded the bond formation. It can be concluded that use of the interlayer materials either prevented the bond formation or resulted in low bond strengths.

As a part of this study, cast Al 6063 alloys were also produced and diffusion bonded. Bonding was carried out under 6 MPa pressure at 520˚C for 3 hours for all of the cast samples based on the results obtained in the initial optimization part of this study. After

bonding, microhardness of the cast alloy decreased from 76.2 HV to 39.9 HV due to homogenization and growth of the grains. Bond strength of the cast alloy was measured as 14.4 MPa. The low bond strength achieved was found to be caused by the presence of unbonded regions, when the fracture surface of the alloy has been examined. To prevent the loss in the strength of the base metal as well as to increase the bond strength Cu and Sn were added separately as alloying elements, and their effects on the properties of the base metal and its diffusion bonding behavior were investigated.

Addition of Cu was accompanied by the formation of Cu_2Al phase during solidification, the amount of which increased with increasing Cu content. Increase in the segregation as a result of the increase in the solute content resulted in decrease in the as-cast grain size. Therefore, grain size of the alloys was found to be decreasing with increasing Cu content leading to increase in the as-cast hardness. Precipitation of $CuMgAl_2$ was observed instead of Mg_2Si for all Cu containing alloys during the diffusion bonding cycle. DSC results showed formation of the GP zones of the $CuAl_2$ for 5 wt% Cu containing sample which justifies the increase in the hardness of the alloy from 88.7 HV to 119 HV after diffusion bonding. Mechanical characterization of the diffusion bonded parts revealed that Cu addition does not contribute to the bond strength of the cast Al-Mg-Si alloy. Both fracture surfaces and measured bond strengths were similar to those of Cu-free alloy. Consequently, addition of Cu to the Al 6063 alloy system eliminated the decrease in the base metal strength during the bonding cycle when the Cu amount was 5 wt%, yet obtained low bond strengths were remained unchanged.

When Sn was added as alloying element, formation of Mg_2Sn phase was observed for similar Mg and Sn contents. Further increase in the Sn content resulted in the formation of additional (Sn) phase which caused the formation of a liquid phase at 203 °C. According to DSC results, amount of this liquid phase is directly related to the amount of the (Sn) phase formed during solidification. Precipitation hardening ability of the alloy disappeared as the amount of Sn introduced into the system was increased, since

Mg available to form Mg_2Si is used for the formation of Mg_2Sn phase. Therefore, increase in the strength of the alloy via aging cannot be achieved. Mechanical characterization of the joints revealed that shear strength of the diffusion bonded joints increases as more Sn is introduced into the system. The unbonded regions observed on the fracture surface of the as-cast Al 6063 alloy were eliminated by Sn addition due to formation of a local liquid phase. For 2.5 and 5 wt% Sn containing alloys a significant decrease in the hardness value of the base metal was observed due to the loss in the precipitation hardening ability of the alloys, and fracture mode was found to transform from ductile to mixed fracture due to the liquid (Sn) phase spread through the interface during the diffusion bonding process. Considering all of these results 0.5 wt% Sn containing alloy was found to be the best choice for diffusion bonding, as it provides higher bond strength compared to Sn-free alloy without deteriorating the strength, age hardening ability and ductile fracture behavior of the alloy.

Further studies are recommended for the future to comment thoroughly on the diffusion bonding behavior of the Al 6063 alloy to be used in electronics cooling systems.

- Thermal conductivity is one of the most important properties for a part to be used in cooling systems. Therefore, thermal conductivity measurements of the produced parts are required once a diffusion bond suitable in terms of mechanical properties is obtained.
- For liquid cooled systems corrosion resistance of the alloy is also important. Corrosion tests can be conducted on the diffusion bonded parts in case they are integrated into a liquid cooled system.
- Due to their low amount precipitates were hard to detect with conventional XRD. Transmission electron microscopy (TEM) studies of the bonded samples are required to better differentiate the phases formed during the bonding process.
- In-situ synchrotron experiments would be beneficial for better understanding of the phase transformations which occur during the diffusion bonding cycle.

- Addition of Cu as alloying element led to an increase in the base metal properties, and addition of Sn increased the bond strength. Therefore, using the 0.5 wt% Sn containing alloy as an interlayer for the diffusion bonding of 5 wt% Cu containing alloy could be considered to increase the strength of both the base metal and diffusion bond simultaneously.

REFERENCES

[1] A. Kraus, A. Bar-Cohen, and A. A. Wative, “Cooling Electronic Equipment,” *Mech. Eng. Handb. Energy Power Third Ed.*, vol. 4, pp. 371–420, 2006.

[2] M. Ohadi and J. Q. J. Qi, “Thermal management of harsh-environment electronics,” *Twent. Annu. IEEE Semicond. Therm. Meas. Manag. Symp. (IEEE Cat. No.04CH37545)*, 2004.

[3] J. B. Marcinichen, J. a. Olivier, N. Lamaison, and J. R. Thome, “Advances in Electronics Cooling,” *Heat Transf. Eng.*, no. May 2015, pp. 434–446, 2012.

[4] N. Espinosa, “Electronics in Industrial How to Properly Cool Electronics in Industrial Applications,” *Processcooling*, no. May, pp. 18–23, 2014.

[5] R. K. Shah, E. C. Subbarao, and R. A. Mashelkar, *Heat Transfer Equipment Design*. Taylor & Francis, 1988.

[6] B. M. Galitseyskiy, “Fundamentals of the Heat Transfer Theory,” in *Mechanical Engineering, Energy Systems and Sustainable Development–Vol.II*, .

[7] A. Laval, “The theory behind heat transfer,” *Nursing standard : official newspaper of the Royal College of Nursing*, vol. 10, no. 39. p. 20, 1996.

[8] I. Obinelo, “Thermal Design in Electronics Packaging.” Degree Controls Inc., 2004.

[9] A. Bar-cohen and K. J. L. Geisler, “Cooling the Electronic Brain,” *Mechanical Engineering*, pp. 38–41, 2011.

[10] S. V. Garimella *et al.*, “Thermal challenges in next generation electronic

systems- Summary of panel presentations and discussions," *IEEE Trans. Components Packag. Technol.*, vol. 25, no. 4, pp. 569–575, 2002.

[11] A. S. Mujumdar and K. Ravi, "ME6204 Convective Heat Transfer Thermal Management of Electronic Components Needs of thermal management for electronic Major Causes of Electronic Failures," no. January, 2006.

[12] "Thermal Design Considerations," in *IC Packages*, Philips Semiconductors, 2000.

[13] R. Manglik, *Heat Transfer Fluid Flow Data Books Vol. II*. Genium Publishing Corporation.

[14] C. A. Soule, "Future trends in heat sink design," *Electronics Cooling*, 2001.

[15] J. Schulz-Harder, "Review on Highly Integrated Solutions for Power Electronic Devices," *5th Int. Conf. Integr. Power Syst. (CIPS), 11-13 March 2008, Nuremberg, Ger.*, pp. 1–7, 2008.

[16] A. Moses, "Heatsink Theory Guide," *Electronics Cooling*, 2002.

[17] A. Dziubi and A. Gontarz, "A New Method for Producing Finned Heat Sinks for Electronic Applications," no. 4, pp. 74–77, 2014.

[18] "Heat Sink Manufacturing Technologies," *Qpedia*, pp. 1–14, 2013.

[19] M. Iyengar, "Design For Manufacturability Of Forced Convection Air Cooled Fully Ducted Heat Sinks," *Electronics Cooling*, 2007.

[20] S. Ashman and S. G. Kandlikar, "A Review of Manufacturing Processes for Microchannel Heat Exchanger Fabrication," *ASME 4th Int. Conf. Nanochannels, Microchannels, Minichannels, Parts A B*, vol. 2006, pp. 855–860, 2006.

[21] D. J. Stephonson, Ed., "Diffusion Bonding 2," 1991, p. 304.

[22] Y. Miwa, K. Noishiki, T. Suzuki, and K. Takatsuki, “Manufacturing technology of diffusion-bonded compact heat exchanger (DCHE),” *R D Res. Dev. Kobe Steel Eng. Reports*, vol. 63, no. 2, pp. 23–27, 2013.

[23] S. K. Mylavarapu, X. Sun, R. N. Christensen, R. R. Unocic, R. E. Glosup, and M. W. Patterson, “Fabrication and design aspects of high-temperature compact diffusion bonded heat exchangers,” *Nucl. Eng. Des.*, vol. 249, pp. 49–56, 2012.

[24] B. Derby and E. Wallach, “Theoretical model for diffusion bonding,” *Met. Sci.*, vol. 16, no. January, pp. 49–56, 1982.

[25] M. Ghosh, K. Bhanumurthy, G. . Kale, J. Krishnan, and S. Chatterjee, “Diffusion bonding of titanium to 304 stainless steel,” *J. Nucl. Mater.*, vol. 322, no. 2–3, pp. 235–241, 2003.

[26] Rusnaldy, “Diffusion bonding: an advanced of material process,” *Rotasi*, vol. 3, pp. 23–27, 2001.

[27] C. S. Lee, H. Li, and R. S. Chandel, “Vacuum-free diffusion bonding of aluminium metal matrix composite,” *J. Mater. Process. Technol.*, vol. 89–90, pp. 326–330, 1999.

[28] D. R. Walmsley, Z. A. Munir, and A. Dean, “An Investigation of Diffusion Welding of Pure and Alloyed Aluminum to Type 316 Stainless Steel,” no. April, pp. 104–112, 1985.

[29] V. B. G. Mahendran , S. Babu, “Analyzing the Effect of Diffusion Bonding Process Parameters on Bond Characteristics of Mg-Al Dissimilar Joints,” *J. Mater. Eng. Perform.*, vol. 19, no. 5, pp. 657–665, 2010.

[30] N. Kurgan, “Investigation of the effect of diffusion bonding parameters on microstructure and mechanical properties of 7075 aluminium alloy,” *Int. J. Adv. Manuf. Technol.*, vol. 71, no. 9–12, pp. 2115–2124, 2014.

[31] S. Chen, F. Ke, M. Zhou, and Y. Bai, “Atomistic investigation of the effects of

temperature and surface roughness on diffusion bonding between Cu and Al," *Acta Mater.*, vol. 55, no. 9, pp. 3169–3175, 2007.

[32] N. F. Kazakov, Ed., *Diffusion Bonding of Materials*, 1st ed. Moscow: Mir Publishers, Pergamon Press, 1985.

[33] A. A. Shirzadi, H. Assadi, and E. R. Wallach, "Interface evolution and bond strength when diffusion bonding materials with stable oxide films," *Surf. Interface Anal.*, vol. 31, no. 7, pp. 609–618, 2001.

[34] P. Natalya and C. de M. Neto, "Diffusion bonding in stainless steel," *COBEM - Congr. Int. Eng. Mecânica*, vol. di, no. 1973, pp. 4–9, 2005.

[35] N. Özdemir, M. Aksoy, and N. Orhan, "Effect of graphite shape in vacuum-free diffusion bonding of nodular cast iron with gray cast iron," *J. Mater. Process. Technol.*, vol. 141, no. 2, pp. 228–233, 2003.

[36] H. Somekawa and K. Higashi, "The Optimal Surface Roughness Condition on Diffusion Bonding," *Mater. Trans.*, vol. 44, no. 8, pp. 1640–1643, 2003.

[37] M. S. Kenevisi and S. M. Mousavi Khoie, "An investigation on microstructure and mechanical properties of Al7075 to Ti–6Al–4V Transient Liquid Phase (TLP) bonded joint," *Mater. Des.*, vol. 38, pp. 19–25, 2012.

[38] A. Shirzadi, "Diffusion Bonding Aluminium Alloys and Composites : New Approaches and Modelling," 1997.

[39] H. M. Tensi and M. Wittman, "Influence of Surface Preparation on the Diffusion Welding of High Strength Aluminium Alloys," in *Diffusion Bonding 2*, 1991, pp. 101–110.

[40] A. . Zuruzi, H. Li, and G. Dong, "Effects of surface roughness on the diffusion bonding of Al alloy 6061 in air," *Mater. Sci. Eng. A*, vol. 270, no. 2, pp. 244–248, 1999.

[41] Y. Huang, N. Ridley, F. J. Humphreys, and J. Z. Cui, “Diffusion bonding of superplastic 7075 aluminium alloy,” *Mater. Sci. Eng. A*, vol. 266, no. 1–2, pp. 295–302, 1999.

[42] D. R. Cooper and J. M. Allwood, “Influence of diffusion mechanisms in aluminium solid-state welding processes,” *Procedia Eng.*, vol. 81, no. October, pp. 2147–2152, 2014.

[43] H. Li, C. Zhang, H. Bin Liu, and M. Q. Li, “Bonding interface characteristic and shear strength of diffusion bonded Ti-17 titanium alloy,” *Trans. Nonferrous Met. Soc. China (English Ed.*, vol. 25, no. 1, pp. 80–87, 2015.

[44] G. E. Totten and D. S. MacKenzie, *Handbook of Aluminum (Volume 2)*. 2003.

[45] U. Aluminum, “The Benefits of Aluminum.” [Online]. Available: www.UnitedAluminum.com.

[46] J. R. Davis, “Aluminum and Aluminum Alloys,” *Light Met. Alloy.*, p. 66, 2001.

[47] A. Verma, S. Kumar, P. S. Grant, and K. A. Q. O’Reilly, “Influence of cooling rate on the Fe intermetallic formation in an AA6063 Al alloy,” *J. Alloys Compd.*, vol. 555, pp. 274–282, 2013.

[48] E. Cevik, Y. Sun, and H. Ahlatci, “Effect of Peak-Aged Heat Treatment on Corrosion Behavior of the AA6063 Alloy Containing Al3Ti,” *Arch. Metall. Mater.*, vol. 57, no. 2, pp. 469–477, 2012.

[49] J. Hirsch, B. Skrotzki, and G. Gottstein, *Aluminium Alloys: The Physical and Mechanical Properties*, no. 1. c. Wiley, 2008.

[50] Hatch J.E., “Aluminum Properties and Physical Metallurgy,” *ASM ,Ohio, US*, p. 424, 1984.

[51] R. S. Rana, R. Purohit, and S. Das, “Reviews on the influences of alloying elements on the microstructure and mechanical properties of aluminum alloys

and aluminum alloy composites," *Int. J. Sci. Res. Publ.*, vol. 2, no. 6, pp. 1–7, 2012.

[52] G. E. Totten and D. S. Mackenzie, *Handbook of Aluminum Nolume 2 - Alloy Production And Materials Manufacturing*. 2003.

[53] B. Milkereit, L. Giersberg, O. Kessler, and C. Schick, "Isothermal time-temperature-precipitation diagram for an aluminum alloy 6005A by in situ DSC experiments," *Materials (Basel).*, vol. 7, no. 4, pp. 2631–2649, 2014.

[54] V. 2 ASM International Handbook, "Properties and selection: Nonferrous alloys and special-purpose materials," *ASM Met. Handb.*, vol. 2, p. 1300, 1990.

[55] "Extruded Aluminum Alloy 6063," vol. 6. Sapagroup, pp. 0–1, 2012.

[56] "6063 - T6 Extrusions." Aalco Metals, London, pp. 9–11, 2009.

[57] M. H. Jacobs, "The structure of the metastable precipitates formed during ageing of an Al-Mg-Si alloy," *Philos. Mag.*, vol. 26, no. 1, pp. 1–13, Jul. 1972.

[58] B. Milkereit, N. Wanderka, C. Schick, and O. Kessler, "Continuous cooling precipitation diagrams of Al-Mg-Si alloys," *Mater. Sci. Eng. A*, vol. 550, pp. 87–96, 2012.

[59] G. A. Edward, K. Stiller, G. L. Dunlop, and M. J. Couper, "The Precipitation Sequence in Al-Mg-Si Alloys," *Acta Mater.*, vol. 46, pp. 3893–3904, 1998.

[60] J. Banhart *et al.*, "Natural ageing in Al-Mg-Si alloys – a process of unexpected complexity Prof . Dr . John Banhart , Head of Institute Zeqin Liang , PhD Student," vol. 12, no. 7, pp. 559–571, 2010.

[61] I. Dutta and S. M. Allen, "A Calorimetric Study of Precipitation in Commercia Aluminum Alloy 6061," *J. Mater. Sci. Lett.*, vol. 10, pp. 323–326, 1991.

[62] L. C. Doan, Y. Ohmori, and K. Nakai, "Precipitation and dissolution reactions in a 6061 aluminum alloy," *Materials Transactions Jim*, vol. 41, no. 2. pp. 300–

305, 2000.

[63] E. A. Stark, “Heat Treatable Aluminum Alloys,” *Acad. Press*, vol. 31, pp. 35–63, 1989.

[64] G. K. Sigworth and T. A. Kuhn, “GRAIN REFINEMENT OF ALUMINUM CASTING ALLOYS,” 2007.

[65] T. E. Quested, “Understanding mechanisms of grain refinement of aluminium alloys by inoculation,” *Mater. Sci. Technol.*, vol. 20, no. November, pp. 1357–1369, 2004.

[66] M. A. Easton and D. H. Stjohn, “Grain Refinement of Aluminum Alloys : Part I . The Nucleant and Solute Paradigms — A Review of the Literature,” *Metall. Mater. Trans. A*, vol. 30, no. June, pp. 1613–1623, 1999.

[67] L. F. Mondolfo, “Aluminum alloys : structure and properties.” Butterworths, London; Boston, 1976.

[68] A. M. A. Mohamed and F. H. Samuel, “A Review on the Heat Treatment of Al-Si-Cu/Mg Casting Alloys,” *Conv. Nov. Appl.*, p. 229, 2012.

[69] C. H. Cáceres, I. L. Svensson, and J. a. Taylor, “Strength-ductility behaviour of Al-Si-Cu-Mg casting alloys in T6 temper,” *International Journal of Cast Metals Research*, vol. 15. pp. 531–543, 2003.

[70] G. Riontino, S. Abis, and C. Bottero, “A DSC Study of Precipitation in Al-Cu-Mg Alloys,” in *Aluminum Alloys,Vol 2*, 1998, pp. 903–908.

[71] S. C. Wang and M. J. Starink, “Precipitates and intermetallic phases in precipitation hardening Al–Cu–Mg–(Li) based alloys,” *Int. Mater. Rev.*, vol. 50, no. 4, pp. 193–215, 2005.

[72] D. A. Petrov, “Voprosy Teorii Splavov Alyuminiya (Problems od Theory of Aluminum Alloys,” *Metallurgizdat*.

[73] V. S. Grebenkin, T. V. Silchenko, and A. A. Gorshkov, “sn,” *Mater. Sci. Heat Treat.*, vol. 3, pp. 50–54, 1972.

[74] E. M. Elgallad, A. M. Samuel, F. H. Samuel, and H. W. Doty, “Effects of Additives on the Microstructures and Tensile Properties of a New Al-Cu Based Alloy Intended for Automotive Castings (10-042),” 2010.

[75] D. Fang, X. Cheng, Y. Li, and Z. Sun, “RSC Advances Microstructure and thermal characteristics of Mg – Sn alloys as phase change materials for thermal,” *RSC Adv.*, vol. 6, no. 400, pp. 96327–96333, 2016.

[76] R. R. Ambriz, V. Mayagoitia, and I. P. N. Ciitec-ipn, “Welding of Aluminum Alloys,” *InstitutePoltechnico, CP*, no. i, pp. 15–30.

[77] R. S. Timsit and B. J. Janeway, “A Novel Brazing Technique for Aluminum,” *Weld. J.*, no. June, pp. 119–128, 1994.

[78] V. Avagyan, “Diffusion brazing and welding of the accelerating structure,” *Proc. IEEE Part. Accel. Conf.*, vol. 2005, pp. 2938–2940, 2005.

[79] Y. Wang, G. Luo, L. Li, Q. Shen, and L. Zhang, “Formation of intermetallic compounds in Mg-Ag-Al joints during diffusion bonding,” *J. Mater. Sci.*, vol. 49, no. 20, pp. 7298–7308, 2014.

[80] P. Eslami and A. K. Taheri, “An investigation on diffusion bonding of aluminum to copper using equal channel angular extrusion process,” *Mater. Lett.*, vol. 65, no. 12, pp. 1862–1864, 2011.

[81] A. Sagai Francis Britto, R. E. Raj, and M. C. Mabel, “Prediction of shear and tensile strength of the diffusion bonded AA5083 and AA7075 aluminium alloy using ANN,” *Mater. Sci. Eng. A*, vol. 692, no. March, pp. 1–8, 2017.

[82] A. Ureña, J. M. Gómez De Salazar, and M. D. Escalera, “Diffusion bonding of an aluminium-copper alloy reinforced with silicon carbide particles (AA2014/SiC/13p) using metallic interlayers,” *Scr. Mater.*, vol. 35, no. 11, pp.

1285–1293, 1996.

[83] G. Chen, Q. Shi, Y. Li, Z. Han, and K. Yuan, “Experimental investigations on the kinetics of void shrinkage in solid state bonding of AA6061 at high temperatures and high pressures,” *Mater. Des.*, vol. 89, pp. 1223–1226, 2016.

[84] A. Urena, J. M. G. De Salazar, J. Quifiones, and J. J. Martin, “TEM Characterization of Diffusion Bonding of Superplastic 8090 Al-Li Alloy,” vol. 34, no. 4, pp. 617–623, 1996.

[85] H. Chen, J. Cao, X. Tian, R. Li, and J. Feng, “Low-temperature diffusion bonding of pure aluminum,” *Appl. Phys. A Mater. Sci. Process.*, vol. 113, no. 1, pp. 101–104, 2013.

[86] T. Enjo and K. Ikeuchi, “Diffusion welding of Al-Cu-Mg series 2017 alloy,” *Trans. JWRI*, vol. 13, no. 2, pp. 63–68, 1984.

[87] Y. E. Wu and Y. L. Lo, “Surface protection for AA8090 aluminum alloy by diffusion bonding,” *Theor. Appl. Fract. Mech.*, vol. 38, no. 1, pp. 71–79, 2002.

[88] Y. E. Wu and Y. L. Lo, “Applying liquid film protection method to solid-state bonding process of AA7075 aluminum alloys,” *J. Mater. Process. Technol.*, vol. 140, no. 1–3 SPEC., pp. 700–704, 2003.

[89] A. S. Zuruzi, H. Li, and G. Dong, “Diffusion bonding of aluminium alloy 6061 in air using an interface treatment technique,” *Mater. Sci. Eng. A*, vol. 259, no. 1, 1999.

[90] I. M. Barta, “Low temperature diffusion bonding of aluminium alloys,” *Weld. J.*, vol. Research S, pp. 241–247, 1964.

[91] E. R. Maddrell and E. R. Wallach, “Diffusion welding of aluminium-lithium alloys,” in *Proc Conf. Recent Trends in Welding Science & Technology*, 1990, p. 541 545.

[92] D. V Dunford, P. G. Partridge, and C. J. Gilmore, “Diffusion Bonding of Al-Li 8090 Alloy,” in *Diffusion Bonding 2*, 1991, pp. 130–143.

[93] R. A. Ricks, G. J. Mahon, N. C. Parson, T. Heinrich, and P. J. Winkler, “Development of Diffusion Bonding Techniques for Al-Li Based AA8090,” in *Diffusion Bonding 2*, 1991, pp. 69–82.

[94] “Standard Test Methods for Tension Testing Wrought and Cast Aluminum- and Magnesium-Alloy Products (Metric).” ASTM International, 2015.

[95] M. V. Kral, P. N. H. Nakashima, and D. R. G. Mitchell, “Electron microscope studies of Al-Fe-Si intermetallics in an Al-11 Pct Si alloy,” *Metall. Mater. Trans. A*, vol. 37, no. 6, pp. 1987–1997, 2006.

[96] W. a. Monteiro, “Microstructural and Mechanical Characterization after Thermomechanical Treatments in 6063 Aluminum Alloy,” *Mater. Sci. Appl.*, vol. 2, no. 11, pp. 1529–1541, 2011.

[97] S. Belmares-Perales and A. A. Zaldívar-Cadena, “Addition of iron for the removal of the β-AlFeSi intermetallic by refining of α-AlFeSi phase in an Al–7.5Si–3.6Cu alloy,” *Mater. Sci. Eng. B*, vol. 174, no. 1, pp. 191–195, 2010.

[98] “Basic Metallurgy : 6000 Series Extrusion Alloys.” Quenching Press, pp. 1–28, 1997.

[99] M. Easton and D. StJohn, “An analysis of the relationship between grain size, solute content, and the potency and number density of nucleant particles,” *Metall. Mater. Trans. A*, vol. 36, no. 7, pp. 1911–1920, 2005.

[100] S. E. Atabay, Z. Esen, and A. F. Dericioglu, “Effect of Sn Alloying on the Diffusion Bonding Behavior of Al-Mg-Si Alloys,” *Metall. Mater. Trans. A Phys. Metall. Mater. Sci.*, pp. 1–7, 2017.